Solutions of Conformal Gravity with Dynamical Mass Generation in the Solar System

A thesis
submitted in partial fulfilment
of the requirements for the Degree
of
Doctor of Philosophy in Physics
in the
University of Canterbury

by

Joshua N. Wood

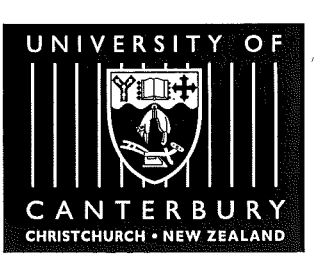

University of Canterbury
2000

Abstract

An investigation is made into the viability of the fourth-order conformal theory of gravity with dynamical mass generation. This is done by considering the analytical behaviour of the equations of motion and using this as a guide to producing numerical solutions to these equations. A review of some criticisms of the fourth-order gravity theory is included.

Numerical solutions of the equations of motion are produced for the domain interior to the source and the exterior region within the solar system, with a variety of source conditions and under different formulations. These are analysed with consideration of reasonable physical and observational requirements, based on the well established solar system gravitational effects. The possibility of extra gravitational effects to explain anomalies in current gravitational theory is investigated. These effects include the possible anomalous acceleration of the Pioneer spacecraft, and could be extended to cover galaxy-scale phenomena such as galactic rotation curves.

Conclusions are then drawn about what formulations and parameter sets are viable for good representation of the physics. The effects of the dynamical mass generation on observed phenomena are discussed, with reference to the potential resolution of gravitational anomalies.

Contents

Chapter 1

Introduction

Theoretical physics has made great advances in this century towards explaining the nature of the fundamental interactions and particles that make up the universe we live in. The essential method in this proceeding explanation of our reality is the unification of the fundamental forces — namely, the strong and weak nuclear forces, the electromagnetic force, and the gravitational force. It is a kind of holy grail for theorists to produce a 'theory of everything' which can include all these forces within a single framework.

The nature of the fundamental forces has been explored via theories of fields, which have developed in ways peculiar to the forces being described. Gravitation is essentially and intrinsically linked to the properties and contents of the space-time in which it is acting, and so is described in terms of metric field tensor $g_{\mu\nu}$ by Einstein's general relativity. This field describes the distances and curvatures of space and time, leading to a beautifully symmetric theory in which the mass and energy content of the universe defines how space is curved, which in turn defines how the mass and energy will move. Developed in 1916, the General Theory of Relativity [1] has been spectacularly successful in describing the gravitational phenomena in the solar system, to the limits of definition of our observations.

Some time after the development of general relativity (GR), quantum field theory (QFT) began to be considered as a good description of the fundamental particles. The theory has considerable initial difficulties, such as the possibility of particles with infinite amounts of energy. These were overcome with the advent of renormalisable theories, which through a redefinition of the idea of what a particle is, allow such infinities to be neatly removed from the theory. Particles are now being treated in a more dynamic way, as being the excitations of a field throughout space-time, rather than being kinematic constructs. Concepts of symmetry invariance, when applied to quantum field theory, allowed the development of the theory of dynamical mass generation by Weinberg, Glashow and Salaam, which

unified the weak nuclear and electromagnetic forces.

This theory of dynamical mass generation by 'spontaneously broken symmetry' (SBS) was a revolutionary concept and took some time to be accepted (see Weinberg's book, 'Dreams of a final theory' [2]), but with the experimental discovery of the W and Z particles at the CERN facility in Switzerland, the theory gained strong credence. It has since been expanded to include the strong nuclear force in the same theoretical framework (quantum chromodynamics, QCD), and is so accepted today that this is referred to as the 'standard model'.

However, the final unification of the four forces remains elusive. The nature of the formulation of general relativity considers matter kinematically, not dynamically. A space-time containing dynamically generated matter is, to Einstein's field equations, essentially a space-time containing nothing. Despite both general relativity and quantum field theory being generally accepted, efforts towards final unification are often in essentially different theories such as superspace or string theories.

1.1 Problems for General Relativity

Despite it's wide acceptance and excellent observational verification in solar system tests, the general theory of relativity is not without it's own foils. Possibly the most obvious difficulty is the 'missing mass' problem, in it's various forms. This is perhaps most easily described in terms of galaxy dynamics.

By measuring the Doppler shift of the frequency of light emitted by a galaxy that is near edge-on to our line of sight here on Earth, the relative velocity of the different parts of such a galaxy can be determined. It is found that the rotational velocity of the stars in the spiral arms of galaxies increase in a way which is not in agreement with the predictions of general relativity. Given the apparent success of GR on local scales, such as within the solar system, the usually presented argument is that the extra gravitational attraction required is provided by 'dark matter' of some kind which is not observed — i.e. there is something out there which we cannot see or detect which is responsible for fixing up the anomalous results. For reasons to do with stability of the rotation of the galaxy, the average spiral galaxy requires about nine times as much dark matter as luminous, observed matter, distributed in a spherical 'halo' around the spiral. The exact composition of the dark matter is speculative, ranging from unknown, exotic fundamental particles that we are currently unaware of, to small stellar

bodies similar to the familiar galactic bodies, but of very low luminosity and profusely distributed.

Another serious question for general relativity is the expansion of the universe. This has always been a slightly nebulous issue, as the end result of the expansion depends on the density of the universe, something not yet determined. Currently, with only considering the observed luminous sources, the expansion of the universe will continue indefinitely as there is not enough matter to reverse the expansion through gravitational attraction. As this has been regarded as an undesirable destiny, mechanisms to retard the expansion have been devised. The most famous is the cosmological constant Λ, an 'ad hoc' term originally added to Einstein's field equations as a 'negative pressure' to augment the gravitational contraction of the universe. The exact value of Λ is arguably the least specified constant in any theory, as arguments from gravitational theories can be made for it to be zero, whilst from particle theory arguments it could be required to be of order 10^{60} or larger.

Recent developments have only exacerbated this problem. Measurements have been made of very distant high redshift type 1a supernovae, the furthest away and thus most ancient of the objects for which we can calculate distances ([3, 4]). These redshifts suggest that objects in distant space are not only receding from us, but that this recession is accelerating. There is no way an accelerating expansion of the universe can be explained with just the gravitational contributions of the matter we can see, some kind of cosmological constant would have to be introduced if this is the case. Just what that cosmological constant physically represents is not certain either, but many suggestions involve some kind of energy stored in the fabric of spacetime [5].

Even closer to home, there is some evidence that gravity may not be working exactly as we expect. In 1997, it was found that the trajectories of the Pioneer space probes, and that of the Ulysses solar probe, were not exactly what had been predicted [6]. Though a great many physical reasons can be thought of for this effect, such as gas release from the craft or heat radiation from it's generators, so far none of these predictions can replicate the effects found in the data. This is an ongoing area of investigation, with the emphasis shifting from physical effects from the craft to gravitational effects, possibly involving new physics [7, 8]. As ranging using active transponder signals from spacecraft could be the most accurate method we have for measurement of motion under gravity, the resolution

of this issue could be very significant.

1.2 Conformal Gravity Theories

Conformal gravity theories are based on the invariance of the action of the theory under stretchings of the space-time manifold — that is, an invariance of scale. In a conformal theory, the metric (which defines the measurement of distances) may be scaled by an arbitrary factor, and the action remains unchanged. This is a powerful symmetry for a theory to have.

Conformal invariance is a property enjoyed by the other fundamental interactions that have been unified, and as a feature results in theories with dimensionless coupling constants (cf. the gravitational constant G, of units Nm^2/kg^2). There is only one action integral which can be used as a basis for a conformally invariant theory of gravity, which was produced by Weyl [9] around the same time as Einstein developed general relativity. The theory was not seriously investigated as a viable theory of gravity as the fourth order differential equations it involves are much more complex than the second order equations of general relativity, which was the 'naturally' expected order for the equations to have. Indeed, in derivations of Einstein's field equations, one of the principles used is that the equations shall be of second order. This is often the least explained requirement in the derivation [10]. Also, the conformal field equations require a traceless energy-momentum tensor, which corresponds to a space-time with no kinematic masses present. To quote P.D. Mannheim, this isn't a very interesting universe, it doesn't have any physicists in it! This has been used as an objection to the possibility of conformal theories having any physical relevance, even though it is a direct requirement for the dynamically generated masses present in the accepted model of the other fundamental interactions. With the dynamical mass generation mechanism, the tracelessness of the conformal energy-momentum tensor becomes an asset.

1.2.1 Existing Work in Conformal Gravity

Despite the complexity of the field equations involved, some work has been done on solutions of conformal gravity theories. An analytic solution to the vacuum field equations, analogous to the Schwarzschild solution of general relativity, was found some time ago ([11, 12, 13]), and some various, generalised solutions for the interior of the gravitating body (typically a star) have followed ([14], etc.). Vari-

ous papers have also been published on the cosmological relevance of conformal gravity theories ([15]), especially with regard to constraining any cosmological constant or for determining the background curvature, if any, of the universe. Extensions of the vacuum solution in explanation of galactic rotation curves have been published ([16, 17]) — which appear quite successful and would obviate the need for the copious amounts of dark matter proposed to explain general relativity's failure to account for these observations.

These papers have, in return, prompted papers in criticism of their theories (e.g. [18]). Conformal gravity theories have a great many obstacles and preconceptions to overcome before they could be expected to be treated as a viable alternate theory of gravity, on a similar footing to general relativity. The difficulties for the theory are mainly computational, though sometimes observational. The preconceptions appear also to be a sizeable obstacle, to both proponents and critics of conformal gravity theories.

For example, we have the issue of tracelessness of the conformal energy-momentum tensor. This has been used as an argument [18] to discredit the theory. However, it is a feature required of any theory that is to be compatible with dynamical mass generation as it is accepted to occur in the standard model of particle physics.

Nevertheless, the proponents of conformal gravity, whilst relying on this compatibility to avoid the argument about the absence of kinematic masses, generally proceed to ignore the dynamical mass generation mechanism in further applications of the theory. So despite a background scalar field being introduced to provide for spontaneous symmetry breaking dynamically generating matter, this scalar field is not accounted for in the solutions of the field equations. For example, papers on galactic rotation curves use a vacuum solution (zero energy-momentum tensor) of the field equations, when the same theory is relying on the presence of a scalar field in the energy-momentum tensor for it's viability.

The undeveloped consideration of the dynamical mass generation mechanism could be the greatest weakness in current publications on conformal gravity. The arguments of some of the critics can be avoided by considering a dynamical source of matter. Even in papers describing the compatibility of dynamical mass generation with geodesic motion [19], the scalar field is carefully simplified in such a way as to produce no observable effects. Once these arguments have been presented, the scalar field is never referred to again.

1.3 Current state of General Relativity

The theory of General Relativity is both well established and very successful on local scales. The accuracy to which the predictions of GR have been confirmed have been a strong influence in the consideration of gravitational theory, and for a great many scientists it is seen as easier to assume that there may be other, exotic kinds of dark matter out there than to consider that GR may not be the whole story. There are still enough unknown areas in the theory that allow excellent descriptions of various dark matter or cosmic acceleration problems to be made within the framework of the standard theory.

The currently favoured model in general relativity is the ΛCDM model, which presumes that the luminous matter we observe in the universe is the minor player gravitationally, with strong contributions from a cosmological constant Λ and the presence of cold dark matter (CDM). This model is able to resolve many issues that trouble the standard theory, and has particularly useful properties for description of structure formation in the early universe. However, it appears that models of this kind have difficulties in describing objects such as galaxies, and recent observations of the cosmic microwave background (CMB) power spectrum suggest that some predictions of the CDM paradigm are not borne out by observation ([20, 21, 22]). The current opinion of some authors is becoming that dark matter models have enough problems of their own that they no longer resolve the difficulties for which they were created any better than alternative gravity theories [23].

1.4 Aim of the Thesis

In this thesis, I propose to investigate conformal gravity with dynamical mass generation as an intrinsic feature, and non-trivial symmetry breaking scalar fields will be considered in their implications for gravitational effects. This can produce some very interesting results, such as apparent near-linear accelerations as possibly observed in the motion of the Pioneer spacecraft, and others. It can also lead to other perspectives of consideration for the Higgs mechanism and it's role in mass generation.

The gravitational system I will investigate is that best known to us, the solar system. Solar data will be used for the general source of gravitational effects, and the results obtained will then be able to be compared to the observed motion of

bodies in our solar system, within tolerances which can be related to the accuracy of the observations. By restricting work to the solar system the predictions of our theory are thus more testable, rather than extending into areas where the observations are in more doubt and the theory less complete. By producing a conformal gravity, dynamical mass model of the solar system we can then compare it's predictions with the observations, and say whether the conformal model is viable with the bounds of observational uncertainty.

1.5 Conventions

As much as possible, we have tried to use conventions following Weinberg [24] for the field equations and definitions of tensor quantities. We assume a metric signature of (-,+,+,+) for all the field equations and equations of motion.

Symbols used in this thesis include the following.

$C_{\lambda\mu\nu\kappa}$	Weyl conformal tensor
$g_{\mu\nu}$	metric tensor
g	metric determinant
$R_{\mu\kappa}$	Ricci tensor
$R^{\alpha}{}_{\alpha}$	Ricci scalar
$T_{\mu\nu}$	energy-momentum tensor
U^{μ}	velocity vector
$W_{\mu\nu}$	Weyl field tensor
$G_{\mu\nu}$	Einstein field tensor
S	mass scale generating scalar field
Ψ	generic fermion field
ρ	density, or alternative radius
p	pressure
a, b	metric coefficients
A, B	alternative metric coefficients
$\bar{a}, \bar{b}$	metric coefficients, conformal line element
$f(r)$	source function for field equations (massive)
$g(r)$	source function for field equations (scalar)
Ω	conformal scale factor
$x = (x^0 = ct, x^1, x^2, x^3)$	point on spacetime manifold
$'$	derivative with respect to radius
$\cdot$	derivative with respect to proper time
R	solar radius
ϵ_m	machine accuracy

Abbreviations used include the following.

GR	General Relativity
CG	Conformal Gravity
S eqn.	S field equation of motion
hseqm.	hydrostatic equilibrium equation
Schwarz.	Schwarzschild
AU	astronomical unit

Chapter 2

The Conformal Field Equations

2.1 Weyl Field Equations

The conformal gravity theory is based on the principle of conformal invariance — that is, the invariance of the action under any conformal stretchings of the space-time manifold. This is represented by the action of a conformal transformation function $\Omega(x)$, which can vary arbitrarily at each point in space, on the metric tensor according to $g_{\mu\nu} \rightarrow \Omega^2 g_{\mu\nu}$. Very few objects are invariant under such a general transformation, and the choice for a gravitational action reduces to

$$I_W = -\alpha \int d^4x \, (-g)^{\frac{1}{2}} \, C_{\lambda\mu\nu\kappa} C^{\lambda\mu\nu\kappa},$$

where

$$C_{\lambda\mu\nu\kappa} = R_{\lambda\mu\nu\kappa} - (g_{\lambda\nu} R_{\mu\kappa} - g_{\lambda\kappa} R_{\mu\nu} - g_{\mu\nu} R_{\lambda\kappa} + g_{\mu\kappa} R_{\lambda\nu})/2 + \frac{R^{\alpha}{}_{\alpha}}{6} (g_{\lambda\nu} g_{\mu\kappa} - g_{\lambda\kappa} g_{\mu\nu})$$

is the conformal Weyl tensor [24] and α is a dimensionless coupling constant. This action is the unique choice for conformal invariance in four-dimensional space-time.

The Weyl tensor itself is a somewhat unwieldy object with which to work, but fortunately by some fairly straightforward arguments we can rewrite this action by discarding the integral of a total divergence [15] as

$$I_W = -2\alpha \int d^4x \, (-g)^{\frac{1}{2}} \left(R_{\mu\kappa} R^{\mu\kappa} - \frac{1}{3} (R^{\alpha}{}_{\alpha})^2 \right),$$

which is in terms of the more familiar Ricci tensor and scalar.

By variation of this action with respect to the metric, we can produce the gravitational tensor $W_{\mu\nu}$, the conformal analogue of the Einstein tensor $G_{\mu\nu}$ of the standard theory. This tensor is found to transform conformally according to $W_{\mu\nu} \rightarrow \Omega^{-2} W_{\mu\nu}$. Given the above form of the gravitational action, and a matter

action I_M, variation produces field equations of the form

$$(-g)^{-\frac{1}{2}} g_{\mu\alpha} g_{\nu\beta} \frac{\delta I_W}{\delta g_{\alpha\beta}} = -2\alpha W_{\mu\nu} = (-g)^{-\frac{1}{2}} g_{\mu\alpha} g_{\nu\beta} \frac{\delta I_M}{\delta g_{\alpha\beta}} = -\frac{1}{2} T_{\mu\nu} \tag{2.1}$$

(first produced by Bach [25]) where the specific form of the tensors $W_{\mu\nu}$ are given by (following DeWitt [26])

$$\begin{aligned} W_{\mu\nu} &= \frac{g_{\mu\nu}}{3} \left(R^{\alpha}{}_{\alpha}\right)^{;\beta}{}_{;\beta} + R_{\mu\nu}{}^{;\beta}{}_{;\beta} - R_{\mu}{}^{\beta}{}_{;\nu;\beta} - R_{\nu}{}^{\beta}{}_{;\mu;\beta} - 2R_{\mu}{}^{\beta} R_{\nu\beta} + \frac{g_{\mu\nu}}{2} R_{\alpha\beta} R^{\alpha\beta} \\ &\quad + \frac{2}{3} \left(R^{\alpha}{}_{\alpha}\right)_{;\mu;\nu} + \frac{2}{3} R^{\alpha}{}_{\alpha} R_{\mu\nu} - \frac{g_{\mu\nu}}{6} \left(R^{\alpha}{}_{\alpha}\right)^2, \end{aligned} \tag{2.2}$$

and the energy-momentum tensor on the right-hand side of equation (2.1) comes from the variation of an appropriate matter action with respect to the metric.

One immediately apparent feature of these tensor equations is that in the vacuum case where $T_{\mu\nu} = 0$, the Schwarzschild solution to the Einstein equations $R_{\mu\nu} = 0$ also satisfies these conformal field equations. However, there can be solutions of the conformal field equations that are more general, as we shall discuss below.

2.1.1 Metric Forms

Having produced the tensor form of the conformal field equations, we must specify a form of the metric, allowing us to express the field equations in terms of the metric coefficients. There are many options, depending on the physical properties of the situation we intend to investigate. Logically, we want to set up our system of equations in a way that reflects the simplest way to view whatever physical system we are concerned with — our coordinates should be set up to exploit any symmetries to the full. The natural place to start is following the route taken in general relativity — let us consider a static, spherically symmetric system. This leads to the 'standard' line element, following Weinberg [24], as given by

$$ds^2 = -b(r)\, dt^2 + a(r)\, dr^2 + r^2 \left(d\theta^2 + \sin^2\theta d\phi^2\right).$$

This is the form of the metric most often encountered in general relativistic solutions of the field equations about gravitating bodies, such as the Schwarzschild solution. This is a perfectly adequate form for us to use, but we can improve on this by making connection with the conformal symmetry we are working under.

Despite the higher order of derivatives present in the Weyl field equations over the Einstein equations, the underlying conformal symmetry of the theory

can be invoked to simplify the line element and thus the expressions for the various curvature tensors. The practical upshot of this is that the equations become not only less complex, but can potentially be written in terms of one less variable. This is a feature exploited in the analytic solutions to the conformal field equations presented in the literature, where the transforming away one of the two metric coefficients allows dramatic simplification of the field equations.

The procedure for transforming the line element to a more obviously conformal representation (as presented by Mannheim [13]) runs as follows.

Starting with the general static, spherically symmetric line element as expressed above, but with a change of radial variable [24]

$$ds^2 = -b(\rho)\,dt^2 + a(\rho)\,d\rho^2 + \rho^2 d\Omega$$

we then rewrite this by change of radial variable to

$$ds^2 = \frac{p^2(r)}{r^2}\left(-B(r)\,dt^2 + A(r)\,dr^2 + r^2 d\Omega\right)$$

where $\rho = p(r), B(r) = \frac{r^2 b(r)}{p^2(r)}, A(r) = \frac{r^2 a(r) p'^2(r)}{p^2(r)}$. The factor $\frac{p(r)}{r}$ is coming in as an overall conformal scaling on the line element, c.f. a conformal transformation effects the line element according to $ds^2 \to \Omega^2 ds^2$.

So far, $p(r)$ is an arbitrary function, but is now chosen to be given by

$$-\frac{1}{p(r)} = \int \frac{dr}{r^2 \left(a(r)\,b(r)\right)^{\frac{1}{2}}}$$

so that

$$ds^2 = \frac{p^2(r)}{r^2}\left(-B(r)\,dt^2 + \frac{dr^2}{B(r)} + r^2 d\Omega\right)$$

which is of the form of a conformal scaling $\Omega = \frac{p(r)}{r}$ on a line element in the standard form but with $A(r) = B(r)^{-1}$. This is exactly a conformal scaling on the result of the Schwarzschild solution to general relativity, where $A(r)$ is found to be equal to $B(r)^{-1}$. This form of the line element allows much simplification of the curvature and field tensors, and hereafter I shall use this in the following notation:

$$ds^2 = \bar{a}^2(r)\left(-\bar{b}(r)\,dt^2 + \frac{dr^2}{\bar{b}(r)} + r^2 d\Omega\right),$$

where $\frac{p(r)}{r}$ has been replaced by $\bar{a}(r)$ and $B(r)$ by $\bar{b}(r)$.

This form of the line element has many advantages when it comes to producing coordinate specific forms of the field equations, which in general come out a

great degree simpler than the corresponding equations in the general spherically symmetric metric above. However, as our theory is conformally invariant, and $W_{\mu\nu}$ transforms as $W_{\mu\nu} \rightarrow \Omega^{-2} W_{\mu\nu}$, the field equations are invariant under a conformal transformation to the line element

$$ds^2 = -B(r)\, dt^2 + \frac{dr^2}{B(r)} + r^2 d\Omega.$$

Thus by a specific choice of conformal transformation on the line element, we can reduce the number of independent variables in the metric by one. In this case, the conformal scaling factor is information that cannot be observed, and the field equations are greatly simplified by it's removal.

This is the form of the line element used in most of the existing publications on conformal gravity theories (e.g. Mannheim [13, 14, 19]). In general, in my calculations I have used the manifestly conformal form of the line element, given in terms of $\bar{a}(r), \bar{b}(r)$. This conformal form simplifies the equations to a large degree, if not so much as removing one metric coefficient completely. The simplifications arising from partially or completely removing one metric coefficient are dramatic, especially when the additional complications of dynamical mass generation are to be considered. This is especially useful when the numerical routines have difficulty coping with the complexity of the more general expressions, whereas they can more easily cope with the simplified form. It also has conceptual advantages in certain cases, such as exterior solutions, where (up to variations induced by a possible Higgs field), the function $\bar{a}(r)$ can be seen as an index of deviation from the Schwarzschild solution of Einstein's field equations, where $A(r) = 1/B(r)$ exactly, and therefore $\bar{a} = 1$.

A side issue arising from this simplification has to do with further conformal transformations. In this case, to remove one metric coefficient completely we have performed a specific conformal transformation to get the line element and metric in a simple form. Though the tensor relation is invariant under any further conformal transformations, it does not appear that this specific, simplified form of the line element would remain as any conformal transformation other than a pure scaling would introduce the new transformation function Ω into the metric coefficients. There are cases in the literature [19] where further conformal transformations are invoked to simplify the system further, for example by reducing a potentially complicated scalar field to a constant value. We do not invoke such transformations in addition to that above, simplifying the line element, as it does not appear that such combinations would be compatible in general. The

practical upshot of this is, that with a simplified form of the line element in use, we do not assume structure of the scalar field can be reduced to a constant, but that the scalar field contains gradients. This is particularly of interest when considering the source terms of the equations, in which the scalar field transforms as $S \rightarrow \Omega^{-1}S$, thus introducing the transformation function explicitly.

2.1.2 Existing Solutions to the Field Equations

Exact Vacuum Solution '89

The most quoted solution to the Weyl conformal field equations to date is the 'vacuum solution' (as presented by Mannheim and Kazanas, Riegert, et. al. [13, 11, 12]), i.e. the solution analogous to the vacuum Schwarzschild solution of general relativity, with the source $T^{\mu\nu}$ set equal to zero. This solution is generally presented as the solution of the radial field equation $W^{rr} = 0$ in a static, spherically symmetric environment. In addition, a conformal transformation has been made to put the metric and line element in the simple form described above. As described above, the standard Schwarzschild solution will solve this equation, as setting $R^{\mu\nu} = 0$ will lead to the vanishing of $W^{\mu\nu}$. However, less trivial solutions are also found, which have certain interesting features. A derivation, as presented in 'Exact Vacuum Solution to Conformal Weyl Gravity' [13] is:

$$\frac{W^{rr}}{b} = \frac{1}{6}b'b''' - \frac{1}{12}b''^2 - \frac{1}{3r}\left(bb''' - b'b''\right) - \frac{1}{3r^2}\left(bb'' + b'^2\right) + \frac{2}{3r^3}bb' - \frac{b^2}{3r^4} + \frac{1}{3r^4},$$

where one metric coefficient has been conformally suppressed. Substitute $b(r) = r^2 f(r)$ and rewrite this equation as:

$$\frac{W^{rr}}{b} = \frac{r^4}{6}\left(f'f''' - \frac{1}{2}f''^2 + \frac{2}{r^8} + \frac{4}{r}f'f'' + \frac{4}{r^2}f'^2\right),$$

then further substitute $f'(r) = y^2(r)\, r^{-4}$ to yield the compact expression

$$\frac{W^{rr}}{b} = \frac{1}{3r^4}\left(1 + y^3 y''\right).$$

This simple expression is then solved for the vacuum $W^{rr} = 0$ case to yield the solution

$$a(r)^{-1} = b(r) = 1 - \frac{\beta(2 - 3\beta\gamma)}{r} - 3\beta\gamma + \gamma r - kr^2 \tag{2.3}$$

where β, γ and k are integration constants.

It is readily apparent that this solution would reduce to the standard Schwarzschild solution if γ and k were to vanish. However, the extra linear potential due to γ

could, if γ is found to have an appropriate value, be used to provide the extra acceleration required to model galactic rotation curves without the need to appeal to dark matter. Papers have been published utilising this procedure [17] which appear to have very promising fits for certain values of γ, with certain other suppositions (such as a further linear potential contribution coming from the background curvature of the universe). However, as yet no complete treatment has derived a suitable value for γ from the integration over the source or from boundary conditions. The magnitude of γ can be estimated by galaxy scale results to be of order 10^{-28} cm^{-1} or smaller for a galaxy, which is not only a suitable magnitude to give restoring contributions to galactic rotation curves but is also interestingly similar to the inverse Hubble length ([27, 28, 29]). The corresponding value for the sun would be $\gamma \sim 10^{-39}$ cm^{-1}, resulting in very small deviations from standard gravitational effects in the solar system [14].

Similarly, the quadratic term kr^2 is identified with a background coming from a de Sitter cosmology. The value of k is linked to the cosmological scalar curvature by the relation $R^{\alpha}{}_{\alpha} = -12k$ (considering cosmological sources only, i.e. $\gamma = 0$). In standard general relativity, such a background cosmological curvature could only be generated by the presence of a cosmological constant but in this conformal theory it is generated naturally. The actual value that this constant takes would be such that it's effects only become apparent on cosmological distance scales, i.e. very small.

Interior Solution

The treatment of interior solutions to the Weyl field equations has been less exact than that of exterior solutions. However, the interior treatment has made some very interesting features of the theory apparent. Specifically, instead of solving the individual field equations, it is found that in the conformal choice of line element with $a = b^{-1}$, the field equation may be combined in a very simple form:

$$\frac{3}{b(r)}\left(W^{t}{}_{t} - W^{r}{}_{r}\right) = \nabla^4 b(r)$$

which, when combined with the Weyl field equations, yields:

$$\nabla^4 b(r) = f(r)$$

where $f(r) = 3\left(T^{t}{}_{t} - T^{r}{}_{r}\right)/4\alpha b(r)$. This source function is unknown without more detailed knowledge of stellar interiors, but the simple equation can be

integrated in terms of the source function $f(r)$. This has been done, integrating over the matter source of gravity in a star ([14], etc.) to yield the following expressions for $b(r)$:

$$b(r > R) = -\frac{1}{6}\int_0^R dr' f(r') \left[3r'^2 r + r'^4/r\right] \tag{2.4}$$

$$b(r < R) = -\frac{1}{6}\int_0^r dr' f(r') \left[3r'^2 r + r'^4/r\right] - \frac{1}{6}\int_r^R dr' f(r') \left[3r'^3 + r^2 r'\right]. \tag{2.5}$$

Mannheim in his 1994 paper [14], then further identifies the components of these integrals (for the exterior case) with the integration constants that appear in the vacuum exterior solution above, giving

$$\beta(2 - 3\beta\gamma) = \frac{1}{6}\int_0^R dr' f(r') r'^4 \tag{2.6}$$

$$\gamma = -\frac{1}{2}\int_0^R dr' f(r') r'^2.$$

This particular method of solution is not taking into account all of the consequences of dynamical mass generation, which would be required for a full conformal gravity theory. This is due to the presence of a traceless energy-momentum tensor which forbids the presence of kinematic particle masses, thus requiring dynamical masses and a scalar Higgs field throughout space, which could contribute vacuum energy to the energy-momentum tensor outside the physical radius of the source object. This will be further investigated in the following sections. In addition, there have been criticisms published on this method which have certain salient points [18], which will also be discussed below.

2.2 Dynamical Mass Generation and Conformal Gravity

The use of the Weyl action leads to field tensors $W_{\mu\nu}$ that are, by definition, traceless. This immediately requires that the energy-momentum tensor of a conformal theory be traceless also. Unfortunately, in standard relativity theory this would correspond to a system with no matter in it, which would not be a very good model of our observable universe! This has often been invoked in papers and comments critical of conformal theories, immediately questioning the relevance of a theory containing no matter to the solar system or galaxy (e.g. [18]).

However, this is not the whole story. The developments in quantum field theory of the last three decades have somewhat demoted the position of kinematic

mass in the fundamental scheme of things — in fact, mass itself is no longer thought of as a fundamental property of particles, but the result of a dynamic interaction with a universal field in spacetime, the Higgs field. On a macroscopic scale, the Higgs field is viewed as a simple scalar value at each point in space, which has a value corresponding to the vacuum energy of space. The particles which we observe all obtain their masses from this field via the mechanism of spontaneous symmetry breaking. Though the Higgs particle itself has remained elusive, the predictions of the theories of dynamical mass generation have been very well borne out by experiments.

If matter can be generated by a mechanism of symmetry breaking, as thought to occur in theories of particle physics, then a traceless energy-momentum tensor changes from a liability to a requirement. This would give a gravitational theory added compatibility with the theories of the other fundamental interactions, which is a feature that gravitation has lacked, leading to the development of very complicated superstring theories in higher dimensions to explain how gravitation fits in with all the other forces. A conformal gravitation theory with dynamical mass generation might be a way to make contact with the other forces without taking off into other dimensions.

To provide the energy-momentum tensor for a conformal gravity theory, the fields Ψ and S are introduced to represent a generic fermion field and a symmetry-breaking scalar field respectively [1]. With these fields, the general conformally invariant matter action is given by (following Mannheim [19]):

$$I_M = -\int d^4x\,(-g)^{\frac{1}{2}}\left[\frac{S^\mu S_\mu}{2} + \lambda S^4 - \frac{S^2 R^\mu{}_\mu}{12} + i\bar{\Psi}\gamma^\mu(x)\left[\partial^\mu + \Gamma^\mu(x)\right]\Psi - hS\bar{\Psi}\Psi\right]$$

where $\Gamma^\mu(x)$ represents the fermion spin connection, h and λ are dimensionless coupling constants, and S_μ represents $\frac{dS}{dx^\mu}$, etc. This matter action is the unique choice in this setting that is simultaneously invariant under the conformal transformations $S \rightarrow \Omega^{-1} S, g_{\mu\nu} \rightarrow \Omega^2\, g_{\mu\nu}$.

Analogous to the procedure used to derive the field equations, variation of this action with respect to the fields S and Ψ produces equations of motion for these fields:

$$i\gamma^\mu(x)\left[\partial_\mu + \Gamma_\mu(x)\right]\Psi - hS\Psi = 0, \tag{2.7}$$

$$S^\mu{}_{;\mu} + \frac{SR^\mu{}_\mu}{6} - 4\lambda S^3 + h\bar{\Psi}\Psi = 0, \tag{2.8}$$

[1] In principle multiple particle fields could be used, whereupon the action would have specific factors in the coupling between the particle and scalar fields to maintain conformal invariance.

while the conformal energy-momentum tensor is produced by variation with respect to the metric tensor, taking the form

$$T_{\mu\nu} = i\bar{\Psi}\gamma_\mu(x)\left[\partial_\nu + \Gamma_\nu(x)\right]\Psi + \frac{2S_\mu S_\nu}{3} - \frac{g_{\mu\nu}S^\alpha S_\alpha}{6} - \frac{SS_{\mu;\nu}}{3} + \frac{g_{\mu\nu}SS^\alpha{}_{;\alpha}}{3} - \frac{S^2}{6}\left(R_{\mu\nu} - \frac{g_{\mu\nu}}{2}R^\alpha{}_\alpha\right) - g_{\mu\nu}\lambda S^4. \quad (2.9)$$

As required, this energy-momentum tensor is traceless as befits a system with dynamical mass generation. This is particularly manifest in a system where the scalar field assumes some constant value $S = S_0$, which is the case generally considered in quantum field theory. Then, by substituting using the S field equation (2.8), the energy-momentum tensor would become

$$T_{\mu\nu} = i\bar{\Psi}\gamma_\mu(x)\left[\partial_\nu + \Gamma_\nu(x)\right]\Psi - \frac{g_{\mu\nu}hS_0\bar{\Psi}\Psi}{4} - \frac{S^2}{6}\left(R_{\mu\nu} - \frac{g_{\mu\nu}}{4}R^\alpha{}_\alpha\right).$$

In this form the tracelessness is apparent — raising an index through $g^{\mu\nu}$ will cancel the $\frac{1}{4}$ factors, and use of the Ψ field equation of motion will then cancel the fermion terms. Then, as $W_{\mu\nu} \to \Omega^{-2}W_{\mu\nu}$, and $T_{\mu\nu}$ must transform in the same way for the field equations to be invariant, the trace of the energy-momentum tensor must transform according to $T^\mu{}_\mu \to \Omega^{-4}T^\mu{}_\mu$. If a conformal transformation Ω is used to take the S field to a non-constant value, the trace remains zero under this transformation.

The scalar field produces a mass scale for the fermion field. According to the fermion equation of motion (2.7), the particle acquires a mass hS from interaction with the scalar field. It is thus important that the scalar field should not vanish, as if this were to occur the fermions would all become massless. This occurrence is held in check by the spontaneous symmetry breaking mechanism present in the matter action — in a ground state region where no excitations of the field were occurring, the spontaneous symmetry breaking should maintain a non-vanishing expectation value of the scalar field.

2.2.1 Conformal Hydrostatic Equilibrium

In addition to being traceless, the energy-momentum tensor must also be covariantly conserved, as in standard gravitational theory. The requirement that $T^{\mu\nu}{}_{;\nu} = 0$ produces a conformal analogue of the standard hydrostatic equilibrium equation, which has the additional feature of reducing to the S field equation exterior to the material source, where the fermion field Ψ vanishes.

In order to produce a hydrostatic equilibrium equation in terms of familiar quantities, some method of identifying the fermion field terms with the more usual physical properties of pressure and density must be found. The procedure described in the literature ([30, 19]) is to quantize the fermion part of the energy-momentum tensor into plane wave eigenstates, which are then incoherently averaged over the component directions to produce perfect fluid expressions for the fermion terms. This is carried out in a constant scalar field gauge, but the most relevant parts are not in fact affected by this, as the fermion terms in the basic energy-momentum tensor do not include the scalar field (2.9). Interaction terms are only introduced by substitution from the equations of motion. The fermion kinetic energy term produces a standard perfect fluid expression, just as used in standard gravitational theory (letting $\hbar = c = 1$):

$$i\bar{\Psi}\gamma^{\mu}\left(x\right)\left[\partial^{\nu}+\Gamma^{\nu}\left(x\right)\right]\Psi\rightarrow\left(\rho_{0}+p_{0}\right)U_{\mu}U_{\nu}+p_{0}g_{\mu\nu} \tag{2.10}$$

where the density and pressure here have the subscript $_0$ as an indication of their derivation in a constant scalar field, which can later be dropped. The interaction term produces another perfect fluid term, which in the constant scalar field gauge is fixed by the requirement that the energy-momentum tensor be traceless. This results in it taking the form

$$-g_{\mu\nu}\frac{hS_{0}\bar{\Psi}\Psi}{4}\rightarrow-g_{\mu\nu}\frac{3p_{0}-\rho_{0}}{4}.$$

This term has no counterpart in standard gravitation, and as it is only introduced in conformal theories through substitutions into the energy-momentum tensor from the equations of motion, it is not necessary that such terms should be manifest. The important result to be utilised is the ability to identify the general fermion kinetic term with a standard perfect fluid, something we have familiarity with from standard treatments of general relativity.

To derive the conformal hydrostatic equilibrium equation, we start from covariant conservation of the energy-momentum tensor:

$$T^{\mu\nu}{}_{;\nu}=\left(\begin{array}{c} i\bar{\Psi}\gamma^{\mu}\left(x\right)\left[\partial^{\nu}+\Gamma^{\nu}\left(x\right)\right]\Psi+\frac{2S^{\mu}S^{\nu}}{3}-\frac{g^{\mu\nu}S^{\alpha}S_{\alpha}}{6}-\frac{SS^{\mu;\nu}}{3}+\frac{g^{\mu\nu}SS^{\alpha}{}_{;\alpha}}{3}\\ -\frac{S^{2}}{6}\left(R^{\mu\nu}-\frac{g^{\mu\nu}}{2}R^{\alpha}{}_{\alpha}\right)-g^{\mu\nu}\lambda S^{4} \end{array}\right)_{;\nu}.$$

We now make use of an identity of covariant derivatives [19] , the derivation of which is presented in the appendices —

$$S^{\mu}\left(S^{\alpha}{}_{;\alpha}+\frac{SR^{\alpha}{}_{\alpha}}{6}-4\lambda S^{3}\right)=\left(\begin{array}{c} \frac{2S^{\mu}S^{\nu}}{3}-\frac{g^{\mu\nu}S^{\alpha}S_{\alpha}}{6}-\frac{SS^{\mu;\nu}}{3}+\frac{g^{\mu\nu}SS^{\alpha}{}_{;\alpha}}{3}\\ -\frac{S^{2}}{6}\left(R^{\mu\nu}-\frac{g^{\mu\nu}}{2}R^{\alpha}{}_{\alpha}\right)-g^{\mu\nu}\lambda S^{4} \end{array}\right)_{;\nu}.$$

This substitution reduces the scalar field dependant terms to those present in the S field equation of motion. We can then substitute using these equations (2.7,2.8) to obtain

$$\begin{aligned}
\left(i\bar{\Psi}\gamma^{\mu}(x)\left[\partial^{\nu}+\Gamma^{\nu}(x)\right]\Psi\right)_{;\nu}+S^{\mu}\left(-h\bar{\Psi}\Psi\right) &= 0,\\
\left(i\bar{\Psi}\gamma^{\mu}(x)\left[\partial^{\nu}+\Gamma^{\nu}(x)\right]\Psi\right)_{;\nu}+\frac{S^{\mu}}{S}\left(i\bar{\Psi}\gamma^{\mu}(x)\left[\partial_{\mu}+\Gamma_{\mu}(x)\right]\Psi\right) &= 0,\\
\left(i\bar{\Psi}\gamma^{\mu}(x)\left[\partial^{\nu}+\Gamma^{\nu}(x)\right]\Psi\right)_{;\nu}+\frac{S^{\mu}}{S}\left(g_{\mu\nu}i\bar{\Psi}\gamma^{\mu}(x)\left[\partial^{\nu}+\Gamma^{\nu}(x)\right]\Psi\right) &= 0,\\
\left(i\bar{\Psi}\gamma^{\mu}(x)\left[\partial^{\nu}+\Gamma^{\nu}(x)\right]\Psi\right)_{;\nu}+\frac{S_{\nu}}{S}\left(i\bar{\Psi}\gamma^{\mu}(x)\left[\partial^{\nu}+\Gamma^{\nu}(x)\right]\Psi\right) &= 0,
\end{aligned}$$

which can be written in the compact form

$$\left(\frac{i\bar{\Psi}\gamma^{\mu}(x)\left[\partial^{\nu}+\Gamma^{\nu}(x)\right]\Psi}{S}\right)_{;\nu}=0.$$

If we can then utilise the above result that the fermion field part can be represented by a standard perfect fluid form, we obtain:

$$\frac{\left(\left(\rho+p\right)U^{\mu}U^{\nu}+pg^{\mu\nu}\right)_{;\nu}}{g_{\mu\nu}\left(\left(\rho+p\right)U^{\mu}U^{\nu}+pg^{\mu\nu}\right)}=\frac{S^{\mu}}{S},$$

reducing the generic fermion field density to more usual matter density and pressure. We can now appeal to standard treatments of hydrostatic equilibrium in perfect fluids [24], utilising the definitions

$$U^{0}=\left(-g_{00}\right)^{-\frac{1}{2}},U^{1..3}=0,g_{\mu\nu}U^{\mu}U^{\nu}=-1$$

to obtain the results

$$\begin{aligned}
\left(\left(\rho+p\right)U^{\mu}U^{\nu}+pg^{\mu\nu}\right)_{;\nu} &\rightarrow p'+\frac{1}{2}\frac{b'}{b}\left(\rho+p\right)\\
g_{\mu\nu}\left(\left(\rho+p\right)U^{\mu}U^{\nu}+pg^{\mu\nu}\right) &\rightarrow 3p-\rho\\
\frac{S^{\mu}}{S} &= \frac{p'+\frac{1}{2}\frac{b'}{b}\left(\rho+p\right)}{3p-\rho}\\
\frac{bS'}{S} &\approx -\frac{p'}{\rho}-\frac{1}{2}\frac{b'}{b}
\end{aligned}\tag{2.11}$$

where $'$ indicates the derivative with respect to radius and in the final step we have assumed $|p|\ll|\rho|$.

This result should be compared to the standard result

$$p'+(\rho+p)\frac{1}{2}\frac{b'}{b}=0.$$

If the scalar field were to take a constant value then the standard result is retrieved exactly, otherwise there is some deviation caused by the structure of the scalar field. This can be qualitatively understood quite well, if the fermion is to acquire a mass hS via it's equation of motion (2.7), then if this is allowed to vary through S we can expect some differences due to pressure and density not obtaining their standard values. That a variation of this kind could occur in the interior of a star is difficult to prove or disprove, as we have no way of measuring the mass of a particle within a stellar body.

The analogous result in the $\bar{a}, \bar{b}$ metric is found to be

$$\frac{S'}{S} \approx -\frac{p'}{\rho} - \frac{1}{2}\frac{\bar{b}'}{\bar{b}} - \frac{\bar{a}'}{\bar{a}}. \tag{2.12}$$

In this case, the conformal scaling field $\bar{a}$ could potentially be just as significant in producing gradients in the scalar field S as the field $\bar{b}$, or equivalently the conformal scaling could have just as significant effect perturbing the standard pressure and density as variations in the scalar field. This equation also suggests some degree of a reciprocating relationship between the $\bar{a}$ and S fields.

With this relationship in hand, it remains to find some appropriate data to apply it to. If information about the pressure, density and metric field b can be approximated, the ratio S'/S can be produced. Exterior to the source, the equations can generally be scaled such that $S = 1$ at the edge of the source, thus this relation provides enough information to start some of the numerical techniques.

2.2.2 Interior and Exterior Quadrature Solution

As noted earlier, interior solutions have been presented in the literature in a quadrature form. The source terms for these expressions are not explicitly given, but expressed as a generic source function $f(r)$, which is presumed to be zero exterior to the source body. These expression are also derived from a line element where $a = b^{-1}$.

It is easily possible to present this quadrature solution with a conformal line element using the metric coefficients $\bar{a}, \bar{b}$. In addition, a source expression can be produced using the scalar field $T^{\mu\nu}$ given above (2.9). This procedure produces the equations

$$W^0{}_0 - W^1{}_1 = \frac{\bar{b}}{3\bar{a}^4}\frac{\left(r\bar{b}\right)''''}{r} = \frac{\bar{b}}{3\bar{a}^4}\nabla^4\bar{b}$$

$$
\begin{aligned}
&= \frac{1}{4\alpha}\left(T^0{}_0 - T^1{}_1\right) \\
&= \frac{1}{4\alpha}\left(-(\rho+p) + \frac{\bar{b}}{\bar{a}^3}\left(\frac{SS''}{\bar{a}} - \frac{2(S')^2}{\bar{a}} - \frac{2\bar{a}'SS'}{\bar{a}} + \bar{a}''S^2 - \frac{2(\bar{a}')^2 S^2}{\bar{a}}\right)\right),
\end{aligned}
$$

where the generic fermion field Ψ has been cast in terms of the usual perfect fluid pressure and density, using the relationships presented above (2.10). Interior to the source body, it would be expected that the pressure and density terms would dominate to a very large degree, resulting in something with similar characteristics to the standard formulation. However, we now also have exterior source terms that will be nonzero if the a or S fields have gradients. This would mean that the quadrature solution of this fourth-order Poisson equation would differ from that presented in [14], in that in the exterior region there would still be source terms exterior to the point of integration. This is a possibility that was described in passing to generate particular solutions of the differential equation containing constant and quadratic terms, in addition to the usual inverse linear term and a linear term, but these were considered uninteresting to the cases being considered. If the source terms extend beyond the usual physical boundary of the body, these terms could well have more significance.

Taking the extended nature of the source into account, an expression for the quadrature solution with the possibility of source exterior to the body concerned would be given by

$$
\begin{aligned}
\bar{b}(r<R) &= -\frac{1}{6}\int_0^r f(r')\left[3r'^2 r + r'^4/r\right]dr' \\
&\quad -\frac{1}{6}\int_r^R f(r')\left[3r'^3 + r'r^2\right]dr' \\
&\quad -\frac{1}{6}\int_R^\infty g(r')\left[3r'^3 + r'r^2\right]dr'
\end{aligned} \tag{2.13}
$$

$$
\begin{aligned}
\bar{b}(r>R) &= -\frac{1}{6}\int_0^R f(r')\left[3r'^2 r + r'^4/r\right]dr' \\
&\quad -\frac{1}{6}\int_R^r g(r')\left[3r'^2 r + r'^4/r\right]dr' \\
&\quad -\frac{1}{6}\int_r^\infty g(r')\left[3r'^3 + r'r^2\right]dr'
\end{aligned} \tag{2.14}
$$

where the source functions are defined from

$$
\begin{aligned}
f(r') &= \frac{1}{4\alpha}\left(-(\rho+p) + \frac{\bar{b}}{\bar{a}^3}\left(\frac{SS''}{\bar{a}} - \frac{2(S')}{\bar{a}} - \frac{2\bar{a}'SS'}{\bar{a}} + \bar{a}''S^2 - \frac{2(\bar{a}')^2 S^2}{\bar{a}}\right)\right) \\
&\approx -\frac{1}{4\alpha}(\rho+p), \\
g(r') &= \frac{1}{4\alpha}\left(\frac{\bar{b}}{\bar{a}^3}\left(\frac{SS''}{\bar{a}} - \frac{2(S')}{\bar{a}} - \frac{2\bar{a}'SS'}{\bar{a}} + \bar{a}''S^2 - \frac{2(\bar{a}')^2 S^2}{\bar{a}}\right)\right).
\end{aligned}
$$

Here we have split the source into two sectors, one dealing with the source interior to the body and another dealing with the source due to the scalar field and conformal scale gradients outside the source. In addition to this particular solution of the fourth-order Poisson equation, there can also be an additive homogeneous solution given by $b_h(r) = k_1 + \frac{k_2}{r} + k_3 r + k_4 r^2$. The value of the constants in this homogeneous contribution would have to be determined from the boundary conditions of the system.

Note, however, that the solution from this quadrature expression is not necessarily a solution of the original field equations from which it was constructed. A linear combination of two equations is not necessarily in itself going to have a solution which also solves the original equations without further constraints. For example, an exterior solution for the homogeneous radial field equation has already been found. By necessity, the solution of the fourth order Poisson equation has one more constant of integration than the third order equation $W^{rr} = 0$, i.e. a general solution of $\nabla^4 \bar{b} = 0$ would be

$$\bar{b}(r) = k_1 + \frac{k_2}{r} + k_3 r + k_4 r^2.$$

Substituting this solution of the homogeneous equation $\nabla^4 \bar{b} = 0$ into the homogeneous field equation $W^{rr} = 0$ results in the constraint

$$3k_2 k_3 - {k_1}^2 + 1 = 0. \tag{2.15}$$

That is, any solution of $\nabla^4 \bar{b} = 0$ is a solution of the radial field equation only when this constraint holds. The solution of the field equations is a solution of this combination of field equations, but not necessarily the other way around. It is not easy to establish if any similar constraint can be written for the particular solutions of the non-homogeneous equation $\nabla^4 \bar{b} = \frac{3\bar{a}^4}{4\alpha b}\left({T^0}_0 - {T^1}_1\right)$, so this constraint is only useful for putting bounds on any homogeneous contribution to the solution for $\bar{b}(r)$. It is because of this kind of ambiguity that solutions for $\bar{b}$ using these quadrature integrals have not been pursued, other than to investigate their own behaviour.

Chapter 3

Conformal Geodesic Motion

In addition to the analytic solutions to the field equations mentioned above, other important relationships can also be provided analytically. These other relationships are used to determine whether the predictions of the theory are compatible with the observations being made of the motions of bodies in the solar system. The field equations themselves tend to be in terms of quantities that are not themselves directly observable (such as the metric coefficients a, b and the scalar field S) or where exact measurement of the quantities is difficult (such as pressure and density interior to the source). The observable quantities we are concerned with are those used to test general relativity — the motion of orbiting bodies and the deflection of photons by gravitational action. The form of the relations describing these effects is similar to that used in general relativity, but generally more complex due to the additional field present. Despite this, the relations can sometimes be reduced to forms that mimic the GR relations but with additional terms or multipliers that show the deviation caused by use of the conformal theory. By studying these relations, we can find useful insights into how the conformal gravity theory will differ from general relativity — specifically, how much the addition of a dynamical mass generation mechanism and use of fourth order equations will affect the apparent observational successes of currently accepted general relativity.

3.1 Dynamical Geodesic Equations

The effects of gravitation, under whatever model, are described in terms of observable quantities by the equations of geodesic motion. These can be used to produce other equations dealing with the deflection of light by gravity, or to produce orbital equations. Only minor modifications to the standard methods are required to encompass the effects of dynamical mass generation.

In the standard discussion of particle motion, as used for kinematic particles, we find the path a test particle takes by producing an action integral for the movement along all paths between two points in spacetime. The geodesic is defined as the stationary path found from the variation of the action integral

$$I_T = -m \int d\tau \tag{3.1}$$

over all paths $x^\lambda(\tau)$ — that is, particles take the shortest path. In flat spacetime this would be a straight line, in general relativity we have the result that spacetime is curved and the shortest path between two points is not always straight.

The energy-momentum tensor corresponding to this action is given by

$$T^{\mu\nu} = \frac{2}{(-g)^{\frac{1}{2}}} \frac{\delta I_T}{\delta g_{\mu\nu}} = \frac{m}{(-g)^{\frac{1}{2}}} \int d\tau \delta^4 (x - y(\tau)) \frac{dy^\mu}{d\tau} \frac{dy^\nu}{d\tau},$$

an analogous process to the derivation of the energy-momentum tensors given above. We then use the result that the energy momentum tensor is covariantly conserved to produce the standard equation of geodesic motion :

$$\frac{d^2x^\lambda}{d\tau^2} + \Gamma^\lambda{}_{\mu\nu} \frac{dx^\mu}{d\tau} \frac{dx^\nu}{d\tau} = 0.$$

(The validity of these standard derivations is discussed in, for example, reference [19]).

Suppose, however, that the particles we are considering obtain their masses by a dynamical process, as introduced above. The particle masses are given from the fermion field equation of motion to be

$$m = hS. \tag{3.2}$$

As we have dynamical mass generation by a symmetry-breaking scalar field $S(x)$, in general the possible variations of $S(x)$ would lead to the masses of the particles having some spacetime dependance, which must be incorporated into the action. What we are seeing here is an additional effect on the motion, that not only does a particle prefer to take the shortest path, but it also prefers to travel along the path that minimises it's effective mass.

Accordingly, substituting (3.2) into (3.1), the action integral becomes

$$I_T = -h \int S(x) \, d\tau,$$

where h is the same dimensionless coupling parameter as above (2.7). If it should turn out that S has a universal constant value then this would just reduce to

the standard action integral. Variation of this action with respect to the possible paths $x^{\lambda}(\tau)$ then leads to the following expression for the stationary trajectory:

$$\frac{d^2x^{\lambda}}{d\tau^2} + \Gamma^{\lambda}{}_{\mu\nu}\frac{dx^{\mu}}{d\tau}\frac{dx^{\nu}}{d\tau} = -\frac{S_{\mu}}{S}\left(g^{\lambda\mu} + \frac{dx^{\lambda}}{d\tau}\frac{dx^{\mu}}{d\tau}\right),$$

a trajectory which can be shown to be conformally invariant.

The departure from motion under the standard geodesic equation can be seen to be drawn from the presence of a non-zero right hand side to this equation, arising from the dynamical mass generation mechanism. If the scalar field were a constant then again, standard geodesic motion is retrieved. If it is not, then the particle propagates with a variable mass, in a way which effects the trajectory. As it is only the final motion of the particles, encompassing all these effects, that is the actual quantity which is observed, the extraction of which components of the motion are due to geometric effects and which related to dynamical mass generation with variable mass is difficult.

In fact, it is a feature that has been exploited in the literature that by a certain (unspecified) conformal transformation, it would be possible to reduce the scalar field to a (non-zero) constant everywhere. This would put all of the motion into the structure of the metric coefficients, which would have changes reciprocal to those in S to maintain the observed trajectory. However, we wish to compare the motion of particles predicted by such a theory to that observed for objects within our solar system, where the form of the metric coefficients is thought to be well known. To this end, it is most convenient to leave structure in the scalar field to allow it to represent deviations from the expected geodesic motion of the purely geometrically based theory used in currently accepted general relativity theory, so that the additional effects we are looking for can be extracted out and investigated in their own right.

This property, that the effects governing the geodesic motion of particles can be shuttled backwards and forwards between the geometry and the mass generation mechanism could be thought of as a manifestation of the symmetry involved. In this case, the physics that is invariant of the conformal transformation is the geodesic path that the particles travel along. By different conformal transformations, coordinate systems with varying scalar fields could be set up, with correspondingly different metric coefficients to maintain the observed geodesic.

3.1.1 Coordinate Forms of the Geodesic Equations

Proper Accelerations of Particles

Using a line element in the standard form (following Weinberg [24]), and the geodesic equations given above, the most simple quantity to produce that is related to the motion of particles is the proper acceleration. The form of the resultant expression is most suitable for determining what extra accelerative effects over those present in general relativity are introduced by the presence of a scalar field. It is not so obvious how proper accelerations relate to the observed, coordinate accelerations but in the coordinate form the separation of the metric related and scalar field related effects becomes less distinct.

Starting from the line element

$$d\tau^2 = c^2 b dt^2 - a dr^2 - r^2\left(d\theta^2 + \sin^2\theta d\phi^2\right) \tag{3.3}$$

and divide by $d\tau^2$

$$1 = c^2 b\dot{t}^2 - a\dot{r}^2 - r^2\left(\dot{\theta}^2 + \sin^2\theta\dot{\phi}^2\right)$$

where $\dot{\text{t}}$ represents $\frac{dt}{d\tau}$ etc. Assuming planar symmetry, restrict the motion to the $\pi/2$ plane :

$$1 = c^2 b\dot{t}^2 - a\dot{r}^2 - r^2\dot{\phi}^2.$$

Now appeal to the geodesic equations. Looking first at the equation for the case $\lambda = t$:

$$\begin{aligned} c\ddot{t} + \frac{b'}{b}c\dot{t}\dot{r} &= -\frac{S'}{S}c\dot{t}\dot{r} \\ \ddot{t} + \dot{t}\left(\frac{\dot{b}}{b} + \frac{\dot{S}}{S}\right) &= 0 \end{aligned}$$

using $\frac{dS}{dr}\frac{dr}{d\tau} = \frac{dS}{d\tau}$,etc. This can be written

$$\begin{aligned} \ddot{t} + \frac{\dot{t}}{bS}\frac{d}{d\tau}(bS) &= 0 \\ (bS)\ddot{t} + \dot{t}\frac{d}{d\tau}(bS) &= 0 \\ \frac{d}{d\tau}\left(bS\dot{t}\right) &= 0 \end{aligned}$$

therefore, the quantity $bS\dot{t}$ is a constant in (proper) time and is given the label l. In standard general relativity the analogous result is

$$\frac{d}{d\tau}\left(b\dot{t}\right) = 0, b\dot{t} = l \tag{3.4}$$

for constant l.

Similarly, for the geodesic equation in the case $\lambda = \phi$,

$$\begin{aligned} \ddot{\phi} + \frac{2}{r}\dot{r}\dot{\phi} &= -\frac{S'}{S}\dot{r}\dot{\phi} \\ \ddot{\phi} + \dot{\phi}\left(\frac{2\dot{r}}{r} + \frac{\dot{S}}{S}\right) &= 0 \\ \left(r^2 S\right)\ddot{\phi} + \dot{\phi}\frac{d}{d\tau}\left(r^2 S\right) &= 0 \\ \frac{d}{d\tau}\left(r^2 S\dot{\phi}\right) &= 0 \\ r^2 S\dot{\phi} &= h \end{aligned} \tag{3.5}$$

for constant h. Again, this process is exactly analogous to that in general relativity up to the presence of the factor S. Should it be necessary to refer to the constant terms generated in the dynamical mass and general relativity in the same context, they shall be delineated by the terms h_{CG} and h_{GR} respectively.

Also from this last geodesic equation we obtain the result that

$$\frac{d\dot{\phi}}{dr} = -\dot{\phi}\left(\frac{2}{r} + \frac{S'}{S}\right).$$

It can also be shown that

$$\frac{d\dot{r}}{dr}\dot{r} = \frac{d\dot{r}}{dr}\frac{dr}{d\tau} = \ddot{r}.$$

Armed with these relations, we proceed to substitute into the line element above

$$\begin{aligned} 1 &= c^2\frac{l^2}{bS^2} - a\dot{r}^2 - r^2\dot{\phi}^2 \\ bS^2 &= c^2 l^2 - abS^2\dot{r}^2 - bS^2 r^2\dot{\phi}^2, \end{aligned}$$

then taking derivative with respect to r we obtain

$$\left(bS^2\right)' = -a'bS^2\dot{r}^2 - ab'S^2\dot{r}^2 - 2abSS'\dot{r}^2 - 2abS^2\ddot{r} - b'S^2r^2\dot{\phi}^2 + 2bs^2r\dot{\phi}^2.$$

If we assume that $a = 1/b$ holds to a good approximation in the exterior (as in the Schwarzschild solution) then this would reduce to

$$\begin{aligned} \left(bS^2\right)' &= -2SS'\dot{r}^2 - 2S^2\ddot{r} - b'S^2r^2\dot{\phi}^2 + 2bS^2r\dot{\phi}^2 \\ \ddot{r} &= br\dot{\phi}^2 - \frac{b'}{2} - \frac{b'r^2\dot{\phi}^2}{2} - \frac{S'}{S}\left(b + \dot{r}^2\right) \end{aligned} \tag{3.6}$$

as our expression for proper acceleration for an exterior, near-Schwarzschild environment. The first three terms exactly replicate the equivalent terms from the proper acceleration in a Schwarzschild environment. The additional terms represent the effects of the scalar field, which is producing an additional attractive motion proportional to the gradient in that field. This would match the intuitive picture of particle propagation in a scalar field increasing with radius — as the dynamical mass of a particle increases with radius, it would be preferential for it to move in the opposite sense. So here we see an acceleration in the opposite direction to the scalar field slope.

Performing this derivation in the $\bar{a}, \bar{b}$ metric produces the analogous result:

$$\ddot{r} = \bar{b} r \dot{\phi}^2 - \frac{\bar{b}'}{2\bar{a}^2} - \frac{\bar{b}' r^2 \dot{\phi}^2}{2} - \frac{S'}{S}\left(\frac{\bar{b}}{\bar{a}^2} + \dot{r}^2\right) - 2\frac{\bar{a}'}{\bar{a}}\left(\frac{\bar{b}}{\bar{a}^2} + \dot{r}^2\right).$$

Coordinate Acceleration

The proper acceleration is a very interesting object theoretically, and can be used to predict what kinds of effects will be observed. However, it is more appropriate to compare observed motions to the coordinate acceleration predicted from these equations. The derivation of a coordinate acceleration for a dynamical mass model is similar to that above. Starting from the line element, we isolate and substitute for $\dot{t}$ using the identity above:

$$\begin{aligned} \frac{b^2 S^2}{l^2} &= bc^2 - a\left(\frac{dr}{dt}\right)^2 - r^2\left(\frac{d\phi}{dt}\right)^2, \\ \frac{1}{l^2} &= \frac{c^2}{bS^2} - \frac{a}{b^2 S^2}\left(\frac{dr}{dt}\right)^2 - \frac{r^2}{b^2 S^2}\left(\frac{d\phi}{dt}\right)^2 \end{aligned}$$

where we have used relations of the form $\frac{dr}{d\tau}\frac{d\tau}{dt} = \frac{dr}{dt}$. Take the derivative with respect to time t, giving the expression

$$\begin{aligned} 0 = & -c^2\left(\frac{1}{b^2 S^2}\frac{db}{dt} - \frac{2}{bS^3}\frac{ds}{dt}\right) \\ & - \left(\left(\frac{1}{b^2 S^2}\frac{da}{dt} - \frac{2a}{b^3 S^2}\frac{db}{dt} - \frac{2a}{b^2 S^3}\frac{dS}{dt}\right)\left(\frac{dr}{dt}\right)^2 + \frac{2a}{b^2 S^2}\frac{dr}{dt}\frac{d^2 r}{dt^2}\right) \\ & - \left(\left(\frac{2r}{b^2 S^2}\frac{dr}{dt} - \frac{2r^2}{b^3 S^2}\frac{db}{dt} - \frac{2r^2}{b^2 S^3}\frac{dS}{dt}\right)\left(\frac{d\phi}{dt}\right)^2 + \frac{2r^2}{b^2 S^2}\frac{d\phi}{dt}\frac{d^2\phi}{dt^2}\right). \end{aligned}$$

Isolating the coordinate acceleration, we find

$$\frac{d^2 r}{dt^2} = -\frac{c^2 b'}{2a} - \frac{c^2 b S'}{aS} - \left(\frac{dr}{dt}\right)^2\left(\frac{a'}{2a} - \frac{b'}{b} - \frac{S'}{S}\right)$$

$$-\left(\frac{d\phi}{dt}\right)^2\left(\frac{r}{a}-\frac{r^2}{a}\frac{b'}{b}-\frac{r^2}{a}\frac{S'}{S}\right)-\frac{r^2\phi'}{a}\frac{d^2\phi}{dt^2} \tag{3.7}$$

where we have used relations of the form $\frac{db}{dt}\frac{dt}{dr}=\frac{db}{dr}$, etc. This expression reduces to it's general relativistic counterpart by letting S take a constant value.

Orbit Equation

Starting from the line element (3.3) again, substitute using the constants described above to get

$$\begin{aligned} 1 &= \frac{c^2l^2}{bS^2}-a\dot{r}^2-\frac{h^2}{r^2S^2}, \\ bS^2 &= c^2l^2-abS^2\dot{r}^2-\frac{bh^2}{r^2}, \end{aligned}$$

then, by rearranging the angular constant expression we find

$$\begin{aligned} \dot{\phi} &= \frac{d\phi}{d\tau}=\frac{d\phi}{dr}\frac{dr}{d\tau}=\frac{h}{r^2S}, \\ \dot{r} &= \frac{dr}{d\tau}=\frac{h}{r^2S}\frac{dr}{d\phi}. \end{aligned}$$

Substituting this in, we find

$$bS^2=c^2l^2-ab\frac{h^2}{r^4}\left(\frac{dr}{d\phi}\right)^2-\frac{bh^2}{r^2}.$$

Change radial variable r to inverse radius u, with the accompanying change in the derivative $\frac{dr}{d\phi}=-\frac{1}{u^2}\frac{du}{d\phi}$:

$$bS^2=c^2l^2-abh^2\left(\frac{du}{d\phi}\right)^2-bh^2u^2$$

and differentiate with respect to ϕ. We then obtain

$$\begin{aligned} S^2\frac{db}{d\phi}+2bS\frac{dS}{d\phi} &= -h^2\left(\left(\frac{du}{d\phi}\right)^2\left(\frac{da}{d\phi}b+a\frac{db}{d\phi}\right)+2ab\frac{du}{d\phi}\frac{d^2u}{d\phi^2}+2bu\frac{du}{d\phi}+u^2\frac{db}{d\phi}\right), \\ \frac{du}{d\phi}\left(S^2\frac{db}{du}+2bS\frac{dS}{du}\right) &= -h^2\frac{du}{d\phi}\left(\left(\frac{du}{d\phi}\right)^2\left(\frac{da}{du}b+a\frac{db}{du}\right)+2ab\frac{d^2u}{d\phi^2}+2bu+u^2\frac{db}{du}\right). \end{aligned}$$

For motion that is non-circular, $\frac{du}{d\phi}\neq 0$. We can then rearrange to solve for $\frac{d^2u}{d\phi^2}$, obtaining the relation

$$\frac{d^2u}{d\phi^2}=-\frac{\left(\left(\frac{du}{d\phi}\right)^2\left(\frac{da}{du}b+a\frac{db}{du}\right)+2bu+u^2\frac{db}{du}\right)}{2ab}-\frac{S^2}{2abh^2}\frac{db}{du}-\frac{S}{ah^2}\frac{ds}{du}. \tag{3.8}$$

The exterior, general relativity limit of this equation would be to let $a = b^{-1}, S = 1$ everywhere (any other constant value of S would be merely redefining the scale of the constant h). In this case, the equation reduces to

$$\frac{d^2u}{d\phi^2} = -\frac{\left(2bu + u^2\frac{db}{du}\right)}{2} - \frac{1}{2h^2}\frac{db}{du}.$$

Substituting the Schwarzschild expression $b(r) = 1 - 2mu$ retrieves the standard result

$$\frac{d^2u}{d\phi^2} = -u + 3mu^2 + \frac{m}{h^2}. \tag{3.9}$$

This result can also be derived in the $\bar{a}, \bar{b}$ conformal metric:

$$1 = c^2\bar{a}^2\bar{b}\dot{t}^2 - \frac{\bar{a}^2}{\bar{b}}\dot{r}^2 - \bar{a}^2r^2\dot{\phi}^2.$$

Substituting for the proper derivatives using the geodesic equations, analogous to those above

$$\begin{aligned}
\dot{\phi} &= \frac{d\phi}{d\tau} = \frac{h}{\bar{a}^2Sr^2}, \\
\dot{t} &= \frac{dt}{d\tau} = \frac{l}{\bar{a}^2\bar{b}S}, \\
1 &= \frac{c^2l^2}{\bar{a}^2\bar{b}S} - \left(\frac{dr}{d\phi}\right)^2\frac{h^2}{\bar{a}^2\bar{b}S^2r^4} - \frac{h^2}{r^2S^2}.
\end{aligned}$$

Solve for $\frac{dr}{d\phi}$ to obtain

$$\left(\frac{dr}{d\phi}\right)^2\frac{1}{r^4} = \frac{c^2l^2}{h^2} - \frac{\bar{b}}{r^2} - \frac{\bar{a}^2\bar{b}S^2}{h^2},$$

and change variables to inverse radius u :

$$\left(\frac{du}{d\phi}\right)^2 = \frac{c^2l^2}{h^2} - \bar{b}u^2 - \frac{\bar{a}^2\bar{b}S^2}{h^2}.$$

Differentiate with respect to ϕ and obtain

$$2\frac{du}{d\phi}\frac{d^2u}{d\phi^2} = -\frac{d\bar{b}}{d\phi}u^2 - 2\bar{b}u\frac{du}{d\phi} - \frac{1}{h^2}\left(2\bar{a}\bar{b}S^2\frac{d\bar{a}}{d\phi} + \bar{a}^2S^2\frac{d\bar{b}}{d\phi} + 2\bar{a}^2\bar{b}S\frac{dS}{d\phi}\right),$$

which for $\frac{du}{d\phi} \neq 0$ gives

$$\frac{d^2u}{d\phi^2} = -\frac{d\bar{b}}{du}\frac{u^2}{2} - \bar{b}u - \frac{1}{h^2}\left(\bar{a}\bar{b}S^2\frac{d\bar{a}}{du} + \frac{\bar{a}^2S^2}{2}\frac{d\bar{b}}{du} + \bar{a}^2\bar{b}S\frac{dS}{du}\right). \tag{3.10}$$

In this case, the reduction to GR would be by setting $\bar{a} = 1, S = 1$ which returns the GR expression exactly.

3.2 Application to Particle Motion

3.2.1 Features

In deciding to investigate the fourth-order conformal gravity theory, there were a number of motivations. Some of these came from the potential uses of the theory to match observations of large-scale phenomena more accurately from first principles (as opposed to using *ad hoc* theories of dark matter), or to potentially resolve issues to do with cosmological constants and inflation [31]. The theory is also intrinsically attractive due to the additional symmetry it contains. However, in order to be usefully employed and tested, the theory has to be applied to local phenomena for which we have obtained confident measurements.

To be successfully applied on local (solar system) scales, the conformal gravity theory must produce predictions of particle (or any body) motions that match those observed, at least as well as the currently accepted theories. This means that any extra effects must be limited to within the accuracy of our current measurements of particle motion, or be actually desirable effects to account for anomalies in the observations. The effects of the conformal gravity theory should also be seen to extend to reasonable large-scale limits, preferably including any desirable features of this theory on those scales.

The observations we are trying to match are generally those of orbiting bodies. Most important to match among these are the orbital motions of the planets, of which we have reasonably accurate (and ever increasingly so) observations, at least for the inner planets which have been well observed for multiple orbits. In addition, the orbital motion of space probes has to be matched, and in this case we can have particularly continuous and accurate data. However, the usefulness of data from space probes is very particular to the spacecraft in question, as the geodesic motion of the body is obscured if the craft is itself changing its orbit by use of corrective thrusters.

At a first level, the predictions of conformal gravity theory should well approximate those of Keplerian orbits. Given the form of the exterior solution without source for the conformal field equations (2.3), provided the extra constants of the theory are small enough there should be good agreement on this scale. This is completely analogous to the treatment of general relativity.

The next level of the predictions would be to see how they compare to the predictions of general relativity itself. General relativity provided the solution to a slight, but noticeable anomaly in the Newtonian prediction of the motion of the

inner planets. It was found the orbits of the planets precess, such that the point of closest approach to the sun moves around the sun slowly over time. This effect is most noticeable for the planet Mercury, closest to the sun and having the shortest orbital period. This effect cannot be explained by Newtonian gravity theory, but was well modelled in general relativity. Such an effect must be reproduced by conformal gravity theory if it is to be a reasonable model of gravitation.

Another prediction of general relativity was the deflection of light by gravitational fields. This was predicted by Einstein and subsequently observed during eclipses, when light just at the edge of the sun could be observed. Light at the edge of the sun would experience the greatest deflection by gravity that we could observe. Again, this was a feature absent from Newtonian gravitation (as light has no mass, it does not experience gravity in Newtonian physics), and it's prediction and verification was one of the major supporting events leading to the acceptance of general relativity theory.

Essentially, this means that the first thing that conformal gravity must do is replicate the results of general relativity, to within the uncertainty in the measurements. Additional desirable features of conformal theory should not have effects that disrupt these results. However, we also want conformal gravity to have certain differences on larger scales, so some precursors of these effects should be present on local scales. The differences on large scales are not such a restriction as the uncertainty in the measurements is of a different character — if dark matter is not observed, and conformal gravity produces effects reproducing observation without it, then discrepancies from GR in this respect are not an obstacle.

3.2.2 Usage of the Orbital Equation

The two effects produced in the general relativistic treatment of gravitation mentioned above, that set it apart from prior Newtonian mechanics, can be demonstrated by use of the orbit equation as derived under conformal theory above (3.8). If we take the exterior, general relativistic version of the orbit equation (3.9):

$$\frac{d^2u}{d\phi^2} + u = 3mu^2 + \frac{m}{h^2}$$

we can compare this to the earlier, Newtonian result

$$\frac{d^2u}{d\phi^2} + u = \frac{m}{h^2}$$

which would predict an orbit without precession. If we change the form of the orbit equation

$$\frac{d^2u}{d\phi^2} + u\left(1 - 3mu\right) = \frac{m}{h^2}$$

we see that if $3mu$ is small this corresponds to the Keplerian orbit. This term is largest for small radius (large u), so the largest effect should be noticed in the orbit of Mercury. Taking the observed elements of Mercury's orbit, we find that $3mu = 8.1 \times 10^{-8} \ll 1$. The orbit is very close to Keplerian. It is therefore an appropriate method to solve the orbit equation by successive approximations, given the small perturbation the relativistic effects have on the orbit.

The solution to the Newtonian equation for the orbit is

$$u = u_0\left(1 + e\cos\phi\right)$$

for eccentricity e and $u_0 = \frac{m}{h^2}$. Substituting this solution into the right hand side of the orbit equation (3.9), we obtain

$$\begin{aligned}\frac{d^2u}{d\phi^2} + u - \frac{m}{h^2} &= 3m\left(u_0\left(1 + e\cos\phi\right)\right)^2, \\ &= \frac{3m^3}{h^4} + \frac{6m^3}{h^4}e\cos\phi + \frac{3m^3}{h^4}e^2\cos^2\phi.\end{aligned}$$

As we are considering nearly circular orbits, we drop the term in e^2 compared to the term in e. The solution to this new equation is given by

$$u = \left(\frac{m}{h^2} + \frac{3m^3}{h^4}\right)\left(1 + e\cos\phi\right) + \frac{3m^3}{h^4}e\phi\sin\phi.$$

There is an evident precessional term $\phi\sin\phi$. This term has a secular contribution that grows with the angle traversed, i.e. grows with the number of orbits. As this extra contribution is a small quantity, we can use the relation

$$\cos\phi + \varepsilon\phi\sin\phi \simeq \cos\left(\phi - \varepsilon\phi\right)$$

for the small quantity $\varepsilon = \frac{3m^3e}{h^4}$. This leads to the following form for the orbit

$$u = \frac{m}{h^2}\left(1 + \frac{3m^2}{h^2}\right)\left(1 + e\cos\left(\omega\phi\right)\right)$$

where $\omega = 1 - \varepsilon$ as defined above. If the orbital properties of Mercury are used in this relation, then the resulting precession from this effect comes out to be 42.98 arc seconds/century, which is in good agreement with the extra precession required to match observations to theory, which give a geometric precession

(precession with all effects of the other planets, etc., removed) of 43.1 ± 0.1 arc seconds/century.

The other result, the deflection of starlight grazing the limb of the sun, is well described by the same system of equations. Light travels along 'null' geodesics, for which the line element $ds^2 = -d\tau^2 = 0$. Considering the geodesic equation in the angle ϕ,

$$\dot{\phi} = \frac{d\phi}{d\tau} = \frac{d\phi}{dr}\frac{dr}{d\tau} = \frac{h}{r^2}$$

for Schwarzschild geometry, and since $d\phi \neq 0$, then $h \to \infty$ for photons. This would seem reasonable for particles with zero rest mass. The Schwarzschild orbit equation then reduces to

$$\frac{d^2u}{d\phi^2} + u = 3mu^2,$$

which can again be solved by successive approximations.

First, consider the solution of the homogeneous equation

$$\frac{d^2u}{d\phi^2} + u = 0,$$

which is given by

$$u = u_{\max} \cos\phi$$

where $u_{\max} = 1/R_0$ for a photon trajectory grazing the limb of the sun. Substitute that back into the original equation:

$$\frac{d^2u}{d\phi^2} + u = 3m\frac{\cos^2\phi}{{R_0}^2},$$

which has solution

$$u = \frac{\cos\phi}{R_0} + \frac{m}{{R_0}^2}\left(\cos^2\phi + 2\sin^2\phi\right).$$

Changing to Cartesian coordinates, we can solve for large distances from the sun, and consider the asymptotic angles that the trajectory makes to an x axis along the line between the centre of the sun and the point of closest approach:

$$\begin{aligned} R_0 &= x + \frac{m}{R_0}\frac{(x^2+2y^2)}{(x^2+y^2)^{\frac{1}{2}}}, \\ y &= \mp\frac{R_0}{2m}x \pm \frac{{R_0}^2}{2m} \end{aligned}$$

for large y, leading for a deflection angle δ given by

$$\tan\delta = 4\frac{m}{R_0}$$

or, for small δ

$$\delta = 4\frac{m}{R_0}.$$

Given the solar values $m = 1500\text{m}$, $R_0 = 7 \times 10^8\text{m}$, the deflection observed at the limb of the sun should be about 1.75". Observations of star fields during eclipses, compared to the star fields normally, find the deflection of starlight is well described by such a model. A recent experimental result on this effect [32] found the deflection at optical wavelengths to be 1.66 ± 0.19" in 1973. Deflections of radio waves are a little easier to measure as it is not necessary to wait for an eclipse, and rays of impact parameters closer to the solar 'surface' can be observed. Allowances have to be made for refraction of the rays in the solar corona, but up to this accuracy results from Very Long Baseline Interferometry have verified the predicted deflection to an accuracy of $\theta_{\text{exp}}/\theta_{\text{theory}} = 1.0001 \pm 0.0001$ [33].

3.2.3 Higgs-Dependant Acceleration

Having produced observable effects of general relativity, we now consider - how do these effects compare when we are considering a conformal gravity theory? Naturally, we do not want a 'better' theory to throw out the good features of the theory it is replacing or extending. Ideally, we would like the effects of conformal gravity on the tests of general relativity to produce much the same results, through much the same procedures.

Qualitatively, the conformal theory looks pretty good in this respect. If we have a solution to the conformal field equations like the vacuum solution (2.3), and variation in the scalar field is small, then the orbit equations would have much the same derivation and the values used would also be very similar to the Schwarzschild solution.

This can be made a little more definite by considering that first quantity we produced in our study of particle motion, the proper acceleration:

$$\ddot{r} = br\dot{\phi}^2 - \frac{b'}{2} - \frac{b'r^2\dot{\phi}^2}{2} - \frac{S'}{S}\left(b + \dot{r}^2\right).$$

This expression shows exactly the same effects as observed in general relativity, except with additional terms dependant on the scalar field gradient. So long as the scalar field gradient is not large within the solar system, the results of GR will not be perturbed significantly. Essentially, this would put a bound on the magnitude of the S field gradient — if proper velocities were a quantity that could be easily measured. However, as this is not the case, this relation serves only to

suggest that the dynamics of the scalar field could contribute extra accelerations, and that such must be small on local scales.

Of greater use is the orbit equation in the $\bar{a}, \bar{b}$ metric:

$$\frac{d^2u}{d\phi^2} = -\frac{d\bar{b}}{du}\frac{u^2}{2} - \bar{b}u - \frac{1}{h^2}\left(\bar{a}\bar{b}S^2\frac{d\bar{a}}{du} + \frac{\bar{a}^2S^2}{2}\frac{d\bar{b}}{du} + \bar{a}^2\bar{b}S\frac{dS}{du}\right).$$

This shows the full effect of a conformal metric with the conformal geodesic equations, in the presence of a scalar field. It is very easy to see that the effects of any scalar field gradients, or any effects of the $\bar{a}$ field, are not going to be apparent in the easily observed solar system tests of gravity theories.

To demonstrate this, for the deflection of starlight the vital consideration is that the angular momentum constant h goes to infinity for a photon. When this is the case, the denominator of all the terms involving the $\bar{a}$ and S field gradients contains h^2, so any effects they could have vanish in the case of photons. Similarly, any effects due to the value of the fields (should it be far from the value 1) is lost in the same manner. Once all the $1/h^2$ dependant terms have been discarded, the orbit equation reduces exactly to the Schwarzschild equivalent.

In the case of the precession of orbiting bodies, it should be noted that the secular $\phi \sin \phi$ term is generated by the successive approximation process when the Newtonian solution of the orbit for u is substituted back into the differential equation. In the conformal orbit equation, no additional u dependant terms have been generated, so no additional substitutions of the Newtonian form will be present to produce any additional secular contributions. Any deviations from the orbit produced by the extra conformal contributions will be of the same order as the non-secular general relativistic corrections, which are too small to be observed.

So it would appear that although the geodesic and orbital equations in conformal gravity have differing contributions than those in general relativity, as far as observable effects in the local solar system are concerned the predictions should be much the same for both theories. These are the requirements that concern us most as they are the most accurately measured and best understood effects. The potential for large-scale gravitational differences is there so long as they are very small on solar system scales, but this is an area where the data becomes less certain, as does the understanding of exactly what is being observed and the processes at work. For this study, good agreement with the local observation is the test of usefulness for the conformal gravity theory.

3.2.4 Application to the Possible Anomalous Acceleration of Pioneer Spacecraft, *et. al.*

In late 1998, a paper was published by J D Anderson, *et al.,* in Physical Review Letters [6] that detailed a possible anomaly in the motion of the space probes Pioneer 10 and 11, which was also potentially evident for the sun probe Ulysses. This anomaly was a very small, apparently constant acceleration towards the sun, observed in the outer regions of the solar system from 30-60 AU. This acceleration was detected from the frequency shift observed in the transponder signals from the probes. Much work has been done to determine the source of the anomaly, and to date very many explanations have been put forward, ranging from the obvious physical effects of gas leaks or radiated energy from the power sources, to tidal effects in the transponder equipment, to new physics. As yet all the obvious explanations have largely been discounted, leaving the possibility that some additional gravitational effect may be responsible.

The effect has features that would be attractive to a conformal gravity explanation. Firstly, the effect appears close to constant in the outer solar system where it can be observed. This is not a property that the mechanical explanations would enjoy, but is a property that could arise in the conformal theory either through an explicit linear potential in the exterior solution or a near-constant gradient in the scalar field. Secondly, the effect is very small, such that at closer distances to the sun it is swamped by the usual general relativistic and Newtonian effects. This is also commeasurate with an effect from a scalar field linked to spacetime curvature.

One difficulty with explaining gravitational anomalies of this kind with scalar fields or linearly rising potentials in general would be why similar effects, though larger in scale, are not observed for massive orbiting bodies such as the planets. The anomalous acceleration on Pioneer 10 is found to have a magnitude of $8.1 \times 10^{-10}\text{ms}^{-2}$. The current planetary ranging data for Mars, obtained from the Viking missions [34], would limit any anomalous radial acceleration on Earth or Mars to be no more than $0.1 \times 10^{-10}\text{ms}^{-2}$ [6]. A scalar field coupled to curvature could potentially help address this, as a planet or similar body is not a good approximation to a test particle, and will have it's own effects on the curvature, and thus the scalar field that generates the acceleration. It is conceivable that this kind of self-interaction could mitigate the effect of extra acceleration on massive bodies due to the scalar field.

It may therefore be useful to consider this data as a candidate for a conformal theory explanation — to see if a conformal gravitation theory can explain this observation any better than standard general relativity. In order to reproduce the effect as noted for the Pioneer spacecraft, then an acceleration of order $8 \times 10^{-10}\text{ms}^{-2}$ is required. If this is to be produced from an acceleration due to the background scalar field, then from the coordinate acceleration expression (3.7) the magnitude of the scalar field gradient $\frac{S'}{S}$ would need to be 10^{-26}m^{-1} in the vicinity of 30-60 AU from the sun. This would seem to be an appropriately small value of deviation from general relativity.

If another explanation of the Pioneer acceleration is found to hold, then this data could become a sensitive negative test for conformal gravity in the same way — whatever extra acceleration is generated by the scalar field, it would then have to not exceed this limit. In such a case, the limit for the scalar field gradient would have to be at least an order of magnitude less than the accuracy of this anomalous acceleration, i.e. approximately 10^{-28}m^{-1}.

3.2.5 Analytic S Field Behaviour

Correspondence With an Anomalous Acceleration

As can be seen from the coordinate expression for particle acceleration in a theory with a long-range scalar field (3.7), extra accelerative terms are present over and above those from standard general relativity theory. Conveniently, these extra terms can be isolated completely from the standard results. It is thus a very simple matter to tentatively identify these extra accelerations with any anomalous acceleration of spacecraft, and then see what physical features result for the scalar field and motion of the object.

The scalar field dependant part of the coordinate acceleration expression is

$$\frac{d^2r}{dt^2}_{extra} = -\frac{c^2bS'}{aS} + \left(\frac{dr}{dt}\right)^2\left(\frac{S'}{S}\right) + \left(\frac{d\phi}{dt}\right)^2\left(\frac{r^2}{a}\frac{S'}{S}\right).$$

If we consider an extra acceleration over a vacuum metric field close to Schwarzschild (or equivalently, (2.3) with small γ), and consider particles moving radially and slowly with respect to the speed of light, this expression would reduce to

$$\frac{d^2r}{dt^2}_{extra} = -c^2b^2\frac{d}{dr}\ln(S).$$

By equating the extra acceleration with the possible anomalous acceleration a_{an}, this equation can be solved for the scalar field, giving (letting $\sigma = -\frac{a_{an}}{c^2} \approx$

$1 \times 10^{-26}\mathrm{m}^{-1}$)

$$\begin{aligned} \frac{d}{dr}\ln(S) &= \frac{\sigma}{\left(1-\frac{2\beta}{r}\right)^2}, \\ \ln(S) &= 4\sigma\beta\ln(r-2\beta) - 4\frac{\sigma\beta^2}{(r-2m)} + \sigma r, \\ S &= (r-2m)^{4\sigma\beta}\, e^{\left(\sigma r - \frac{4\sigma\beta^2}{(r-2m)}\right)}. \end{aligned}$$

This solution for the scalar field would result in a scalar field that varies very slowly, with a near constant gradient of order $\sigma \approx 1\times 10^{-26}\mathrm{m}^{-1}$ at 20-60 AU. The scalar field gradient is decreasing on a very extended scale ($S'_{40AU} - S'_{20AU} \approx 1 \times 10^{-10}\mathrm{m}^{-2}$), giving a scalar field that appears to be heading towards an asymptotic limit, but at a very slow rate.

Restricted Analytic Behaviour

The scalar field equation of motion (2.8) is comparatively simple in the context of these conformal field equations, being only second order at most in the fields a, b and S. If certain simplifications are made, it is possible to find analytic solutions that give a reasonable indication of the kind of behaviour that the scalar field exhibits.

As we are expecting that the scalar field will be very close to constant and that the metric will strongly resemble that of the standard theory, we first assume that we can approximate the metric fields by taking their Schwarzschild values. We also assume that the self-coupling constant λ must be very small (this is borne out by later numerical solutions, or can be deduced from relating λ to a cosmological constant [31]), in the limit that λ vanishes the equation of motion reduces to

$$S'' + S'\left(\frac{2\beta}{r^2-2\beta r} + \frac{2}{r}\right) = 0.$$

The solution to this differential equation is easily obtained as

$$S = c_1 \ln\left(1-\frac{2\beta}{r}\right) + c_2. \tag{3.11}$$

The constant c_2 is determined by normalisation of the scalar field, useful options would be normalising to the value that the field takes at infinity i.e. $S_\infty = 1$, or to the value taken at the limb of the sun i.e. $S_R = S_0 = 1$. The latter is

the normalisation generally used for the equations in this work, and produces an expression for the constant c_2 given by

$$c_2 = 1 - c_1 \ln\left(1 - \frac{2\beta}{R}\right).$$

The other constant c_1 requires more information for it's determination, the derivative of the field at a particular point being a particularly convenient choice. The derivative of this analytic solution is given by

$$S' = \frac{2\beta c_1}{r^2 - 2\beta r},$$

thus providing any value of S' at a point immediately specifies c_1 and therefore c_2.

One point that could be provided is a value of the scalar field slope that matches with what would be required to generate an extra acceleration of a magnitude comparable to that as possibly observed for Pioneer 10 and 11. If this data is used, we have the scalar field derivative assuming a value of order 10^{-26} at a range of 40 AU. This information would then give the values $c_1 = 1.20 \times 10^{-4}, c_2 = 1 + 5.14 \times 10^{-10}$ for the constants of integration in the analytic S expression (3.11) above. With these constants, the S field is found to have a value very close to constant and a slope that is very small and decreasing according to an approximately $\frac{1}{r^2}$ relationship (see figures 3.1, 3.2, note that only the first AU is shown for clarity). The scalar field gradient is suitably small and fits the tentative limits at the limb as described earlier (section 2.2.1).

This approximate solution of the scalar field equation of motion shows that the features the scalar field can be expected to have are intuitively reasonable and do not significantly perturb the successes of the results of standard theory. As will be shown later (section 6.1), the approximations used to find this solution, though quite sweeping, are not so extreme as to take the analytic solution of the reduced equation far from the solutions of the full equation. The later numerical solutions of the full equation agree quite well in magnitude and form with this simple analytic solution, and in general the behaviour of the solutions is very similar with only the absolute magnitude of the quantities $(S - 1)$ and S' differing by about 40 percent at the limb of the source. The order of magnitude agrees well but with a slightly different coefficient. This is to be expected as the slope boundary condition applied at 40 AU is in a region where the assumptions hold very well, and cannot be expected to extrapolate perfectly back to the limb regions where any scalar curvature term is likely to be more significant.

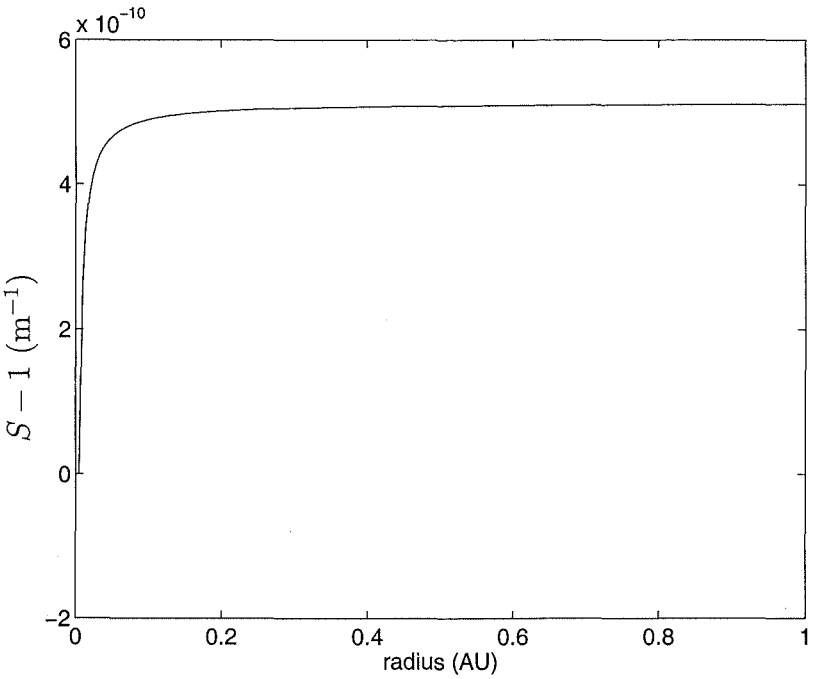

Figure 3.1: Analytic S field solution - $(S-1)$

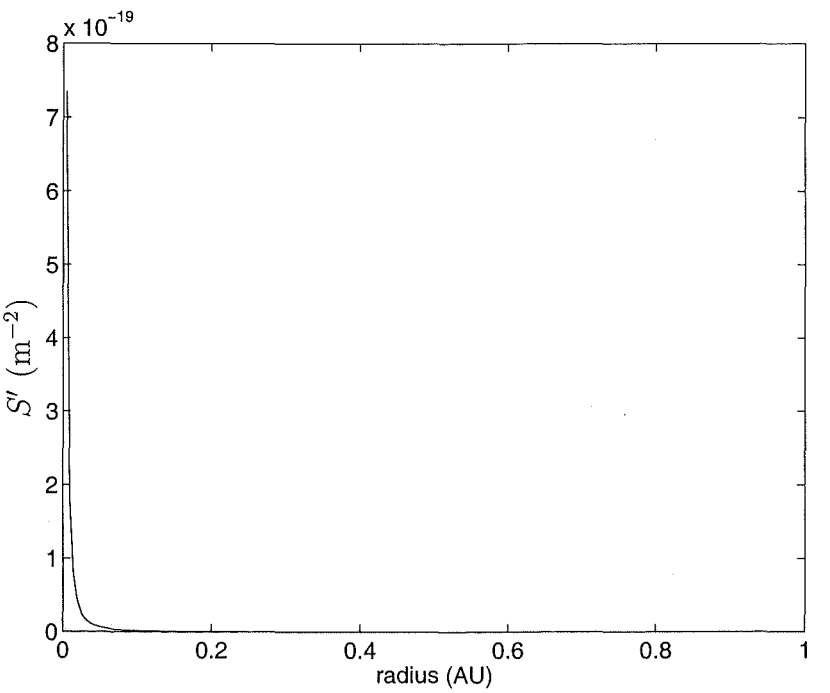

Figure 3.2: Analytic S field solution - S'

The order of magnitude of the scalar field derivative that has been produced is in good accord with what would be required to explain any apparent anomalous acceleration of the Pioneers. The radial dependency of the gradient, however, does not immediately fit that expected for a scalar field generated near-constant acceleration, which would require an almost constant gradient as opposed to an inverse r^2 relationship. Whether this relationship will continue to hold, or is modified by the interaction with the gravitational field equations, will have to be determined by more complete solutions for the metric and scalar field.

3.3 Conformal Transformations and Observable Quantities

Conformal symmetry is a powerful property for a theory to have. Care must be taken in the application of this symmetry and in the subsequent interpretation of results of the theory, to make sure we understand exactly what we are meaning with our results. The conformal transformation $\Omega(x)$ is explicitly dependant upon position in space (and time, in general) — this is a scaling that varies with position. As such, it may become difficult to match predictions of the theory to standard observations which tend to be carried out in systems with uniform scales — our observations of the universe are all given in terms of quantities with familiar, uniform scales like meters and kilograms.

In the literature, the most common treatment of the Weyl field equations involves appeal to conformal symmetry to simplify the equations for analytical solution. The metric is transformed in such a way as to be a conformal scaling of a metric with the coefficients a and b related by $a = b^{-1}$, whereupon a conformal transformation can be made to remove the first of these coefficients, a. In order to do this, a change of variable is first applied to the radial coordinate, then the inverse transformation to the conformal part of the metric coefficients is applied. Quite how the radial coordinate is to behave is unknown at this point, except that it can be shown [18] that the new radial coordinate goes to zero in the limit that the old radial coordinate vanishes, i.e. if $p(r)$ is the new radial coordinate from the original r, then $p(r) \to 0$ implies $r \to 0$.

Beyond this application of conformal symmetry, it is also standard to invoke conformal symmetry to simplify the scalar field also. The method in this case is to assert that whatever structure may be present in the scalar field can be transformed away by some particular conformal transformation, with the equivalent physics in the new metric being determined by the nonzero value of the now

constant scalar field. Such a transformation can not in general be specified, but for a scalar field without singularities such a transformation would be possible.

However, this second conformal transformation must be applied to all the fields of the theory, and it's application will introduce new factors into the metric coefficients — effectively undoing some part of the previous transformation that put the metric coefficients in the form $a = b^{-1}$. In addition, this introduces another unobservable scaling to the metric which would have to be taken into account when trying to match to observations. For these reasons, in this numerical work the assumption that these transformations can be successively applied and retain all the simplification has not been relied upon. In this work, as many fields have been retained as is workable in each case.

Some more recent work in the field has followed this trend and has restricted simplifications, for example a recent article on the 'Newtonian limit of conformal gravity' [35]. In this particular work, the metric is transformed to a conformal form (in our notation, the metric is in terms of $\bar{a}, \bar{b}$) and is not conformally reduced further. The conformal symmetry is invoked to bring the scalar field to a constant value only. The field equations are only marginally more complicated in this form, though they do involve a second variable which does considerably complicate the solution process.

It should also be noted that existing work in the literature does not specifically set out to perform both of these conformal transformations at the outset. The way that the equations are handled is to treat the left and right hand sides with a degree of separation, and the simplifications are typically made to one side at a time. This occurs because the field equations have not been solved in terms of a full energy-momentum tensor in the literature — the components of $W^{\mu\nu}$ are expanded in terms of the metric, which is simplified by a conformal transformation to depend only upon b. The source terms are not expanded in terms of a metric, and are worked with in terms of tensor quantities. This allows a lot of discussion of properties of the geodesic equations and covariant conservation of the energy-momentum tensor, which is simplified by a conformal transformation to a gauge where S takes a constant, nonzero value. The complete, expanded system is not solved for, however it is easy to assume that both conformal transformations could be made successively to simplify this procedure. This has not been proven to be the case and seems very unlikely for any physical situation.

Chapter 4

Criticisms of Conformal Gravity

A number of papers have been published since the presentation of a vacuum solution of the conformal field equations, trying to expand or elaborate on the possibilities of fourth-order gravity theory. Some have been possible extensions, others seeking clarification of what the coefficients might be, and some have tried to show potential downfalls of the theory. The area is still in the very early stages of development, so many of the ideas being proposed, whether in favour or against conformal theories, can appear trivial or inapplicable in many cases. Nevertheless, all these criticisms or difficulties need to be addressed — it is not until a theory has been exhaustively tested that it can be considered practically useful or predictive.

4.1 'Solution Matching in Weyl Gravity' — Perlick & Xu

Possibly the most quoted paper criticising the potential of conformal gravity theory is the 1995 paper by Perlick and Xu [18]. This paper is a direct reply to the work of Mannheim and Kazanas in their papers of 1989-94 ([13, 14, 16, 19]), and attempts to show that a fourth-order theory cannot produce observationally acceptable results on the scale of the solar system, or anywhere else.

They present three main objections to the previous work. The first objection is that the Weyl tensor is necessarily traceless, thus requiring a traceless energy-momentum tensor, which is not a good representation of kinematic mass. This could also create difficulties in matching boundary conditions between areas of matter density and the vacuum, such as at the limb of the sun.

This objection has already been answered in the literature, and in the discussion above. The apparent lack of kinematic mass is not considered a disadvantage for conformal gravity theory, but rather a requirement and a potentially useful link to quantum theory of matter generation. Matter in a conformal gravity

theory must be generated dynamically though interaction with some scalar field, as is thought to occur in the currently accepted model of particle physics. The standard model of particle physics is also conformally invariant, with dimensionless coupling constants, which would suggest that a gravity theory with the same features could be more easily integrated into a complete theoretical framework.

The second objection that Perlick and Xu present is related to the conformal invariance property. It is a property of the conformal field tensor that any solution of the vacuum field equations remains a solution if it is multiplied by a conformal scale factor. Any conformal multiple of the metric is also a valid metric! This means that when considering geodesics, null intervals are fixed (any scaling of zero is still zero) but a timelike interval is not fixed — it can vary with a scaling of the metric. If this is the case then no one orbit can be picked out for any massive particle without further information, and the theory is non-predictive.

To illustrate, the trajectory of a particle can be produced by the variation of the action integral

$$I = -m \int d\tau$$

with respect to the paths taken $x^{\lambda}(\tau)$. Given that the interval transforms according to $d\tau \rightarrow \Omega d\tau$,any conformal transformation would introduce an extra variable into the integral, dependant on the conformal transformation that is made, so that the stationary path is not necessarily constant — the interval for a timelike trajectory is not constant.

Fortunately, the resolution of this difficulty is inherent in the resolution of the difficulty mentioned above. The solution of the conformal field equations is not enough on it's own, the geometry is not the whole story when it comes to describing a realistic system with particles present. To consider massive particles, we have to include a scalar field to provide a mass-generation scale. The value that this field takes participates in the mass-generation mechanism, and needs to be included in any action representing the path taken by the particle. As it happens, the scalar field required for mass generation must be of order m^{-1}, and transforms conformally according to $S \rightarrow \Omega^{-1} S$. Particles acquire a mass from this scalar field according to $m = hS$. Substituting this result into the action integral produces

$$I = -h \int S(x)\, d\tau.$$

If we look at the conformal transformation of this action under $g_{\mu\nu}(x) \rightarrow \Omega^2(x)\, g_{\mu\nu}(x)$, it is manifest that the factors of the conformal transformation Ω cancel — re-

moving the ambiguity. This only occurs for a field with these dimensions, any other choice would result in some factor of Ω remaining in the integral, and then indeed the action would be dependant on the conformal scaling, a quantity that is generally not known *a priori*. This cannot occur in a conformal theory, which must have a completely conformal action.

The third objection presented is the most serious and takes up the bulk of the paper. The problem is, that a solution of a differential equation must, if it is to be physically representative, satisfy boundary conditions that are appropriate to it. For the exterior solution (2.3), these would be conditions at the inner boundary with the source and at infinity. These conditions should provide data for the constants of the solution, in this case β, γ and k. Perlick and Xu do acknowledge that Mannheim and Kazanas are aware of this issue, and discussions of general, interior solutions were made in a later paper [14]. These relate the constants β and γ to integrals over the source, in terms of a general source function, as described above. One valid point made by Perlick and Xu is that a solution of the homogeneous equation may also be added to give a full solution of the differential equation, which has not been done. This would then have to be constrained by boundary conditions also. However, matching at the boundaries is not something Mannheim and Kazanas have addressed, beyond stating that the interior and exterior solutions appear to be compatible.

The paper then goes on to describe a method of matching an interior integral with the exterior solution. Their finding is that for this system, the boundary conditions at the limb of the source are such that the coefficient γ for a linear term can not be small enough to match observation in the solar system — their calculations limit this coefficient by $\gamma \geq \frac{\beta}{R^2}$, which would be readily apparent in the solar system. Thus a theory constructed on this basis could have no physical relevance to the solar system, and by extension, to anything else.

The calculations used to arrive at this result are sound, and indeed do result in such a limit. To use Mannheim and Kazanas's own results, they also show by reference to the results $\beta(2-3\beta\gamma) = \frac{1}{6}\int_0^R dr' f(r') r'^4, \gamma = -\frac{1}{2}\int_0^R dr' f(r') r'^2$ that the same kind of limit arises from the internal quadrature solution. The argument runs thus:

$$-\gamma = \frac{1}{2}\int_0^R f(r')\frac{r'^4}{r'^2}dr' \geq \frac{1}{2}\int_0^R f(r')\frac{r'^4}{r^2}dr' = \frac{3\beta}{r^2}(2-3\beta\gamma)$$

for some $r \geq R$, that is, at any such r, the contribution from γr is of order $\frac{\beta}{r}$ and not smaller.

This result can be arrived at even more simply by transforming to a dimensionless radial variable according to $\bar{r} = \frac{r'}{R}$. Then the two integral expressions for the coefficients of the theory reduce to

$$\begin{aligned} \beta(2 - 3\beta\gamma) &= \frac{R^4}{6}\int_0^1 d\bar{r} f(\bar{r})\bar{r}^4 \\ \gamma &= -\frac{R^2}{2}\int_0^1 d\bar{r} f(\bar{r})\bar{r}^2. \end{aligned}$$

It is obvious that the integral $\int_0^1 d\bar{r} f(\bar{r})\bar{r}^4 < \int_0^1 d\bar{r} f(\bar{r})\bar{r}^2$ for r running between zero and one. Therefore

$$|\gamma| \geq \frac{3}{R^2}|\beta(2 - 3\beta\gamma)|,$$

as given above.

The main difficulty with this procedure is that they are attempting to match an interior integral with the exterior, $T^{\mu\nu} = 0$ solution. In order to resolve the inherent features of a conformal theory, as described above, a scalar field must be included in the source $T^{\mu\nu}$. If this is done it is not necessary that the source vanish when the fermionic mass terms are zero. Source terms are introduced though the varying scalar field, the scalar curvature and the scalar field self-coupling λ. Even if the scalar field were to be constant, the usual assumption in the literature, there would still be source terms which would not in general be constant. Thus matching to a vacuum solution with $T^{\mu\nu} = 0$ is not a useful approach for a fully conformal theory with the required scalar field.

4.2 Wood & Nemiroff 1991

Another paper published in 1991 was 'Constraints on Weyl Gravity on Subgalactic Distance Scales' [36]. This paper attempts to establish what limits could be placed upon the magnitude of any linear potential coefficient γ. The paper assumes that the value of γ is a universal constant, and takes a value such as quoted by Mannheim and Kazanas in their papers which suggest that a linear potential would be useful for explaining galactic rotation curves ([13, 16]), that is about 10^{-28}cm^{-1}.

With this universal constant, small effects could potentially be noticed in the orbits of distant solar system objects, given enough resolution of observation. If such a constant were used for test bodies in a laboratory, then this could be distinguished from their usual inverse radius squared attraction quite easily. The conclusion that arises is that a constant value for γ of this magnitude is

not compatible with observation, and the constant value would have to be many orders of magnitude smaller.

This is perfectly compatible with the development of the conformal theory - the interior properties of the source should contribute to the generation of γ. Exactly how this occurs is the issue to be resolved, the suggestions in the literature 2.6 have their own difficulties that must be addressed. Specifically, if a scalar field is included then there is not going to be a single constant γ for all exterior space, rather the value would be continuing to change asymptotically towards some value at infinity. This would occur even if the scalar field is constant, via the scalar curvature and scalar field self-interaction. A universal constant γ is not feasible in such a system, or even a locally constant value. Related material in a similar vein can also be found in a paper by Walker [29].

4.3 Other Concerns

One particularly interesting result was found that derives from the S field equation of motion (2.8) in the exterior case. If we were to allow conformal transformations to be performed successively, so as to let $a = 1/b$ and $S = S_0$, a constant value, then the S equation of motion would reduce to the form

$$\frac{S_0 R^{\mu}{}_{\mu}}{6} - 4\lambda {S_0}^3 = 0$$

or

$$R^{\mu}{}_{\mu} = 24\lambda {S_0}^2.$$

As λ and S_0 are assumed constant, this condition in the exterior results in the requirement that the scalar curvature $R^{\mu}{}_{\mu}$ take some constant value. If we expand the scalar curvature in terms of the metric coefficients, we obtain

$$b_{rr} + \frac{4b_r}{r} + \frac{2b}{r^2} - \frac{2}{r^2} = k$$

for some constant value k. This differential equation has the easily found solution

$$b = 1 + \frac{\eta}{r} + \frac{k}{12}r^2 + \left(\xi - \frac{1}{k}\right)\frac{1}{r^2}.$$

This solution, if taken as a constraint upon what constants we could use for the coefficients in the corresponding vacuum solution of the conformal field equations (2.3), has an important immediate consequence — there is no linear term. If this is the case, then the conformal vacuum solution reduces to a Schwarzschild

solution in a deSitter background specified by the constant cosmological curvature k. This would mean that linear potentials could not be used to give a dark matter free explanation of the galactic rotation curves. A constant-valued scalar field destroys some of the desirable features of the model.

Also, we have a pair of integration constants arising from the homogeneous part of the solution — η and ξ. The first, η, can be readily identified with the usual β term. The second coefficient ξ had better equal k^{-1} to a phenomenal accuracy otherwise, as k is expected to be of order 10^{-60} or so, there will be huge deviations from Schwarzschild on solar system scales. This kind of fine-tuning of constants against each other is a little unsatisfactory, if mathematically allowable. It is an especially worrisome feature when tiny deviations from the exactly required value would completely upset the viability of the model. If the scalar field were to vary, however, this situation would not arise.

There are other potential difficulties that are inherent with the conformal gravity theory. With a fourth-order theory, the high derivatives can lead to the quantum theory becoming susceptible to ghosts, though in this case the symmetry may constrain this effect [37]. However, in a similar vein, the dimensionless coupling constant between the geometry and matter tensors gives a conformal theory a better chance of being renormalizable than general relativity. Such discussion is beyond the scope of this work.

Chapter 5

Implementation of a Numerical Solution to Conformal Gravity

We now have an appreciation of what conformal gravity theory entails and what features it might have. So now we come to the crux of it — can we get a reasonable physical representation of the universe using this theory? The features we found in the geodesic and orbit equations *suggest* that the differences of the theory from standard gravity should not destroy the desired features of general relativity, and that the additional features of conformal gravity could resolve some of the remaining mysteries. In order for the conformal theory to be viable, this has to be shown to be true!

So we now make the focus of this study a feasibility study into the use of fourth-order conformal gravity theories including dynamical mass — just what can we do with them, can they possibly be set up to explain the physics of the universe as we observe it, especially with regards to nearby phenomena in our own spatial neighbourhood, the solar system. The feasibility of conformal theories is continuing to be investigated in other ways, and sometimes new data comes to light to help refine the investigation, such as the observation of the anomalous space probe accelerations. Though some of the most compelling results in the literature come from cosmological or galactic implications of fourth-order theories, I choose to focus on areas more amenable to study and comparison to well understood observation, and on the possible nature of connections to dynamical mass generation. So the investigations have mainly involved the motion of bodies within solar system limits, including any possible effects of a background Higgs-type field.

Straight away it becomes apparent that finding solutions to the conformal field equations is not a trivial task — the nonlinearity of the equations when a source is present, and the inclusion of an additional variable in the scalar field, make the

possibility of an analytic solution remote. In searching for any analytic solutions to give an idea of what behaviour the conformal metric and scalar field might display, success was obtained for very simplified, linearised systems in terms of one variable only. This does give some indication of the kind of behaviour we can expect from a fuller solution, and points the way to the techniques that can actually solve this problem — numerical methods.

5.1 Numerical Techniques

It is immediately apparent from considering the form of the Weyl field equations that they are much more complicated objects than the Einstein field equations of general relativity. Indeed, a fourth-order, nonlinear set of differential equations is most often a very difficult thing to solve - even the second order Einstein equations have a small number of analytic solutions. Modern computing power makes numerical solutions of these equations a feasible option, as today's desktop computers have the speed and capacity to attempt such large numerical systems that once would have required a mainframe. Even in the course of my studies the computing power on my desk has increased nearly tenfold. Such solutions should be enough to determine whether a theory with this basis can be viewed as a useful description of the physics.

There are a wide variety of numerical techniques that can be applied to problems of this kind, and an equally wide variety of existing mathematical packages out available that claim to be able to use various of these methods. Some of these packages were trialled, and indeed some of them could perform some of the basic techniques of interest, forming a starting point for the further research. However, most had limitations of some form, whether in ease of use, apparent reliability of results, or in extensibility. Eventually the limits of the packages we were working with were reached, and I decided to implement my own programs for the numerical techniques. This had several advantages, such as customisability, extensibility, and exact knowledge of what processes were going on — which improves the confidence in the results. The disadvantages would be in the development time and that some packages may have higher-power routines available that I did not choose to implement. These disadvantages were vastly overwhelmed by the advantages in extensibility of having a custom suite of routines.

The main techniques used to provide solutions of the various field and dynamical equations of the theory fall into two categories — extrapolation methods

and relaxation methods. Of the extrapolation methods, the most commonly used was the standard Runge-Kutta integration. This particular method is a tried and true numerical workhorse, to which many elaborations and improvements have been made over the years. The evolution of the Runge-Kutta methods resulted in the Burlisch-Stoer integration method, which was another option in the eventual suite of routines that became available.

Occasionally, some equations proved difficult to solve with this type of method. In this case, there was the option to use the 'predictor-corrector' method. This particular numerical technique seems to be falling from favour due to a lack of flexibility, but it handles smoothly varying functions particularly well in some cases, and came in handy for certain recalcitrant equations.

The other category of methods, relaxation, consists of finite-difference Newton-Raphson iterations. These methods seek to solve the equations over the whole of the domain, and over all the variables, simultaneously. These are particularly useful when there is the possibility of extrapolation introducing large errors, and unlike extrapolation include boundary conditions at both ends of the domain of interest.

These all had their uses in certain cases as the equations are highly sensitive to the particular formulation. Very often it was found that where one method would fail another would succeed. Initially we were considering using essentially only the finite-difference Newton-Raphson methods for calculation, but the other methods proved useful for setting up initial data for the Newton-Raphsons and for certain intractable systems.

5.1.1 Extrapolation Methods

The Runge-Kutta method used was the traditional fourth-order method, with the ability to use variable stepsizes, which was often suppressed to produce data on a constant mesh for simple use in a subsequent Newton-Raphson method. These methods were initially used to provide the trial solutions to the Newton-Raphson methods or to investigate the potential behaviour of functions with different parameters. However, this technique became more useful through the project as the systems became more complicated. The Runge-Kutta technique is well suited to 'brute-force' solution of complicated systems — if they are formulated correctly, and you are willing to let the computer use a lot of time and memory, it can grind it's way through most problems. Of course, you have to know something

about the results you expect in this case, to make sure the solution you obtain is reasonable.

The process of the method involves taking the value of the function at a point and computing its' derivatives. These are then used to extrapolate the function forward in the domain of interest. The resulting point has its' derivatives calculated, which is used to modify the original extrapolation. The process is repeated, depending on the order of the method, and eventually a final estimate of the function at the next interval of the domain is obtained. The method then repeats for the new value of the function. These methods are quite robust, and if set up correctly can produce reasonable results for moderately complicated equations with all kinds of values of the parameters. This made them useful for seeing what bounds could be placed on the parameters of the theory and still get reasonable results out.

The potential downside of Runge-Kutta methods (or any extrapolation method) is propagation of errors, as points are continuously extrapolated from the results of previous extrapolations so any errors introduced at some point are likely to throw further calculations off track. This can be particularly evident in equations which have solutions involving contributions growing with radius, with a coefficient that could take many values. For example, the vacuum solution of the field equations (2.3) has a linearly growing term with coefficient γ, presumed to be small. If a slight numerical or extrapolation error is made at a point, this could appear to the equations as if a larger value of this coefficient has been included, which effects the following extrapolation. Such effects tend to grow if the method is not set up to handle them, which is why some knowledge of what solution is expected is an advantage.

This kind of effect can be minimised by using higher order methods and finer steps for extrapolation. Higher order methods use more subdivisions per extrapolation step to get better estimates of where the next point should be. The information gained by referring to more subdivided points for each step gives the method a better ability to handle gradients. Finer extrapolation stepsizes are the brute-force method, if the extrapolation step is smaller then a better estimate of the new point is obtained, as long as the function does not vary greatly within the stepsize — which becomes more unlikely as the stepsize is reduced.

Burlisch-Stoer methods are an extension to the variable-stepsize Runge-Kutta algorithm. As the accuracy of the method tends to increase with decreasing

stepsize (up to the numerical limits of the computer system), the Burlisch-Stoer method aims to exploit this property by predicting what value an extrapolated point would take for an infinitely small stepsize. This is done by subdividing the step interval several times, producing a series of estimates of the next point's value dependant on stepsize. Working on the assumption that the value of the next point is some function of the stepsize, this series of estimates is extrapolated down to an infinitely small value, and the result used for the new point. The stepsize for the actual extrapolation interval is variable, increasing when the error estimates of the method are small and decreasing conversely. These methods can be particularly efficient for functions that are not varying too sharply, as large extrapolation stepsizes can be used with high accuracy.

Predictor-corrector methods would appear from the literature to be dropping out of favour compared to high order adaptive-stepsize Runge-Kutta or Burlisch-Stoer methods. However they are noted as being useful for particularly complicated though smooth functions. As cases like this were found in my work, which the other methods didn't always handle well, this method was a potential option.

This technique was again mainly used to find initial data for later computations, but it has the advantage over Runge-Kutta in that it can use data provided on a grid (such as the output of previous Runge-Kutta extrapolations) as it does not perform internal subdivisions for its operation. Rather, it extrapolates new points from the data of several previous points as it marches through the domain of interest. A new point is extrapolated by using the information about the value and slope of the function from several earlier steps to predict the next point. This point then has it's own slope calculated, which is used to re-interpolate the point, thus 'correcting' it. This correction can be repeated with the (supposedly) improved estimate of the point, and the prediction and correction operations can be repeated many times — though typically more than two iterations will not provide any real improvement in the result.

The main disadvantage of this method is having to supply several starting points rather than one, so it presumes better knowledge of the boundary conditions. This does restrict what systems it can be applied to. In practice, the problems it was applied to were generally those where the solution was believed to be asymptotically flat, so a fair approximation to the boundary condition can be supplied by an *exactly* flat set of data points at a large distance from the origin of the system.

5.1.2 Newton-Raphson Methods

The method of a finite-difference Newton-Raphson engine is simple. The differential equations are discretised by replacing derivatives with appropriate expressions involving the values of the function over a few points, placing the domain of the functions to be solved for on a grid of mesh points. At each point the finite-difference approximations to the differential equations are evaluated, along with a Jacobian matrix formed from the derivatives of these difference equations with respect to the variables. This produces a matrix system which can be solved for a 'descent' direction, in this case a vector of adjustments to the values of the functions at all the mesh points. This adjustment should bring the variables towards a solution of the finite-difference equations.

The values of all the variables at all the mesh points are solved for simultaneously. The advantage of this type of method is that it is known to have rapid (second order) convergence to a solution, *if* the initial trial solution is close enough to the true solution. However, like all Newton's method implementations, unless it is modified, the method is not globally convergent and if the initial trial solution is significantly removed from the final solution then the method becomes divergent and no solution will be reached. What counts as 'significantly removed' depends on each system to be solved.

This method has several useful features from the point of view of trying to solve the field equations. First, this is the only method which can explicitly include boundary conditions at more than one point, as the entire domain is solved for simultaneously. This is very often what I want to do to match observation or physical requirements. For example, a solution of the field equations across the interior of the sun should produce fields that match well in value to the observations at the limb of the sun, but at the origin we don't know what values the fields can take. However, from symmetry we know that many of the fields should have zero slope at the origin, which is a boundary condition we can apply in the Newton-Raphson iteration.

Another advantage is that the method is easy to set up to incorporate previous results. Typically the method is working on a grid of evenly spaced points (otherwise the finite-difference expressions for derivatives get more complicated), which can be set to match the interval (or a multiple of the interval) of a previous Runge-Kutta or similar method.

The other advantage that these methods have over extrapolation methods is

that they are not so sensitive to extrapolation errors. As the Jacobian matrix of derivatives is solved at every point, each point is connected to it's neighbours by the derivatives, so any artificially introduced slopes or deformations in the values will reduce the accuracy of the solution, which should be picked up in the next iteration. The result is that any error-introduced effects should not be as cumulative as they would be in an extrapolation method.

The type of error that can occur instead in relaxation methods is a little different. Consider solving the vacuum field equation, knowing the analytic solution (2.3), as above. In this case any small errors that induce an inappropriate value of γ will not throw off the derivative at the next point, so will not accumulate across the domain. Instead, errors could induce a different value of γ at every point. This could easily happen if the starting solution is not close to the true solution, so that large corrections are made, which can easily overshoot the mark. This variation of γ is then limited by the derivative terms in the field equation — if γ were to vary randomly, the function would not be continuous in higher orders so will not solve the field equations so well. This deviation would then be corrected in subsequent iterations.

This kind of effect can easily be observed — for example, if boundary conditions are chosen that do not exactly match the rest of the domain's solution to the equations, then a disturbance of this kind will propagate out slowly through the domain with successive iterations. A case like this could be observed in the case for predictor-corrector methods described above, where an asymptotically flat function is enforced to have vanishing slope at some finite radius. The function would then have a discontinuous first derivative at that boundary, which the iterations will try to correct by adjusting the points adjacent to the boundary to better match the slope required by the equations. As the finite-difference expressions for the derivatives involve only a few neighbouring points, this adjusting will propagate out from the point of discontinuity a few points at a time, getting smaller and smaller as the discrepancy is 'spread out' over more of the domain.

5.1.3 Stability Issues

To be a useful method, a particular numerical technique must have a high degree of stability, especially when dealing with nonlinear, high order equations. Often it was found that with these equations the border between instability and stability was a very fine one. The exact representation of the system of equations could

have a direct impact on whether the method would prove stable or not. This includes not only such choices as whether to reduce a system of higher-order differential equations to coupled first-order equations, but also such simple choices as whether to solve for the variable, a radialised variable, or some scaled variable. Such simple differences in the systems to be solved could make large differences in the stability of the programs.

The Newton-Raphson methods were the most temperamental, due to the nature of how they work. As we noted, a starting solution that is too far off the final solution will cause instability — in tests on these systems, sometimes the difference could be as small as 1%. In addition, the way in which the system is formulated has direct effects of stability. To perform a Newton-Raphson iteration cycle involves solving the matrix system $Ax = b$ for x — requiring some eliminative process or matrix inversion. This is always greatly simplified by the finite-difference method which produces a diagonal structure for the matrix A as the equations at a point can only depend on the values of the variables a finite number of points to either side - typically only one to three points for second to sixth order Taylor expansions. The block-diagonal structure allows large savings in memory required to store the matrix and in the computations to solve the matrix. However some care is required in making sure that the matrix is far from singular — often systems where one variable is present only weakly in high derivatives with respect to the other variables can lead to ill-conditioned matrices, producing unreliable results. Sometimes this could be alleviated by reformulating the equations — for example, by solving the equations for the variable multiplied by radius rather than the variable itself, which in some external systems helped prevent terms getting too small for the numerical engine.

The Runge-Kutta and predictor-corrector methods tended to work more consistently — once set up properly, they do tend to operate robustly. However, as they are processes of extrapolation they are more sensitive to the boundary conditions and could sometimes flip between solutions with expected behaviour to solutions with unphysical behaviour dependant on very fine adjustment of the initial data supplied. Again, this could sometimes be alleviated by reformulating the equations in terms of differently scaled variables.

However, sometimes difficult issues arise where the different methods are affected in different ways by the same changes. The number of intervals on which the numerical engines operate is the principle example of such an effect. If the

number of subintervals of the domain (number of nodes) is low, then processes which process the domain as a step-by-step process (Runge-Kutta methods, integrals, etc.) are not particularly accurate. In order to model the effects of the function accurately, the subinterval size must be small (number of nodes large). However, the finite-difference methods use Taylor expansions to produce finite-difference approximations to the derivatives of the variables. If the difference between the value of a function at two adjacent nodes is very small, errors from the floating point representation can creep in. If the number of nodes is large with a slowly varying function, then the difference between two nodes is likely to be small, increasing the chances of roundoff or truncation errors. Given that the fields of the equations we are solving are generally varying very slowly, especially once away from the source, this kind of effect could introduce much difficulty to the program.

5.1.4 Computational Accuracy

Despite the speed and large storage capacities of modern desktop computers, some limitations have not changed a lot. Accuracy of numerical computations is limited largely by the storage format of individual numbers in computer memory, and the formats available for storing numbers haven't changed much since the early days of computer languages.

For the purposes of most numerical calculations, we are not dealing with integer quantities, but rather decimal ones. Floating point numbers are represented by computers in a format of

$$(sign) * mantissa * 2^{\text{exponent-bias}}$$

where the mantissa and exponent are base two numbers of varying numbers of digits dependant on the exact format and the platform, typically single precision numbers can represent about 7 decimal significant figures and double precision about 16.

This representation, though organised to be the best we can use, has certain inherent difficulties. The first and most obvious is that the mantissa and exponent are base two numbers and so many numbers that are exact in decimal figures are only approximated by the computer. For example, we are used to there being no exact decimal representation of 1/3, but in a binary format 0.01 is not an exact figure but in single precision turns out to be 10737418/1073741824 — 0.01 to about 8 figures, but no more.

The problem with using this kind of representation is most manifest when subtracting two numbers of similar magnitude — something which comes up a lot in many mathematical processes. Then the tail of the approximation can be made more significant than it should be, introducing spurious figures into the result. Any results of a numerical process should be taken with this property in mind — we need to know how many figures are likely to remain significant through the calculations. In general this will be something like the 7 or 16 decimal figures mentioned above, but the accuracy of the last two or three of these figures may be in doubt.

This gives rise to the discussion of a quantity referred to as the *machine accuracy*, ϵ_m. This quantity is defined from the way floating point numbers are added together. This is done by taking the smaller of the two and shifting the exponent up by powers of two and the mantissa down, until the exponent matches that of the larger number. If this is done too many times the mantissa is wiped clear and you end up adding zero. So the machine accuracy is defined as the smallest number that can be added to one, and achieve a result different from one. This number is about 5.0×10^{-7} in single precision and maybe 5.0×10^{-16} in double precision. Note that this number is in no way related to the smallest number the computer can represent — this is much smaller. This represents some limit to the effect of adding numbers of very different magnitudes.

In the process of any extended calculation, it can be expected that some error of order ϵ_m will be introduced at each operation. If you were feeling lucky, you could expect that for N operations you might have a total error of order $\sqrt{N}\ \epsilon_m$, from random errors of positive or negative sign. More likely the system will have some sort of bias and error is of order $N\ \epsilon_m$. Errors introduced in this way are usually referred to as roundoff errors, and in most cases there is not a lot that can be done about them.

The other main form of error in numerical techniques is that introduced by the techniques themselves. For example, a numerical integration is not done over a continuous domain but is performed over a series of subintervals. Whatever the size of the subintervals is, it will not give exactly the same result as the analytic result, though it can be close for small enough intervals. Another example would be dropping terms in a series expansion after a certain limit. In this case, though some truncation error is unavoidable, some of it can be minimised by the program design. There are some sequences or combinations of operations to

watch out for and avoid — a good reference on these issues is *Numerical Recipes: the Art of Scientific Programming*[38], which goes into some detail about relevant programming techniques.

5.2 Boundary Conditions

All of the numerical methods described above will take differential behaviour of a function and produce curves of how that function would behave across the domain of investigation. At some point we must pin down the solutions with some physical information — typically, the derivative information from the equations will provide a curve through any point, but only a very few, or one, such curve will have physical relevance to us. The values of the boundary conditions are provided from information about the function's behaviour at important boundaries, such as the centre of the source or origin of the coordinate system (usually the same point) , the edge of the source, and in the limit as the radius goes to large or infinite values. Some of these can be matched to experimental data, while others must be conjectured from reasonable physical expectations.

The boundary conditions need to be applied only at one end of the Runge-Kutta or predictor-corrector methods (and are thus perhaps more properly called initial conditions), and at both end of the Newton-Raphson systems. In the cases of the extrapolation methods, specific values of point and slope for all the variables of interest are provided at the initial point. Note this may actually be many derivatives of the variables if a high-order differential equation has been recast into a system of coupled first-order equations.

For Newton-Raphson methods, extra mesh points can be constructed exterior to the domain of interest, which provide the extra information for finite-difference approximations to the derivatives at the boundary points. The values of these points can be provided explicitly or calculated from the finite-difference routines, depending on what the boundary condition is. If a fixed value of the field must be obtained, then extra points are provided explicitly. If boundary conditions apply to the gradient instead, such as requiring a slope to vanish at large radius, then the finite-difference equations can be arranged to specify the slope in terms of one exterior point and several interior ones (the exact number depending on the order of finite-difference expansion), providing us with a relationship to satisfy the boundary condition in terms of one new point. This means that the boundary points become special cases, with their own specific finite-difference expansions.

5.2.1 Photospheric Boundary Condition Data

The most convenient object to model as the source of gravitation, and the most useful for comparing the results of the numerical engines to observation, is the sun. The sun also has a variety of observations that have been made upon it available. From these it is possible to extract information to give approximate values of the physical and geometric quantities present in the equations I am solving — the approximate orders of pressure, density, scalar field slope, and metric coefficients.

Boundary conditions for models of stellar interiors, no matter how simplified, are a tricky proposition. The problem is the determination of where is the boundary surface? The sun is a tenuously extended object, with the photosphere giving way to the chromosphere and corona, eventually merging into the solar wind. As far as mass distributions go, there is an ever-decreasing density out into the solar system, with a small net material flux. A more useful definition of the solar surface is probably in the photosphere, the area within the sun from which light we receive emanates. In this case the physical quantities pressure and density are not going to be exactly zero at this boundary. These boundary conditions are only approximations, though they appear to be quite good ones in most models.

Data on the density and pressure distributions of the sun's photosphere are obtained from measurements of limb-darkening, the apparent drop in brightness at the edge of the solar disk. Elaborate models of the processes involved have been created to obtain the physical properties of the solar atmosphere from the limb-darkening data. The results are usually most valid in the region at a depth of around one mean free path of a photon in the solar atmosphere. The results used to get some estimates of the physical properties pressure and density came from a paper by Vernazza, *et al.* [39] which gives a profile of the photosphere with enough information to produce a gradient in pressure near the edge of the sun. This can then be used to give a representative value of the quantity $\frac{p'}{\rho}$. These are reasonable values to use as they would be provided at a depth that on the scale of the stepsize of the numerical values is very close to the boundary of the sun.

Representative values of this kind are suitable to use in numerical solutions of the differential equations. They would only be approximations in any analytic solution, but in the numerical methods performed on grids the effective resolution is much more coarse. In a typical run of a Runge-Kutta method an individual step

may be kilometers wide, or of orders higher, so changes on a scale less than this are not going to effect the results of the process. In a Newton-Raphson iteration, the stepsize could be hundreds of kilometers. Similarly, it is not unreasonable to use Schwarzschild values for the quantity $\frac{b'}{b}$ at this radius as compared to the stepsize involved the photospheric depth considered is essentially at the radius of the sun.

5.2.2 Boundary Conditions at the Origin

The other most important point, mathematically, is at the origin. Whereas boundary conditions for the exterior domain involve matching the solutions of the equations to the observed physical results and observations, those at the origin are more to do with making sure the equations describe reasonable physical quantities.

It is soon noted that the mathematical forms of the various quantites involved in this theory often involve terms with inverse radial dependance, often to several orders in radius r. Obviously, these terms potentially could cause difficulty at the origin where any terms that remain with such a dependance would cause the equations to go infinite at the origin. The limit of the equations as r approaches the origin can be taken using l'Hopitals' rule, to provide finite-valued equations at the origin. However, often the equations can be badly behaved numerically in the vicinity of the origin due to the presence of $\frac{1}{r}$ terms which have small numerical coefficients which might analytically cancel, but due to floating point or accumulated numerical errors do not exactly cancel out. In this case Taylor expansions of the derivatives in the vicinity of the origin can often remedy this problem.

The most obvious consequence of requiring the equations and the representations of physical quantities (such as the scalar curvature, expressed in terms of $\bar{a}(r)$ and $\bar{b}(r)$) to be finite at the origin is that the first derivatives of all the physical quantites $\bar{a}(r), \bar{b}(r), S(r), \rho(r)$, and $p(r)$ must vanish. This could be expected from symmetry of the system — the profiles of these quantities should be reflected through the origin due to spherical symmetry. Similarly, the second and third derivative of the metric functions must also vanish, as can be shown by use of Taylor expansions. In addition, due to the presence of terms of the form $\frac{\bar{b}-1}{r^n}$, it is found that the metric coefficient $\bar{b}$ must reduce to 1 at the origin. This has a physical consequence that at the origin of a distribution of matter, the

spacetime will be conformal to flat spacetime. However, the scalar curvature can be non-zero due to the presence of the second derivative of the metric coefficient $\bar{a}$ in the definition of scalar curvature, which is not required to vanish.

These regularity conditions can be used to expand the discussion started earlier about the viability of the interior quadrature solution presented in the literature (2.5,2.4). The regularity constraints can be merged with the constraints upon the solution of $\nabla^4 b = 0$ that are required for it to also be a solution of the field equations.

The argument is presented in terms of the possible homogeneous sector of the interior solution. The homogeneous contribution from $\nabla^4 b = 0$ is

$$b_h(r) = k_1 + \frac{k_2}{r} + k_3 r + k_4 r^2.$$

This must obey the constraint

$$3k_2 k_3 - {k_1}^2 + 1 = 0$$

in order to satisfy the field equations. In order that this constraint holds, it is immediately specified that k_2 must vanish, otherwise there is an infinite contribution to $b_h(r)$ at the origin. Then the constraint upon the homogeneous contribution at the origin becomes

$$1 - {k_1}^2 = 0.$$

This is obviously only solved for $k_1 = \pm 1$, and if this constant is to be acceptably merged with an exterior solution and to maintain signature, the positive sign should be selected. This gives us the following homogeneous contribution:

$$b_h(r) = 1 + k_3 r + k_4 r^2.$$

Consider now the interior quadrature solution given above, if the source exterior to radius R is dropped, as in the literature (2.5). The same constraints apply to $\bar{b}(r)$ as used in this solution. At the origin, this expression for $b(r)$ reduces to

$$b(0) = 1 - \frac{1}{2}\int_0^R dr' f(r') r'^3,$$

including the homogeneous contribution. Note, however for regularity at the origin we have that $b(0) = 1$. As $f(r')$ is assumed positive definite for the extended source [14], the only way this could hold would be if $f(r')$ were to vanish. This, however is a very uninteresting solution — nothing is present, and no β or γ can be generated using the quadrature solutions. It would appear that this method of solution is not viable.

5.3 Implementation

5.3.1 Numerical Requirements

Using the analytic expressions in the previous section, and by requiring the solution to match the observed successes of general relativity theory (the observed deflection of starlight, the precession of Mercury, *et. al.*), a set of reasonable requirements for any numerical solutions can be established. The requirements for the solutions of the field equations and equations of motion to be acceptable are:

- that the deviation of the metric fields from the GR values cannot be large in the exterior region — it must approximate the GR solution to within reasonable experimental bounds. This requirement means that $a \approx b^{-1}$, or $\bar{a} \approx 1$, with $b(r)$ or $\bar{b}(r)$ being approximately the GR value, respectively, and that $b(r)$ should take approximately the Schwarzschild value at the limb of the sun.

- that the gradient of the scalar field be small, or rather that $\frac{S'}{S}$ be small. If the scalar field were to provide the Pioneer spacecraft acceleration, then the magnitude of the normalised scalar gradient would be 10^{-26}. To produce this value at 20-40 AU, at the limb of the sun an appropriate value for $\frac{S'}{S}$ would be of order 10^{-18}.

- that the scalar field does not become zero. This would allow a point in space where the particles generated by the symmetry-breaking mechanism have zero mass.

These are the optimal requirements for any results of our numerical solutions. These features are augmented by the particular requirements of the case being solved, which can be simplified by the numeric nature of the process. For example, it is expected that the field $\bar{a}(r)$ is to become asymptotically flat, and to asymptotically take the value one. In far-field solutions, a reasonable boundary condition for large r would be to require that the derivative $\bar{a}'(r)$ vanish, even though it is not necessarily at infinity at the last interval of the method. If the field is such that the stepsize or magnitude of the quantities makes this a bad approximation, the variables can be transformed to a non-uniform mesh where the point at infinity is part of the domain. This, however, requires more careful

construction of derivatives and may not be useful in all cases such as finite-difference methods.

The fermion field present, representing usual matter contributions and being obtainable in terms of pressure and density fields, has only weak constraints applied to it at this point. Exterior to the source body, the fermion field is presumed to vanish, thus setting Ψ, p, and ρ all equal to zero. In the interior of the source body, the values of these fields can have a certain degree of freedom in our solutions as data to match them to is lacking. The most important feature that they should possess is that they produce solutions that match the boundary conditions and that are physical across their entire domain. Beyond that, we can consider a variety of physical configurations, of various degrees of approximation.

Solutions of the standard theory

In the standard theory, the only analytic solution for the interior of a spherical gravitating body is for a body possessing the unusual property of constant density. This kind of object does not appear to be physically very likely, unless you want to consider the gravitation of artificial bodies, but has some utility in that it provides some bounds on what can be expected for a more realistic physical model, where an analytic solution is not available.

A commonly used approach to modelling the interior of stellar bodies is to assume some equation of state relating the pressure and density, which can then be solved for through the hydrostatic equilibrium relationship. A large set of solutions have been produced assuming that the equation of state follows the form

$$p(r) = K\rho^{1+1/n}(r),$$

where K and n are constants. A body obeying this kind of relationship is referred to as a polytrope of order n. By substituting this equation of state into the standard hydrostatic equilibrium relationship, and introducing the dimensionless function θ according to

$$\rho(r) = \rho_0\theta^n(r), p(r) = p_0\theta^{n+1}(r),$$

the following differential equation is obtained for the quantity θ :

$$\frac{(n+1)\,p_0}{4\pi G{\rho_0}^2}\frac{1}{r^2}\frac{d}{dr}\left(r^2\frac{d\theta}{dr}\right) = -\theta^n.$$

Introducing a dimensionless radial constant ξ according to

$$r = r_n \xi,$$

where the scale length is defined from

$$r_n{}^2 = \frac{(n+1)\, p_0}{4\pi G {\rho_0}^2},$$

the equation above reduces to

$$\frac{1}{\xi^2}\frac{d}{d\xi}\left(\xi^2 \frac{d\theta}{d\xi}\right) = -\theta^2.$$

This is the Lane-Emden equation, which unfortunately has few analytic solutions — for objects of bounded radius, only solutions with $n = 0$ and $n = 1$ exist — corresponding to constant density, or density given by $\frac{\sin\xi}{\xi}$, respectively.

So what values of n correspond to physically interesting objects? As it happens, there are two particularly interesting values to consider. For a completely degenerate, non-relativistic electron gas the order would be $n = 1.5$, and for a fully relativistic case $n = 3$. These values can be used to a reasonable degree of approximation in the modelling of stellar interiors, the $n = 1.5$ case being most useful in convective zones and the $n = 3$ case being a good model in the non-convective parts of a star (the bulk of stars like the sun, in terms of mass). As these cases have no analytic solution, they must be produced numerically by methods such as those described above. A straightforward Runge-Kutta engine will rapidly produce the functions $\theta(\xi)$ for these orders, which take the value zero at the 'edge' of the sun, allowing a scaling between the dimensionless radius ξ and coordinate radius r. With these functions, we can construct profiles of the density and pressure across the stellar polytrope we are considering.

It is not easy to construct an analogous procedure in the conformal theory. In this case, the hydrostatic equilibrium equation involves both metric coefficients and the scalar field S. In addition, the standard theory derivation relies on simple arguments about the weight of a spherical shell of matter, according to the standard Newtonian potential. Because of this restriction no effects of matter (or anything else) outside the radius of interest are included, so the effect of any linear component to the gravitational potential cannot be simply included in this form. Using the Newtonian gravitational potential allows an equation that does not involve the metric coefficients but only the density and pressure.

In the conformal gravity model, we do not want to make such bold assumptions. The metric coefficients could be eliminated, but only by assuming that at some point inside the source the metric is determined entirely by the region interior to that point — that is, we are everywhere providing an exterior solution with infinitesimally increasing coefficients. This also requires that both metric coefficients be known, in addition to the scalar field. Without the simplifying mechanism of reducing the metric coefficients to terms involving the density, we have a problem in density, two metric coefficients and the scalar field. Possibly this number could be reduced by appealing to conformal transformations, but without a surer knowledge of how the metric coefficients are generated by the density, pressure and scalar field, the conformal hydrostatic equilibrium system is not going to be amenable to solution in the same way as standard theory.

What all this means in practice is that we can't assume a direct correlation between the physical characteristics of models using the standard theory and those using a conformal theory. We can consider the solutions of standard theory to give us a pointer to likely values the conformal solutions may take, especially as we expect in the limit of near-constant scalar field that the predictions of both theories should be very similar (assuming linear potential effects from the field equations are small, as they would have to be exterior). They can certainly give us a strong indication of what we should perhaps expect to occur for quantities like the scalar curvature interior to the body, it's magnitude, sign and gradients.

However, it is not a requirement that the pressure and density match up well with standard theory models — we expect that there will be differences, if particle mass is correlated to the scalar field, let alone if the metric field is noticeably different. Standard models of the interior have produced good agreement with the observed solar properties — luminosity, temperature, chemical abundances, etc., but these are all properties observed at the surface and a multitude of internal configurations can produce the same surface properties. (Incidentally, one of the only probes we have of the solar interior is the production rate of neutrinos, which has been stubbornly resistant to matching models with experiment). The most important property any models need is to match the observations at the surface, as this is the only hard data we have on hand. In producing conformal gravity models of the stellar interior, a variety of physical profiles have been used. Some are very unlikely to bear much relationship to the actual profiles of the pressure and density present in the sun, but my first requirement for the models is that

they produce useful solutions in a gravitational sense. The astrophysics of their energy production and convection mechanisms, etc., can be refined at a later date! Right now, it is required to show just how viable a gravitational model conformal theory is — and that is what the models will set out to do.

Chapter 6

Numerical Results

A large number of numerical engines were created in the course of this project. Their purposes fell into three categories — first, the initial programs written for familiarisation with the methods and to establish what the capabilities of the software packages and methods might be. These were followed by simple engines designed to produce some initial data for later, more elaborate engines and to explore the behavior of the differential equations to be solved. Typically these engines operated over limited domains and were in terms of only one variable. Finally, the full problems were approached by programs of higher complexity which produce results in terms of as many variables as can simultaneously be solved for.

The first category of numerical engine need not be described in great detail, given the discussion presented above. Once some understanding of what the operating platforms and methods were capable of, a few programs were produced to test the vacuum solutions of general relativity and conformal gravity on a very local scale. These proved to work satisfactorily, so work progressed to solving systems for information where we did not already possess analytic solutions.

6.1 Exterior Solutions

The first candidate for serious numerical solution was the scalar field S. This field is well set up for numerical solution if reasonable data can be provided for the metric. The scalar field can be solved for through it's own equation of motion (2.8), which is nicely amenable to Runge-Kutta solution. The equation of motion is rewritten as a set of coupled first-order equations and boundary conditions are applied at the limb of the sun, integrating outwards.

The value of S at the boundary is not determined by any physical requirement. Instead, it is possible to normalise the scalar field such that it's value is one at

the limb of the sun. All this requires is a redefinition of the constant λ, which is of undetermined (though expected to be very small) value — so scaling it by another undetermined constant is not an issue.

This leaves the initial slope of the scalar field. The hydrostatic equilibrium equation can be formulated in the standard metric with a scalar field (2.11), and data at the limb of the sun can be provided to a reasonable approximation given that the stepsize of the integration we are to perform is suitably large that the photosphere can be considered to be the exterior limit of the sun. Under this approximation, data can be provided from models of the photosphere [39] for pressure and density. On the length scale of a Runge-Kutta extending multiple solar radii, it can be taken that the photospheric data is at the edge of the sun where the exterior solution to the field equations must match the internal solution. Therefore, the values of the metric fields can be approximated from the usual Schwarzschild (or conformal vacuum) solution. Combining this data gives a rough upper limit for the initial scalar field gradient, which is of order $10^{-14}\mathrm{m}^{-2}$.

This value can be refined if more information about large-scale scalar field effects is provided. In this case, we could decide to produce a scalar field capable of reproducing the unmodelled acceleration of the Pioneer spacecraft. By use of the coordinate acceleration equations derived above (3.7), it can be determined that the scalar field should have a gradient of order $2 \times 10^{-26}\mathrm{m}^{-2}$ in the region 30-60 AU. The initial gradient can be adjusted iteratively to produce a far-field value of this order.

The S field equation was found to produce a robust Runge-Kutta system, capable of extension to large radius without introduction of large roundoff or computational errors, and tolerant of a reasonable range of it's parameters (the initial gradient and the constant λ). The equation was initially formulated in the standard (Weinberg) metric, and exterior vacuum solutions were used as the initial approximation for the metric fields. In the standard form of the metric, this means that $a = 1/b$ and $b(r) = 1 - \frac{\beta(2-3\beta\gamma)}{r} - 3\beta\gamma + \gamma r - kr^2$ (2.3), where both γ and k are very small or zero.

It was found that the behaviour of the S field matched up very well with expectation — the field takes apparently asymptotically rising form, rapidly approaching a near-constant value and having a small gradient everywhere in the exterior region. The behaviour of the S field is not very sensitive to any conformal deviations of the metric field from the GR Schwarzschild solution —

for any reasonable values of the linear coefficient γ, the solution for S is modified only very slightly. Similar effects are noted for the quadratic coefficient k, which is limited to be of magnitude approximately 10^{-40} m^{-2} or less — values many orders of magnitude smaller still are reasonable for this de Sitter background-like term. In fact the scalar field does not rely upon the presence of a non-standard metric field for it's generation, and is still generated in the same form for the usual Schwarzschild metric field. This would mean that even if the metric is entirely as it is found to be from standard gravitational theory, a scalar field coupled to gravity that provides a mass scale for dynamical mass generation can still be produced and have gradients — in fact, it would appear that a constant scalar field would be much more unlikely.

The quantities that the scalar field is sensitive to are the self-coupling constant λ and it's own initial conditions. The self-coupling term in λS^3 provides very strong accelerations in the scalar field - that is, it produces very rapidly increasing gradients that increase faster the larger S gets (for positive λ). Essentially, if the value of λ is too large then at some critical radius the scalar field will start to grow unboundedly, heading for infinity at an ever increasing rate. This would not seem very physical, after a long placid run of near-constant value with an asymptotically vanishing gradient! These considerations lead to λ adopting a very small value, of order 10^{-42} or smaller. This is also borne out by possible cosmological arguments which would link the self-coupling constant λ with the cosmological constant Λ, thus linking λ with cosmological distance scales [31].

The sensitivity to the initially supplied gradient was found to have quite a useful form. The variation of the scalar field tends to proceed in much the same fashion and over much the same magnitude range for reasonable values of the initial gradient — that is, plots of the scalar field show essentially identical curves for different initial gradients, except shifted in magnitude, and with only a small variation in the actual range of values covered in any one run. The value of the field gradient at the far end (a scale of 40 AU used for the large-scale runs, in general) was found to be approximately $6-7$ orders of magnitude below the initial value. This rule of thumb allowed rapid determination of an initial gradient that would reproduce the Pioneer acceleration in the outer solar system, a value which turned out to be around $2 \times 10^{-18}\mathrm{m}^{-2}$.

Here are some plots of the first half an astronomical unit of the large-scale plot (figures 6.1, 6.2). The integration can be carried out successfully across the

entire solar system, with only the first half AU range being shown for clarity. The scalar field is shown as a difference from one to show up the structure of the solutions. Note the rapidly asymptotic behaviour — the scalar field assumes a near-constant value very rapidly, with a very small gradient that varies slowly at large radius. The behaviour of the scalar field is in good accord with what was predicted earlier in the restricted analytic solution (3.11), and the variation in the field is suitably small so as not to disturb the successes of the standard theory.

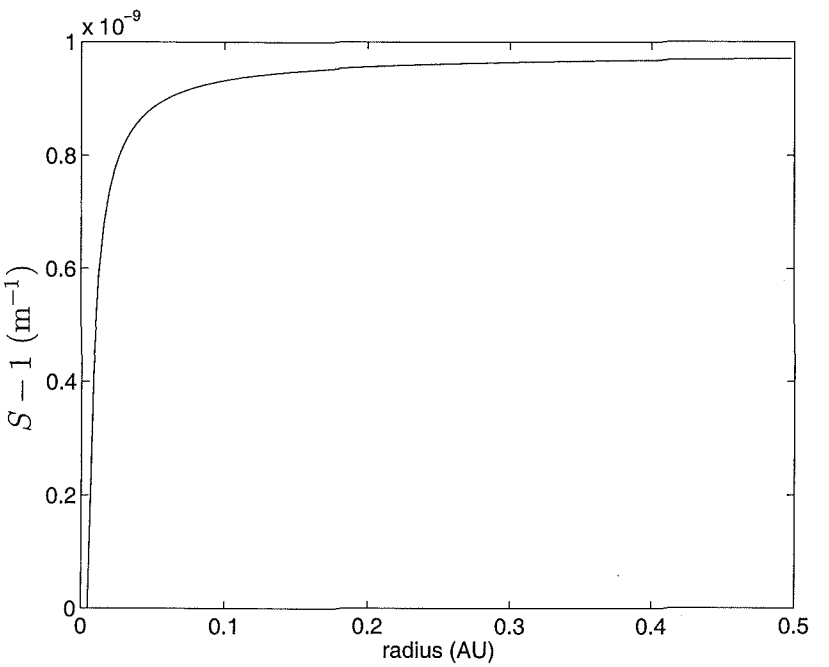

Figure 6.1: Exterior Scalar Field

The next problem to be investigated was the compatibility of this newly produced scalar field with the vacuum solution to the conformal field equations. With a nonzero scalar field, the energy-momentum tensor will be nonzero, and the field equations will not represent a vacuum system. Thus the metric coefficients could then potentially have particular solutions as well as homogeneous solutions of the field equations, affecting their value and therefore changing the coefficients in the scalar field equation of motion. Given that a metric field significantly different from Schwarzschild would be unacceptable in the local solar system, some sort of compatibility test for the metric field with a nonzero source from the scalar field was in order.

To perform this test a numerical method that could handle variation of an

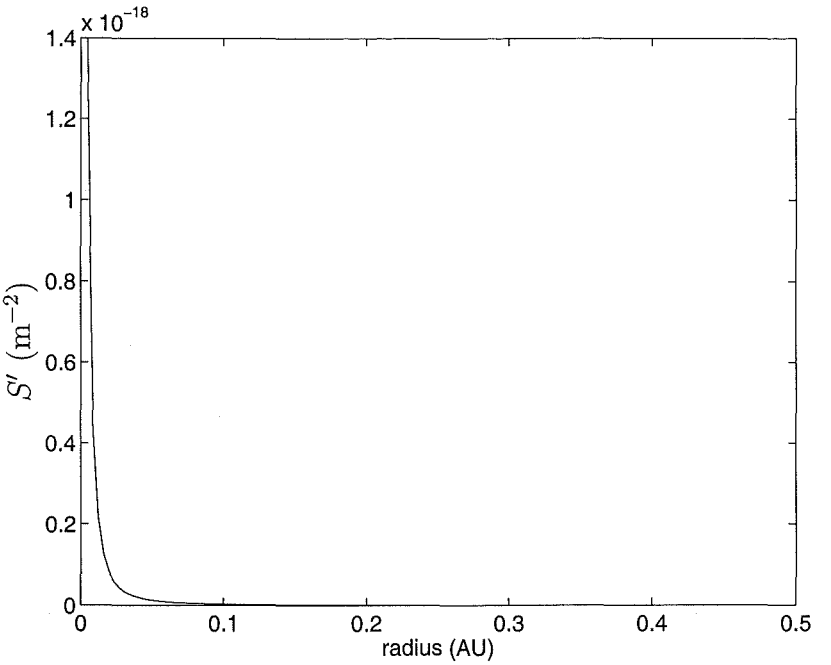

Figure 6.2: Exterior Scalar Field Gradient

existing solution (Schwarzschild exterior solution) with the presence of a small perturbation in the source was required. The Newton-Raphson finite difference method is well suited to such a case, as the solution to the non-vacuum field equation for small source should be very much like the vacuum solution, and if it were not found to behave similarly then that would be a strong negative mark against the theory anyway. Another advantage of the Newton-Raphson method is that it uses data on an evenly spaced mesh of points, so a fixed stepsize Runge-Kutta integration for the scalar field can provide the data very simply.

The test was performed using the standard metric with the assumption that $a = 1/b$, either from conformal transformation or to a good approximation. The range of the test was not large — a few solar radii. This was due to the constraints of the methods being employed at the time, and also covered one of the more important areas, that where the metric fields are varying most strongly. A fixed-stepsize Runge-Kutta integration and the Schwarzschild solution provided data for the initial scalar and metric fields, respectively. The Newton-Raphson method was then allowed to iterate on this system to solve the radial field equation with the presence of a source.

It must be noted that there was one parameter, α, which as yet had no good information regarding it's magnitude (or even sign!). At best, it was desired that

α be reasonably large so that any undue effects that might arise from a non-zero source would be washed out by this overall constant, which multiplies the denominator (2.2) and therefore reduces the magnitude of the source. However, the normalisation of the scalar field can be absorbed into alpha such that the source terms contain a scalar field of order one. The Runge-Kutta iterations would then suggest that the source terms arising from λ and the derivatives of S would be of small magnitude anyway — order 10^{-26} or smaller. With a source of this magnitude, α does not have to be large to prevent the metric fields leaving their vacuum solutions. The first compatibility tests of the kind being discussed were performed before a thorough scaling of α (or S) had been made possible, and were performed on data derived using photospheric limits on what values the scalar field could assume. Later, once some idea of the magnitude of acceptable values of α had been determined, these values were substituted back into the consistency testing program to improve it's connection with the rest of the numerical programs. The results were essentially unchanged by this alteration of the parameters.

The results of this compatibility test were strongly encouraging. Even with a value of α such as one, the metric field b was not significantly changed from it's initial state, and the residuals of the field equations were very small. In a typical run, the value of b would be altered by fluctuations of order one part in 10^{14}, and these variations were observed to oscillate in an essentially random manner around the initial vacuum solution. These are very small effects on the scale of the Schwarzschild solution, which would take the value $1 - 10^{-13}$ at a radius of around 10^{16}m — a distance of about a light year, and far outside the solar system. The residuals to the field equations took values of order 10^{-45}. If the source terms were removed, by setting the scalar field equal to zero throughout the domain, then the vacuum solution was returned exactly, with residuals again of order 10^{-45}, for $\alpha = 1$. This check against the known homogenous solution gives strong confindence in the results of this method.

In fact, it turned out that the variation of b was only strongly sensitive to the self-coupling constant λ. The initial runs, which had only an approximate scale for the values of α and S, were made with larger values of λ than would be permitted with the improved S field Runge-Kutta integrations that were subsequently made. Once the smaller values of λ were used, the variation of b dropped below levels comparable to the machine accuracy.

This engine was extended to allow the scalar field to also vary to suit solution of the radial field equation and the S field equation of motion. The Newton-Raphson method was extended to use two variables in two equations, and both fields were allowed to vary. The results were almost unchanged — the metric field fluctuated by a similar amount as above, order 10^{-14}, and the scalar field was also perturbed by amounts of this order. The residuals were comparable to those obtained in the previous result. The perturbation in the metric field showed no correlation with radius, the fluctuations were essentially random and show no trend with the number of iterations (figure 6.3).

The scalar field, when allowed to vary, showed a more distinct trend (figure 6.4). The value was unchanged at the interior end of the domain but had an increasing negative trend with radius, flattening off with increasing radius. This could be due to the effect of the variation in b absorbing some of the effects of the scalar field, such that S does not have to vary as strongly. These effects are reduced for larger values of α, which also gives smaller residuals for the Newton-Raphson.

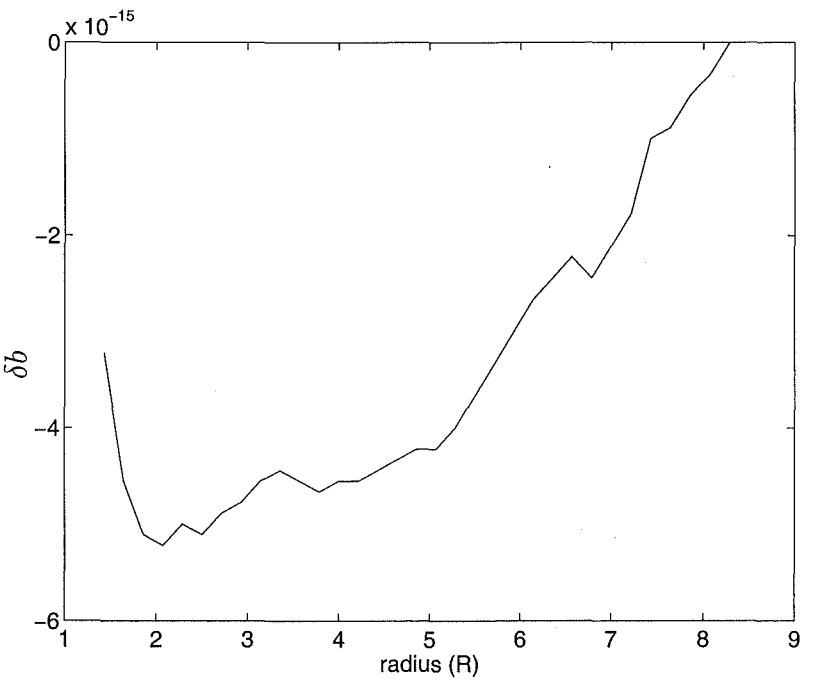

Figure 6.3: metric variation δb

Given that the scalar field does not appear to perturb the metric field far from it's vacuum values, the next field to investigate is the conformal metric coefficient $\bar{a}$. In the conformal metric, this coefficient has the useful relationship to the

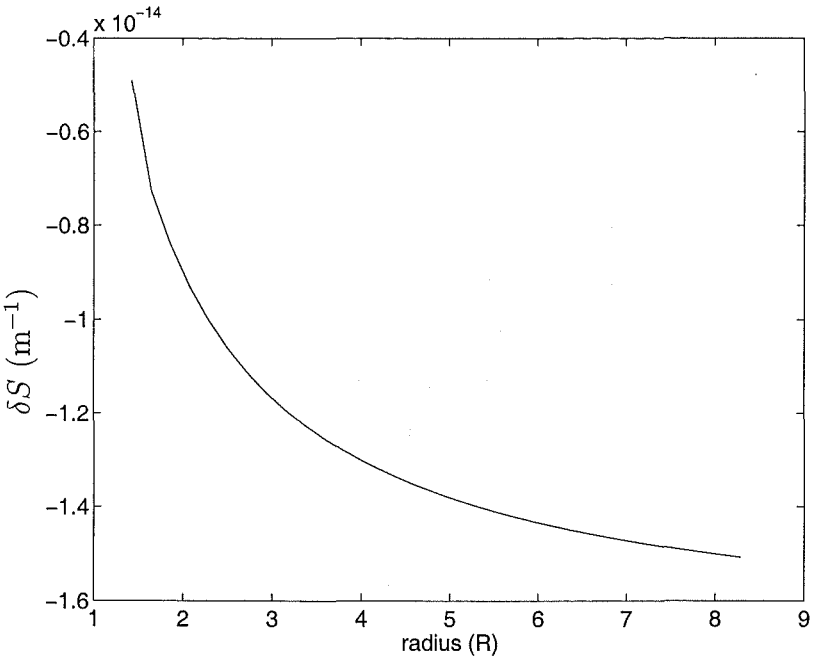

Figure 6.4: scalar field variation δS

standard coefficients that a value of $\bar{a} = 1$ corresponds to a standard metric in which $a = 1/b$. As this is an assumption, or provided by conformal transformation in the exterior solution of the conformal field equations, a solution found for $\bar{a}$ which has any value differing from one has a direct correlation with how closely $a = 1/b$ is obeyed in the standard metric — or if you like, how much the conformal solution differs from usual Schwarzschild spacetime.

As we expect the conformal metric to closely resemble Schwarzschild, that would have the immediate consequence that the value of $\bar{a}$ should be close to one. A reasonable assumption for the large-scale behaviour of $\bar{a}$ for a central-body problem is that $\bar{a}$ asymptotically approaches one with increasing radius. What behaviour it might have interior or near the limb of the sun is more difficult to predict, though through compatibility with the Schwarzschild solution, values of $\bar{a}$ less than one are more favoured than those greater than one. If $\bar{a}$ were to assume a value greater than one, it would be difficult to produce the standard metric fields a, b with their usual behaviour with regard to magnitude greater or less than one.

The procedure adopted to produce some starting values for $\bar{a}$ was to first produce a first order differential equation for $\bar{a}$ from the field equations. The radial field equation was solved for $\bar{a}'$ - this introduced a potential ambiguity of

sign through a square root term, however a little investigation of the terms shows that one sign would cause large gradients in $\bar{a}$ even without source terms in S and b, as this would seem unphysical this solution was disregarded in favour of the solution with the opposite sign. This resulted in an equation in terms of the scalar field and it's first two derivatives, and the metric coefficient $\bar{b}$ and it's first three derivatives. If $\bar{b}$ was assumed to be a solution of the vacuum equations to good order, then the equation could be reduced to being in terms of only the first derivative of $\bar{b}$.

It would be desirable that the metric be close to a vacuum solution for methods of this kind to work. The field $\bar{a}$ only has derivatives introduced through the source terms in $T_{\mu\nu}$, all of which are scaled by the inverse of the coupling constant α. When the field equation $W_{rr} = \frac{1}{4\alpha}T_{\mu\nu}$ is solved for $\bar{a}'$, the constant α multiplies the whole of the left hand side of the equation. This means that if the left hand side is non-zero, then any deviation from a vacuum solution produces gradients in $\bar{a}$ proportional to $\alpha^{\frac{1}{2}}$. If α is at all large, then these contributions will dominate severely, producing large gradients in $\bar{a}$ and letting this conformal scale take values far from one. In this case, the spacetime metric would be far from Schwarzschild — which would not fit our requirements. A large value of α, however, is just what is needed to make solutions of the conformal field equations close to vacuum solutions. The best resolution to this situation is that regardless of the actual magnitude of α, $\bar{b}(r)$ should be close to a vacuum solution, and that α be not too large in magnitude.

With a differential equation for $\bar{a}$ in hand, it remained to find an appropriate method with which to solve the equation. The first useful method used was a predictor-corrector extrapolation. This had the advantage of being able to operate on data provided on a grid, and being able to iterate from some initial conditions to an unknown final condition, combining some of the features of both Runge-Kutta and Newton-Raphson methods. The iteration could be started at some large distance in which the $\bar{a}$ field is presumed to behave very closely to the asymptotic behaviour. An initial field could be provided with a value of one at the outer few mesh points, and derivatives calculated there, and the method then allowed to extrapolate the fields inwards with the exact data for the b and S fields previously produced specified on the grid.

The results were encouraging — the method performed well, with no problematical points or numerical difficulties. The $\bar{a}$ field was found to behave much

as anticipated — it remained very close to the value of one in the far field, only deviating from this value near the source, where it decreased quite steeply towards the limb of the source. Turned around, the field was found to rise quickly from it's initial value at the limb of the source and rapidly approach an asymptotic value of one. However, the method could not be entirely relied upon for numerical values as when the method was operated in the absence of a source, extrapolation errors contributed to a minor perturbation on what should otherwise be a constant field. Essentially, truncation errors introduced a zero error in this method, so that it could only be used to show differences between values and not to provide absolute values — for example, the trend for the $\bar{a}$ field to decrease strongly at the limb with increasing source mass was readily apparent.

This method thus gave pointers to what kind and magnitude of values could be expected for $\bar{a}$ near the limb of the sun, but not with reliable numerical value. This led to consideration of a Runge-Kutta method. In this case, the S field would have to be solved for simultaneously as the method requires values for its source fields at points in between the final mesh spacing. As this is the way the methods should be heading, that is to concurrently solve for all the fields so that at every stage the extrapolation for one variable involves the current best value of it's source terms, this was no hardship. The Runge-Kutta method was set up to run from large radius inwards to the limb of the source, starting with an S field matched up to the results of the outwardly iterating S field Runge-Kutta above.

This time, the results were very acceptable. The original initial conditions for S were returned to a reasonable accuracy (consider that the original integration for S considered $\bar{a} = 1$ to hold everywhere), and the $\bar{a}$ field was returned with the same behaviour as indicated by the predictor-corrector method. Also, the scalar field was regenerated in the same configuration as before. However, if the source were removed then a constant $\bar{a} = 1$ field was generated everywhere, as to be expected for empty space. The numerical results of this method can be used with a much higher degree of confidence. Again, only the first part of the domain of integration is displayed for clarity of presentation (figures 6.5, 6.6).

The predictor-corrector method could also be used with non-analytic data for the field $\bar{b}(r)$, that is a vector of the field values that has been previously generated. This allowed some testing of compatible metric fields, and some idea of just what magnitudes are allowable for alpha when the metric field does

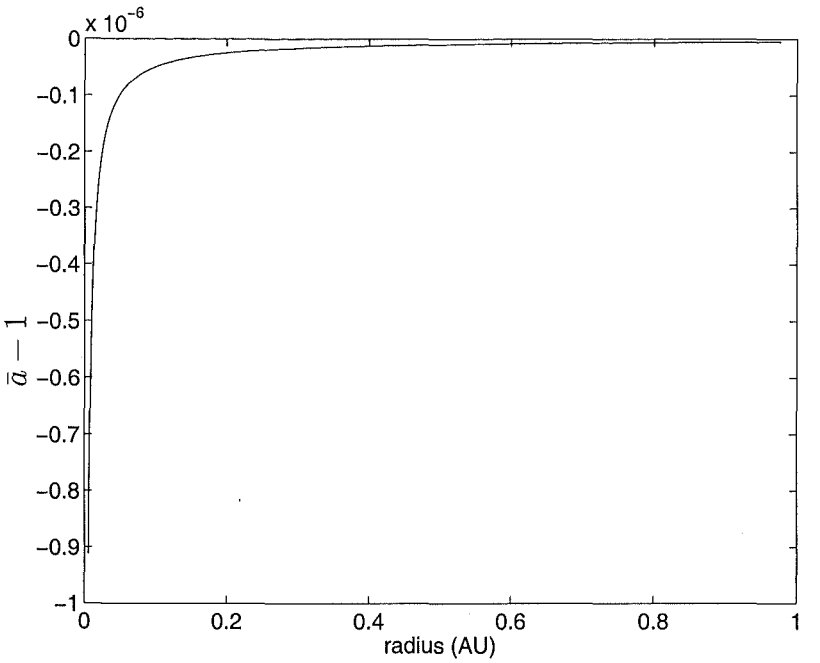

Figure 6.5: $\delta\bar{a}$ field - Runge-Kutta method

not well satisfy the homogeneous field equation. This program produced results as expected — if the metric field were allowed to vary from the homogeneous solution, then a large magnitude of α directly multiplied that effect into a large deviation in $\bar{a}$. At this stage, without an exterior solution for $\bar{b}$, the utility of this program was limited.

At this stage, a solution for $\bar{b}$ needed to be found for the non-homogeneous case. This required a better estimate of the value of α than the previous methods could furnish us with — the S field equation does not involve α, and solving for $\bar{a}$ has only told us that the magnitude of the difference of $\bar{b}$ from it's homogeneous value must be inversely related to α somehow. In order to get a good value for α, the radial field equation would have to be solved in the presence of stronger source to match a specific boundary condition. This can best be done by considering an interior solution.

6.2 Interior Solutions

The interior solution presented a more daunting problem at first, as there would be more fields to worry about (pressure, density) and many simplifying assumptions could be unlikely to be valid — certainly, assuming S is constant (or $\bar{a} = 1$)

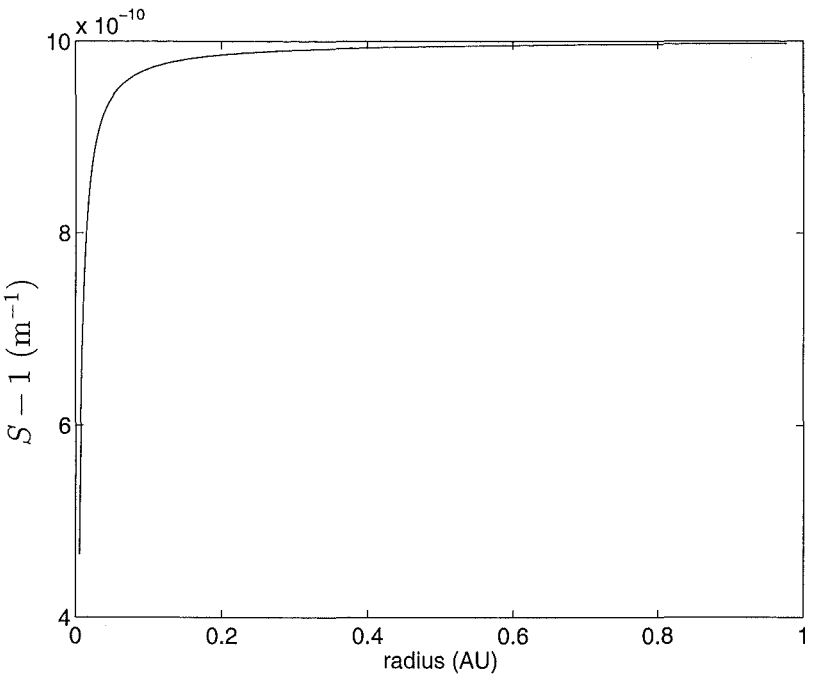

Figure 6.6: δS field - Runge-Kutta method

is a strong constraint in the interior, where we do not have any evidence to support these propositions, and where the source terms for the field equations can depend strongly on these quantities. These simplifications should still be considered, if only as providing test cases for the fuller solutions. The experiences gained in the earlier programs allowed interior solution methods to have certain flexibility about what equations and variables were to be considered simultaneously, which made development of consistent and reliable programs more rapid.

From the start, it was apparent that many quantities would have to be solved for, preferably simultaneously — though if differing methods of solution were more appropriate for different variables, a self-consistent approach of altering one variable at a time whilst holding the other constant and iterating was also considered. The most significant variable to solve for is the metric coefficient $\bar{b}$, and in order to solve for this quantity source terms must be obtained — which are in terms of p, S, and $\bar{a}$, when using the radial field equation. Even if assumptions are made to remove $\bar{a}$ or S from the equations, it is still necessary to be prepared to consider cases where S was not constant or $\bar{a}$ not one, and p has to be provided somehow in all cases.

Defining the pressure (or density) is not as straightforward as it might seem to be. For a start, the source for the metric coefficient $\bar{b}$ involves the pressure, but

in many treatments of stellar modelling it is the density that is provided, as the pressure would depend upon the temperature as well as the particle distribution. Ideally some kind of equation of state should be determined, so that knowing one or the other of these physical quantities is sufficient. Also, the pressure and density we are using in the conformal field equations are not necessarily simply related to the usual pressure and density. The pressure and density in the field equations are found by an averaging process over the kinetic energy terms of the generic fermion field Ψ [19], so are more closely related to number density than mass density. If the average particle mass is known then this can reduce to the same information, but we are dealing with a system incorporating dynamical mass generation, so the particle masses, provided by the $hS\bar{\Psi}\Psi$ term, could depend upon position through S.

As it turns out, a little dimensional analysis can show the relationship between the field equation number-type densities and pressures and the usual kinematic ones. The conversion between quantities is scaled by the absolute magnitude of the scalar field, which was normalised out of the equations and into the undetermined constants of the theory. Therefore, the density coefficient can be related, for a specific value of α, to the magnitude of the scalar field S_0. This means that a range of orders of magnitude can be trialled for the physical quantities, as their relationship to the observable values is scaled by S_0, a parameter of the theory. The density coefficient in these equations is not constrained to match the observed density until S_0 is specified, or more generally (in practice) the value of S_0 is specified by matching the density coefficient and the observed density for a specific value of α.

It remained to provide either one of pressure and density and an equation of state, or to provide both. Some kind of physical model must be assumed in either case. The initial models trialled followed the methods of treatment in standard theory — start from a constant density model, and move on to more likely algebraic profiles, to models more directly derived from the equations. These models incorporated a density specified as an algebraic expression, and pressure was either provided similarly or derived using the hydrostatic equilibrium relation. The use of the hydrostatic equilibrium equation to solve for pressure depended on whether this equation was required to provide solutions for any other variables — it is also a good candidate for solutions for $\bar{a}$.

These models were successful, producing fields for $\bar{b}$ and S for given density

and pressure profiles. They could also be programmed to recalculate pressure as they progressed through the domain of integration, updating it via the hydrostatic equilibrium equation to account for the newly generated values of the fields, and this process could then be iterated. The results were encouraging but did not at this stage allow for the possibility of variable S and $\bar{a}$ fields simultaneously. The goal became a system that could take a specified density and pressure and solve for both metric coefficients, and the scalar field, all at once.

6.2.1 Full Interior Solution

A program capable of solving the three-variable interior problem was eventually produced. This new program performed a Runge-Kutta extrapolation in terms of all the variables, with pressure and density specified as functions across the interior space, scaled by their central values. It was also made possible to turn the governing differential equations for the different fields on or off independently, which turned out to be a vital consideration for getting the program to operate, and also allows very simple imposition of the simplifications $\bar{a} = 1$ and $S = S_0$.

The three differential equations used to extrapolate out the behaviour of the various fields (in the initial version) were the radial field equation, the S field equation of motion, and the conformal hydrostatic equilibrium equation. Both of the latter two equations can be subsumed by the covariant conservation of the energy-momentum tensor, $T^{\mu\nu}{}_{;\nu} = 0$. However, the S field equation of motion can be derived independently, and the difference of the two equations gives the hydrostatic equilibrium equation.

The parameters that this engine depends upon are the constants of the theory α and λ, the central pressure and density, and the initial values of the fields and their derivatives at $r = 0$. Derivatives need only be provided to first order for $\bar{a}$ and S, and to third order in $\bar{b}$. However, due to regularity conditions nearly all the values and derivatives of the fields are already specified — all the first derivatives must vanish, $\bar{b}$ must equal one, S can be normalised to one, and the second and third derivatives of $\bar{b}$ must also vanish. This leaves only the initial value of $\bar{a}$. In order for the solution to be realistic, the initial value of $\bar{a}$ must be close to one. Ideally, the value of this parameter should be specified by the physical properties of the source, that is the total mass and it's distribution, and in an analytic solution it may be possible to extract this data from the beginning. Without that information, it is still possible to restrict the value of this parameter

- the behaviour of the $\bar{a}$ field is strongly dependant on it's initial value, and must fit in with what is required at the limb of the source. Additionally, λ is not free to take large values due to it's exterior contributions, and is restricted to values that are sufficiently small as to have a very minor effect interior.

The behaviour of the full differential system for all three variables, the metric coefficients $\bar{a}$ and $\bar{b}$, and the scalar field S, turned out to be more complex than expected. There is a very strong connection between the gradients of the $\bar{a}$ and S fields through the scalar field equation of motion and the hydrostatic equilibrium equation (or alternatively, through the covariant conservation of $T^{\mu\nu}$). Almost inevitably, a gradient in one of these fields leads to a corresponding gradient of the opposite sign in the other field, up to areas of strong driving behaviour in the remaining fields $(\bar{b}, p, \rho)$. This meant that solutions to a system solving for only two of the variables need not necessarily be that close to a solution when all three are considered. For example, a solution for $\bar{b}$ and S produces mild gradients in both fields, assuming $\bar{a}$ is equal to one. If $\bar{a}$ is included with the same parameters, it is quite likely that the initially small gradients in S will drive gradients in $\bar{a}$, which in turn lead to stronger gradients in S than were earlier observed. The now-varying $\bar{a}$ field also leads to differing behaviour of the metric coefficient $\bar{b}$, though to a much lesser degree than it does in the S field.

The most vital fact to get out of this is that because of this strong connection and potential feedback system, there are many combinations of parameters (central density, α, etc.) which lead to unstable solutions — gradients in one or another of the fields race off to infinity. These can be rejected physically, but the allowed domains in parameter space are difficult to determine — an inadmissable value for α at some central density might well be allowed if the density is changed. There are also solutions which become unstable in the midst of regions of apparent stability, which unfortunately suffer from some numerical instability for particular values of the parameters. The exact combinations that contribute to this kind of behaviour are also difficult to determine in general — a wide range of possible parameter values must be trialled. It is possible that more than one combination of parameters, for a given profile of pressure and density, could match the boundary conditions. This ambiguity can be reduced to some degree when α is further constrained to take values compatible with the exterior solutions.

Also, the behaviour of the fields was not always as expected. The exact be-

haviour of the different fields depends strongly upon the initial pressure and density profiles provided. Most significantly, the pressure gradient and the pressure-density ratio have a strong contribution to the magnitude of the $\bar{a}$ field gradient (which in turn strongly influences the gradient in S). The gradient in $\bar{a}$ tends to produce an absolute range of value in the $\bar{a}$ field that is significantly larger than what might have been initially expected — for example, in the general relativistic solution of a constant density model, the range of the metric coefficient b is $0.9999936 - 0.9999957$, and the range of a is from $1 - 1.000004$, a range of 0.01%. For a typical early solution of the conformal interior problem, with a central pressure of order $3 \times 10^{-17} \mathrm{m}^{-4}$, the range of the field $\bar{a}$ is from $0.873791 - 0.999998$, that is a range of around 14% of its central value. The outer limb value matches nicely with the exterior requirements that $\bar{a}$ take a value very close to one, but the central value is very far from this — given that the central value of $\bar{b}$ is to be one for regularity, and that at the origin $b \to \bar{a}^2\bar{b}$, the central value of the metric coefficient b would be approximately 0.763 — very different from the intuitive picture we came in with from standard theory. Significantly, the field $\bar{a}$ is often the major contributor to producing a value for b that matches up with a Schwarzschild-like boundary value.

This kind of behaviour provides further realistic constraints on what values the parameters can take. Though solutions like the above may be acceptable solutions as far as the boundary conditions are concerned, they are physically disconcerting. Different values of the physical parameters can produce more acceptable solutions, both in terms of the realism of the physical distribution of the source and in terms of the resulting metric coefficients.

The ratio of pressure to density turns out to be a significant quantity in controlling what solutions come out to be reasonable. This, combined with the initial value of $\bar{a}$, the coupling constant α, and the limb values of the physical quantities (assuming they are not set to zero) are the most significant parameters for producing interior models that satisfy the boundary conditions, in approximate order of importance.

It turned out that the best initial guess for the pressure/density ratio, for systems where the pressure gradient is low, is 1/3 — exactly what would be the case in standard theory for ultra-relativistic particles. This is the value that would correspond to the fermion sector of the energy-momentum tensor being traceless, in the absence of a varying scalar field. This is an interesting result

in it's own right, as in the literature the most common case considered is for a constant-valued scalar field, requiring the fermion sector to have exactly this value for tracelessness, irrespective of the energy the particles might have [15]. The solutions obtained using the numerical engine with variable scalar field do not have $\rho = 3p$ as in the constant S case, but have some variation from this value, representing the part of the tracelessness requirement that is being met by the interactions with the non-constant S field. The magnitude of this variation depends upon the structure of the pressure and density fields - for constant or near constant values, ρ is closer to $3p$. As the fields are made more realistic, the variation in ρ increases.

The initial value of the field $\bar{a}$ is also a crucial parameter for the theory. This parameter has a strong influence on the character of the solutions that are produced. Given that $\bar{a}$ is expected to be near one at the limb, it would be expected that deviation far from one could be adjusted for by using $\bar{a}(0)$ as a shift parameter, at least to some degree. This was in fact found to occur on a coarse scale, but the exact value of $\bar{a}(0)$ also influences the gradients that are generated in all three fields $\bar{a}, \bar{b}$ and S. This means that the fine adjustment of $\bar{a}(0)$ to match the required $\bar{a}(R)$ influences the other boundary values, particularly the value $S(R)$. In addition, the field gradients can be so sensitive to $\bar{a}(0)$ that a slight shift in this value reverses the signs of one or more of the gradients in the fields — and this trend tends to remain across the entire domain.

The effect of $\bar{a}(0)$ on the gradients produced is such that lower values of $\bar{a}(0)$ produce an increasing gradient $\bar{a}'(r)$, which tends to continue across the whole domain, and higher values of $\bar{a}(0)$ lead to decreasing gradients in this field. Typically the gradients of $\bar{b}$ and S are of the opposite sign to that of $\bar{a}$. The region of values that $\bar{a}(0)$ could take to give an approximately constant $\bar{a}$ field, with near zero gradient, turns out to be a region in parameter space that is particularly unstable for the engine. Analytically, the cause of this effect has not been isolated. The value of $\bar{a}(0)$ that provides the turning point between a positive or negative slope $\bar{a}(r)$ curve depends upon the other parameters of the model, particularly α and p/ρ. These parameters also contribute strongly to the magnitude of the $\bar{a}$ field gradients, and generally the best agreement with the boundary requirements is achieved with an $\bar{a}$ field that is very close to constant — which often results in a model that is very close to unstable.

The effect of the limb values of pressure and density is a little harder to

quantify. The model can be quite sensitive to these quantities vanishing, depending on the pressure and density profiles being used. What can happen is that with vanishing limb values, the derivatives of the metric coefficients tend to take anomalously strong, sudden gradients near the limb. These effects were most noticeable in the scalar curvature, which can suddenly 'bow' up from a near constant, small negative value, with a Gaussian-like addition near the limb. With zero limb values, the scalar curvature tends to have a steep drop at the limb, but not to change sign, or have derivatives which are changing sign. For this reason, photospheric-type nonzero limb values are often chosen for these quantities rather than a 'hard' boundary condition of zero. The magnitude of the effect that the limb values has on the solution depends on the pressure and density profiles used, for example some of the Lane-Emden profiles used performed best with a boundary condition given by the usual polytrope relationship with no boundary adjustment, whereas for model functions of trigonometric derivation, lower (or zero) limb values performed badly.

This kind of contribution to the scalar curvature does not seem physically desirable. In fact, it would be considered desirable to have the scalar field maintain the same sign everywhere in the domain of interest, which these types of results do not always allow. If the scalar curvature passes through zero then at that point the spontaneously broken symmetry that generates a nonzero value for the ground state of S for the mass scale breaks down. However, if the scalar curvature is passing through zero at a point where the S field has gradients then the standard symmetry-breaking ground state methods do not hold, as these are designed for a field without gradients — if the field has gradients at this point, then it is not in the ground state. If a conformal transformation is made that brings the scalar field to a (locally) constant value, removing the gradients at that point, then by the equation of motion (2.8) the scalar curvature assumes a constant value at that point. Consequently the scalar curvature cannot vanish for a constant, nonzero scalar field. Therefore, it is permissible for the scalar curvature to pass through zero so long as the scalar field is not constant, and nonzero.

It is also important to note that the scalar curvature is not a conformal tensor. That is, a conformal transformation applied to the metric changes the scalar curvature by a non-trivial relationship involving derivatives of the conformal transformation function Ω. The immediate consequence is that a zero value of

the scalar curvature is not in general invariant under conformal transformations, as might be used to reduce the scalar field to a constant value. This can be easily seen from the conformal metric form of the scalar curvature:

$$R^{\alpha}{}_{\alpha} = \frac{(ab'' + 6a'b' + 6a''b)\, r^2 + (4ab' + 12a'b)\, r + 2ab - 2a}{a^3 r^2}$$

which manifestly has terms present in the conformal scale $\bar{a}$ and its derivatives. A conformal transformation used to bring $S(r)$ to a constant value will introduce an $\bar{a}(r)$ and thus generate a non-zero scalar curvature. This holds even at the origin, where the above expression reduces to

$$\begin{aligned} R^{\alpha}{}_{\alpha} &= \frac{6}{a^3}\left(a'' + 2\frac{a'}{r}\right) \\ &\Rightarrow 6\frac{a''}{a^3} \end{aligned}$$

and the scalar curvature is generated from the second derivative of the conformal scale $\bar{a}$.

In addition, these equations are all set up for a problem of a single body, with spherical symmetry around the origin. Some of the regularity conditions are relaxed if the problem is considered in Cartesian coordinates. The system does not consider any possible contributions to the scalar curvature or metric coefficients due to distant bodies or background curvature. These effects could be significant in a more complete treatment.

The limb values also directly contribute to the magnitude of the pressure and density gradients — the physical quantities have to get to these limits from their central value! The quantity with most impact on the solutions is the pressure gradient, which becomes a direct source for the $\bar{a}$ field through the hydrostatic equilibrium relationship (2.12). As can be seen from this equation, the pressure contributes through the term in $\frac{p'}{\rho}$, causing the $\bar{a}$ gradient to increase with the pressure gradient, scaled down by the density. This illustrates the overall importance of the pressure/density ratio, which tends to be more important than the absolute values of either pressure or density as the $\bar{a}$ gradient is also a strong contributor to the differential equations for $\bar{b}$ and S, which are sourced by the magnitude of pressure and density, respectively. Estimates of the ratio of boundary to central pressure and density can be worked out for the standard theory, giving boundary/central pressure and density values of order $10^{-(9-10)}\mathrm{m}^{-4}$.

The first physical model tested was for constant density, for comparison with the standard result and because it reduces the number of parameters we might

need to describe the system. Parameters for this system were quickly found to match up with the boundary conditions in $\bar{b}$ and S', so work immediately proceeded to something a little more realistic.

The first models to try to give some of the physical structure of a stellar body used trigonometric relationships to describe the pressure and density through the star. Profiles of the form

$$\begin{aligned} \rho(r) &= \rho_0 \cos^2\left(\frac{\pi r}{2R}\right) + \rho_0\rho_l, \\ p(r) &= p_0 \cos^2\left(\frac{\pi r}{2R}\right) + p_0 p_l, \end{aligned}$$

where ρ_0 and ρ_l represent the central and limb values of the quantity, proved to be particularly amenable to solution. The profiles and their derivatives are readily calculated, which is a consideration as profiles that are provided on a grid must contain more data points than any Runge-Kutta that is to be generated using those profiles. This is due to the step subdivision performed in the fourth-order Runge-Kutta method. Either the data must contain values at these subintervals or an interpolation is required, which tends to be inaccurate.

With physical profiles of this kind, solutions could be found that matched to the required boundary values of $\bar{b}$ and $\bar{S}$, had a scalar field that nowhere vanish, and had reasonable gradients in the $\bar{b}$ field. The parameters provided to match these conditions are generally quite sensitive, as has been described above — often the desired solutions are near an area of instability of the model. The particular parameter values used for this integration were:

α	6.0×10^{23}
p_0	$3.0 \times 10^{-17}\mathrm{m}^{-4}$
ρ_0	$(9.0 - 3.050888282) \times 10^{-17}\mathrm{m}^{-4}$
$\bar{a}_0$	$(1.0 - 0.1262092)$.

It can be seen that this simplified physical model meets the requirements, but goes through some intuitively unusual routes to get there. The main example is the scalar field gradient, which has obtained the desired value by virtue of having gone strongly negative and then evening off to a much smaller positive value. This requires quite careful fine tuning of the parameters to have the contributions cancel out nicely at the boundary, hence the very specific value of ρ_0 for the given values of the other parameters. Minute changes in the density or initial value of $\bar{a}$, particularly, can throw the agreement with requirements off very easily.

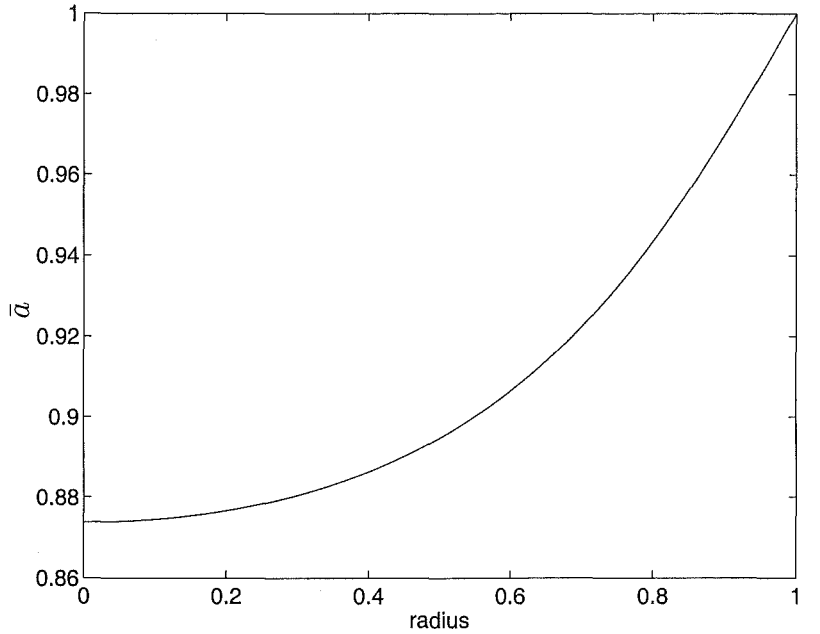

Figure 6.7: $\bar{a}$ metric coefficient, $\cos^2$ model

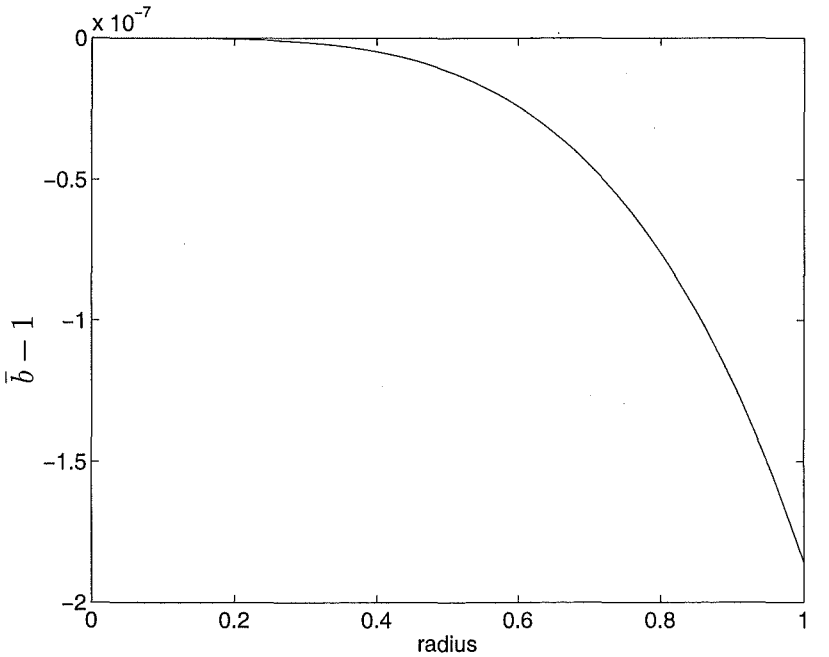

Figure 6.8: metric coefficient $(\bar{b}-1)$, $\cos^2$ model

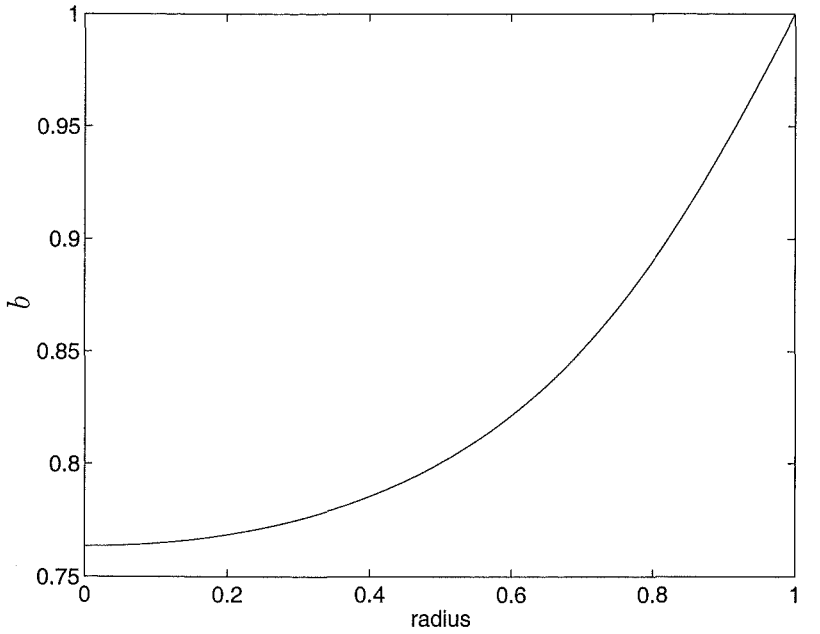

Figure 6.9: b metric coefficient, $\cos^2$ model

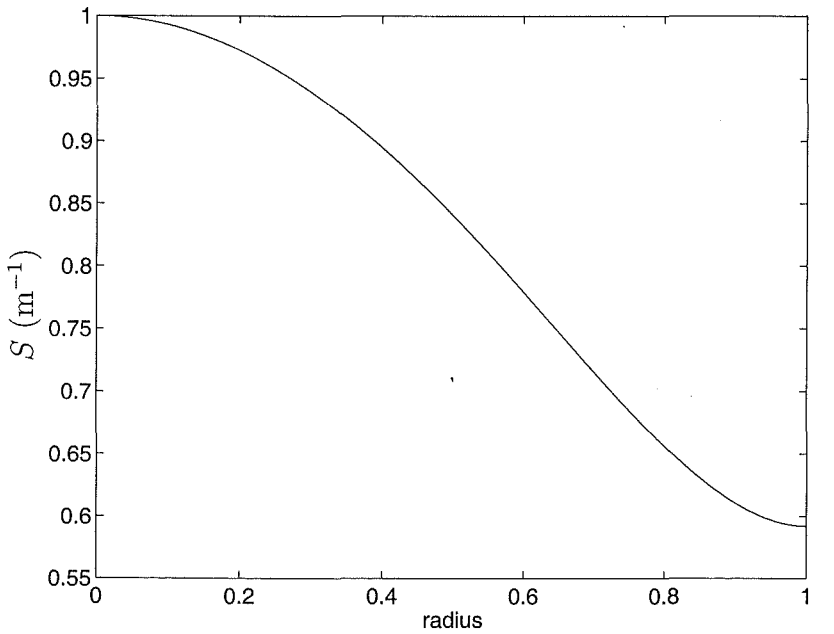

Figure 6.10: scalar field S, $\cos^2$ model

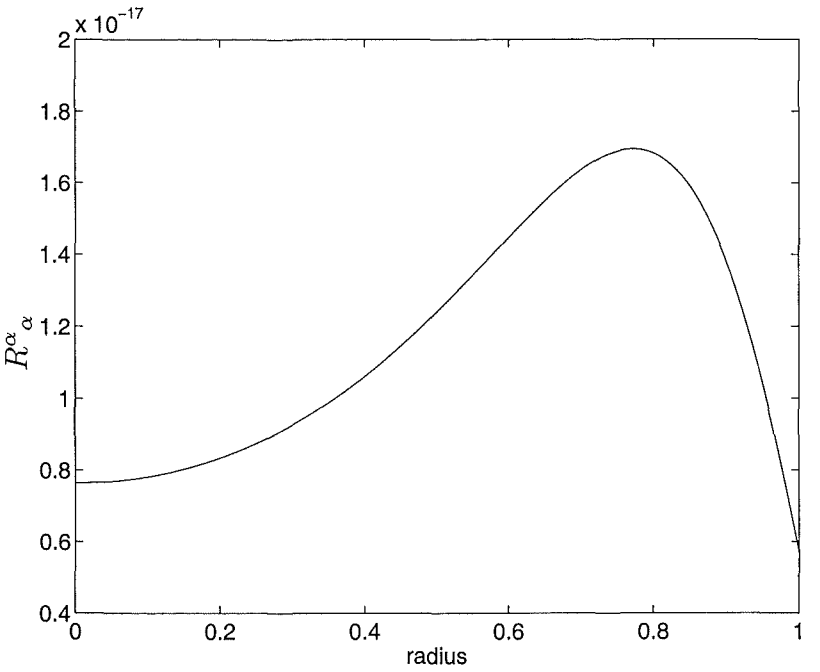

Figure 6.11: scalar curvature, $\cos^2$ model

Another factor of notice is the strong gradients in $\bar{a}$ (figure 6.7). Exterior, it would be expected (if the field is not conformally transformed away) that the value taken would be close to one. Interior, this is not the case and the strong $\bar{a}$ gradients produce large gradients in the b field as well. The contribution of the conformal scale $\bar{a}$ is much more significant than the conformal $\bar{b}$ metric coefficient in producing the required boundary value of the observable b field (figures 6.8, 6.9). The interior $b(r)$ field varies much more strongly than would be expected for a similar model in the standard theory. It is readily apparent that the gradient in $\bar{a}(r)$ is driving the gradient in $b(r)$ that is required at the boundary, as the gradient in $\bar{b}(r)$ is always of the opposite sign.

Here is an example of a solution using a more standard physical model, in this case a Lane-Emden polytrope of order 3/2. That this kind of physical distribution should hold with a conformal hydrostatic equilibrium equation is resting on the assumption that the solutions should not differ greatly from the standard treatment, and could well be unreasonable. However, it's a much better model of the physical properties than a trigonometric function, even if it is inexact. The parameters used in this model were

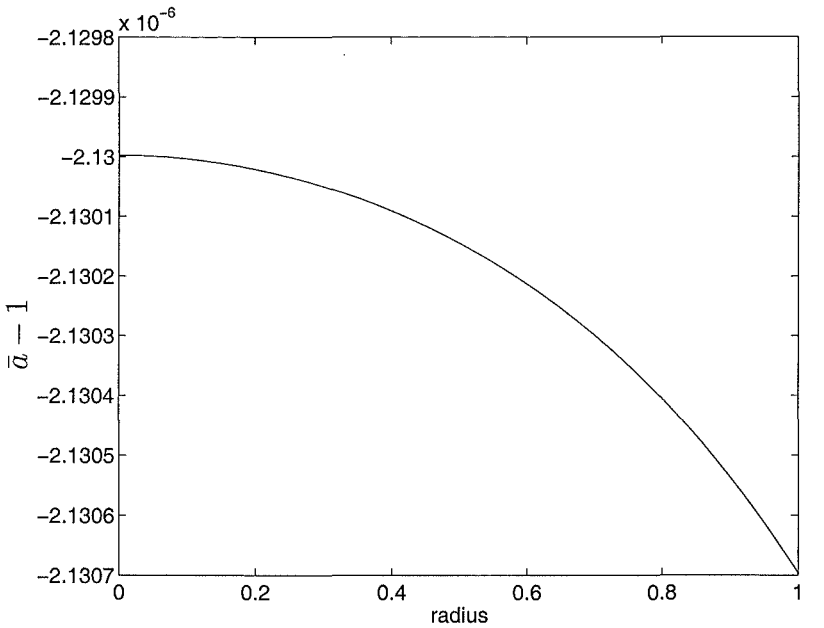

Figure 6.12: $\bar{a}$ metric coefficient, polytrope $\alpha \sim -10^{20}$

α	-5.80×10^{20}
p_0	$5.38856404 \times 10^{-44}\mathrm{m}^{-4}$
ρ_0	$1.9 \times 10^{-30}\mathrm{m}^{-4}$
$\bar{a}_0$	$(1.0 - 0.00000213)$.

Note the much greater difference in magnitude between pressure and density, compared to the earlier models with smaller gradients in these quantities. Also, there is a fundamental change in one of the coefficients — α has changed sign. The results of this integration give good agreement with the requirements for $\bar{b}(R)$ and $S'(R)$, and give a scalar curvature that seems to be consistently negative within the region that it is well represented.

The metric coefficient $\bar{b}(r)$ was found, to the accuracy of the numerical engine, to take the value one across the entire domain. In this solution the contribution of the $\bar{b}$ field to the matching of the observable $b(R)$ has been completely lost, and all of this matching is provided by $\bar{a}(r)$ (figure 6.12). This coefficient is also varying slowly, giving a very slow variation in $b(r)$ across the domain (figure 6.13). This is an interesting result, for if $\bar{a}$ were to be conformally transformed away, then the residual $\bar{b}(r)$ would closely represent flat space throughout the interior, with no possibility of matching to the standard exterior result. Potentially, if the S field cannot somehow be also reduced to constant (as is the current expectation)

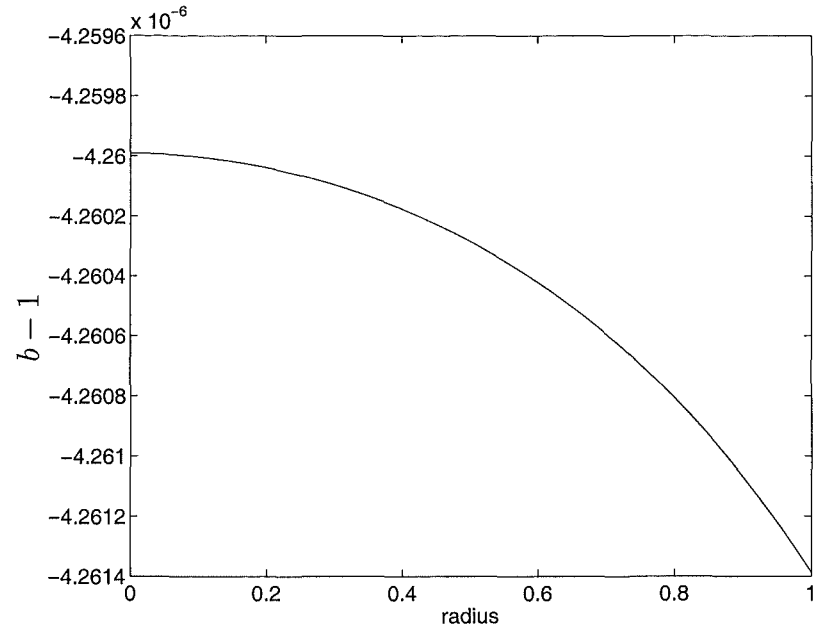

Figure 6.13: b metric coefficient, polytrope $\alpha \sim -10^{20}$

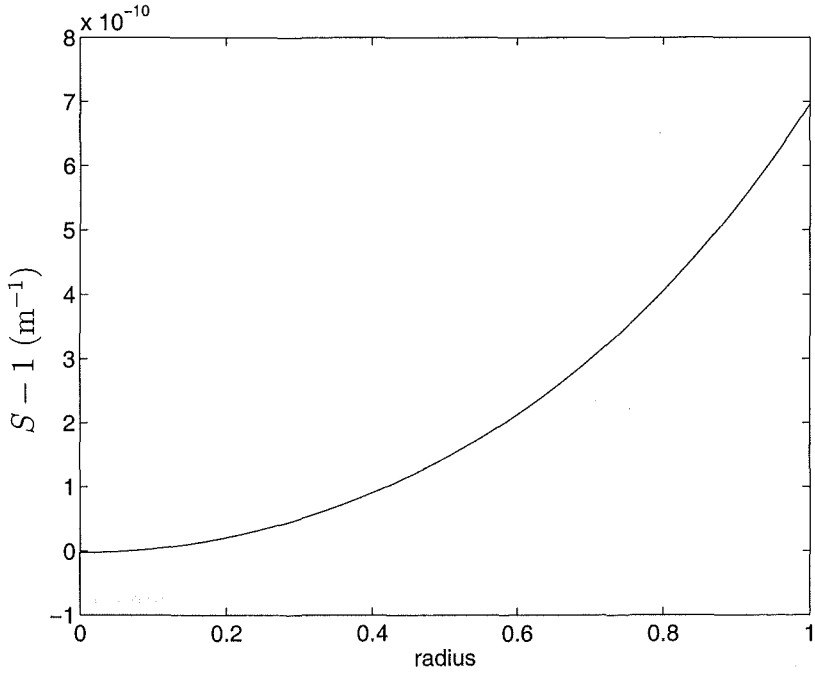

Figure 6.14: scalar field S, polytrope $\alpha \sim -10^{20}$

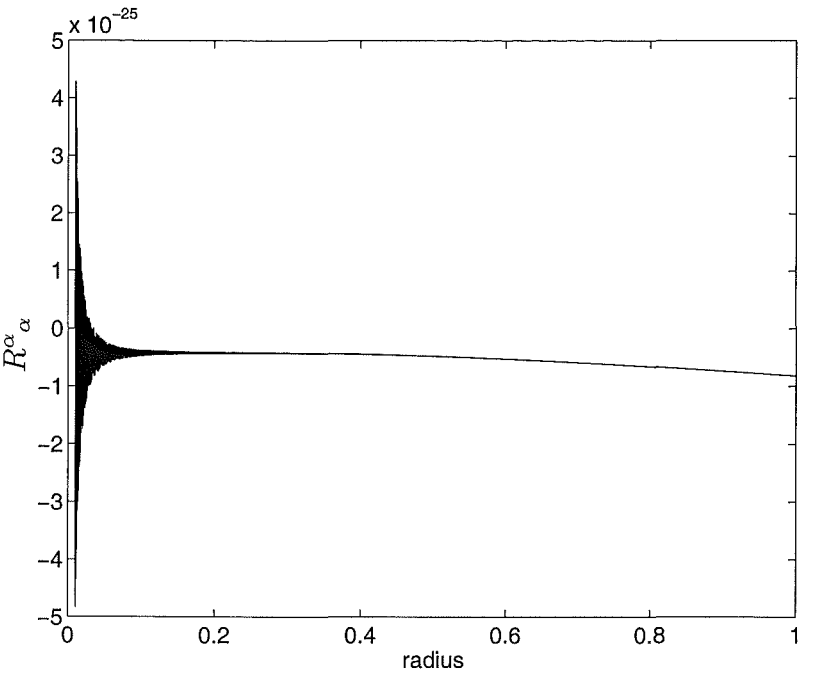

Figure 6.15: scalar curvature, polytrope $\alpha \sim -10^{20}$

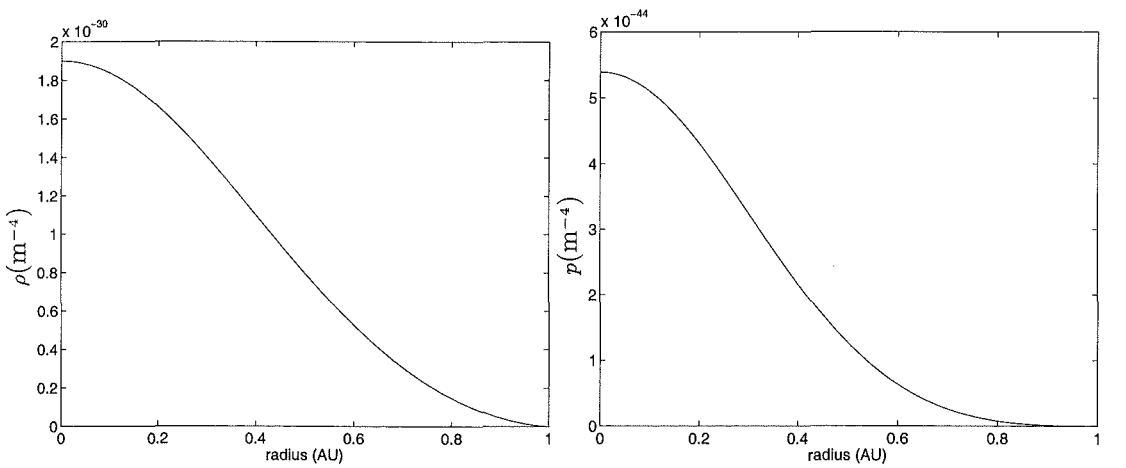

Figure 6.16: physical parameters - Lane-Emden polytrope order $\frac{3}{2}$

then gravitational phenomena would be completely described by interaction with a scalar field gradient.

Note that the scalar curvature, in particular, is showing signs of numerical difficulties — the differences between small quantities used to construct it are resulting in larger truncation error contributions the closer the first and second derivatives of $\bar{a}$ and $\bar{b}$ get to zero (figure 6.15). The average of the noisy region would follow the trend of the better represented area, and maintain sign, but showing that this is to hold is becoming more difficult with these solutions.

The model is also very sensitive to the parameters. In particular, a slight increase in central density (without corresponding changes in $\bar{a}(0)$, etc.) changes the sign of $\bar{a}'$ and S', leading to the opposite behaviour to that expected for the boundary values of S' and $\bar{b}'$. If this occurs, the change in the gradient of $\bar{a}$ means that increasing the model's density results in a value of $\bar{b}(R)$ that is larger for increasing central density, which cannot match up with the exterior solution's behavior. However, in these models the most significant contribution to the limb value of $b(R)$ comes from $\bar{a}(R)$, for which the most significant property is the behaviour of the $\bar{a}$ field across the interior domain. As the gradient of $\bar{a}$ is generally small and has a sign determined by the initial value $\bar{a}(0)$, this means that this becomes the most significant contribution to the boundary matching of $b(R)$.

The value of $\bar{a}(0)$ is currently determined by the success of this boundary matching, ideally it should be determined by an integration over the source itself, including any background effects from the rest of the universe if these are of significant magnitude. This means that if the pressure and density are increased in some consistent manner, the boundary values will not match the equivalent Schwarzschild value without readjustment of $\bar{a}(0)$.

This is a problem of the parameters, we would like $\bar{a}(0)$ as an output of the theory, but with the current methods it is an input to be adjusted. It would be expected that more massive bodies would have stronger gradients in $\bar{a}$, which would still have to match with the exterior far-field expected value of one, so would thus take lower values with increasing source mass. This would have the effect of decreasing the value of b, which is what would be required to match with observation. This behaviour is found to occur in tests on these solutions, for example doubling the pressure and density will produce a viable solution space with the expected magnitude of $b(R)$ if the value of $\bar{a}(0)$ is changed to a value

approximately twice as far from one, i.e. consistent solutions are found in a region where the parameters are adjusted according to

$$\begin{aligned} \rho &\rightarrow 2\rho, \\ p &\rightarrow 2p, \\ \bar{a}(0) &= 1 - \delta\bar{a}(0) \rightarrow 1 - 2\delta\bar{a}(0), \end{aligned}$$

for an initial source mass in the vicinity of the solar mass. With this additional requirement in hand, these interior solutions have good response to changes in the source properties.

It is also possible to produce polytrope solutions with positive values of α. The ratio of pressure to density is a little smaller, and α a little larger but otherwise the parameters are similar. This particular set of values was produced for a polytrope of order three, however it should be noted that the difference between polytropes of orders $\frac{3}{2}$ and 3 is very small as far as boundary condition matching is concerned.

α	2.0855×10^{22}
p_0	$1.800 \times 10^{-47}\mathrm{m}^{-4}$
ρ_0	$1.0 \times 10^{-29}\mathrm{m}^{-4}$
$\bar{a}_0$	$(1.0 - 0.00000218)$.

Again, certain differences in the solution can be observed. The $\bar{a}$ and b fields (figures 6.17, 6.18) are flattening off much more obviously towards the limb of the sun (again, $\bar{b}$ was essentially equal to one everywhere to the program accuracy). The S field has quite different behaviour to the previous negative α solution, which assumed a small negative slope before slowly rising to a limb value (figure 6.14). This time, the solution is taking a more strongly negative initial slope and rising much more slowly across the interior domain (figure 6.19). The scalar curvature is this time of positive sign for a large part of the domain, but changes sign in the outer half, and is showing much less uncertainty (figure 6.21). Note also that the values of the parameters are not constrained to take as precise values as were required in the earlier models - this model is more robust with respect to variation of its parameters.

So which of these two families of polytrope solutions should we consider? The answer to this question must come from considering the behaviour we expect to observe near the limb and exterior to the source body. In the exterior, we have seen that the value of $\bar{a}$ is near to one, and that the solutions where $\bar{a}$ has been

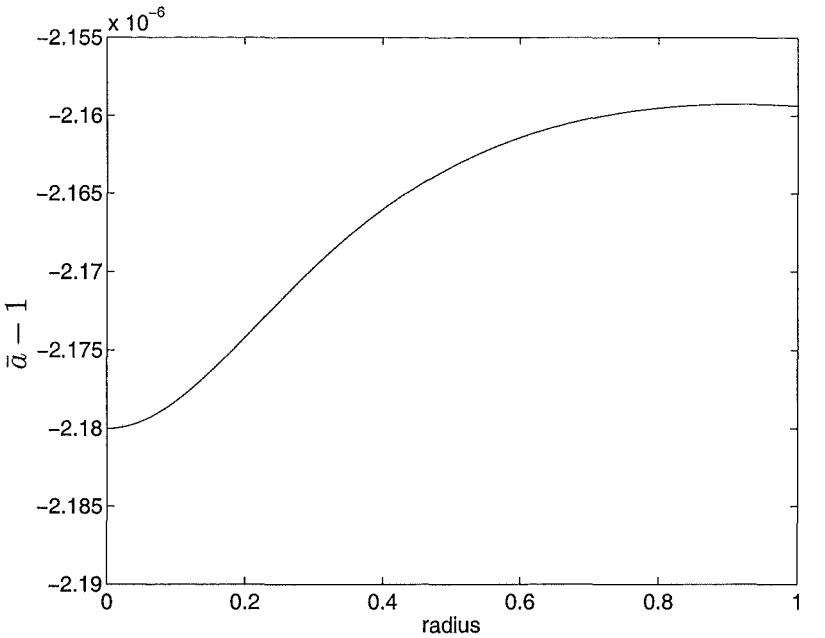

Figure 6.17: metric coefficient $\bar{a}$, polytrope $\alpha \sim 10^{22}$

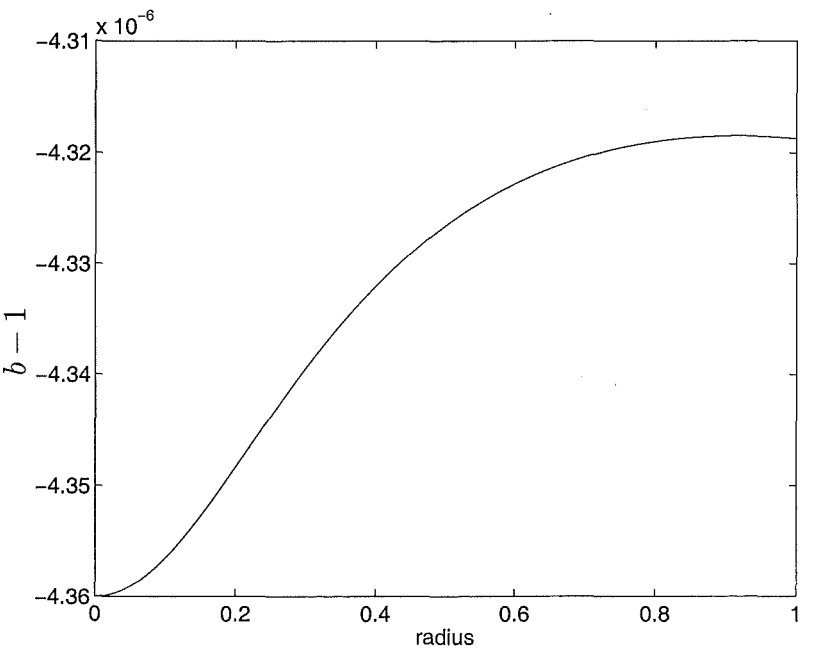

Figure 6.18: metric coefficient b, polytrope $\alpha \sim 10^{22}$

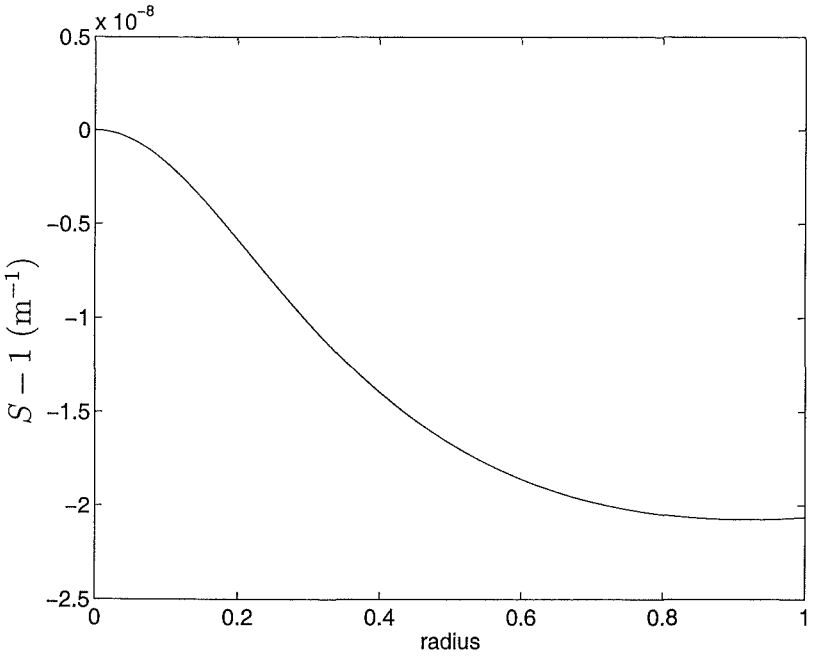

Figure 6.19: scalar field S, polytrope $\alpha \sim 10^{22}$

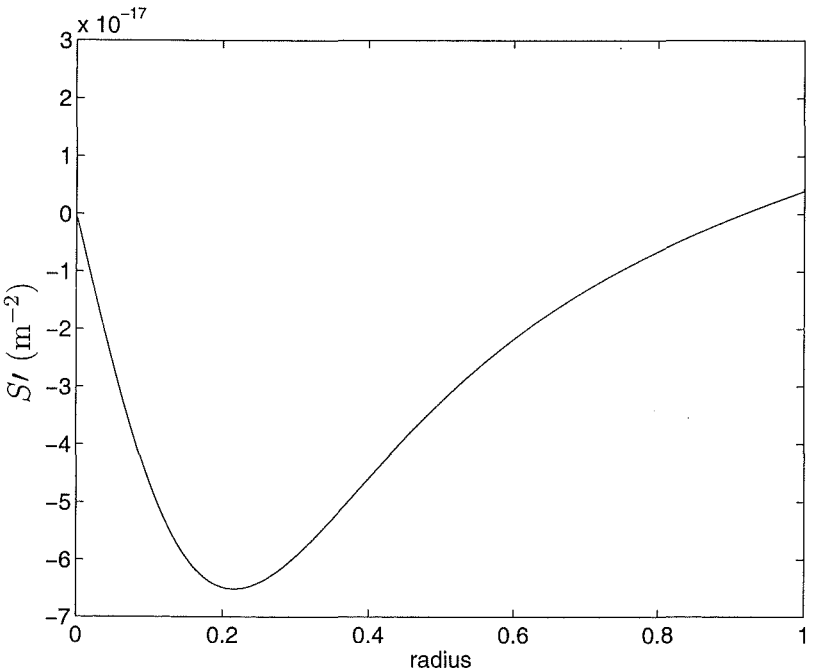

Figure 6.20: scalar field gradient, polytrope $\alpha \sim 10^{22}$

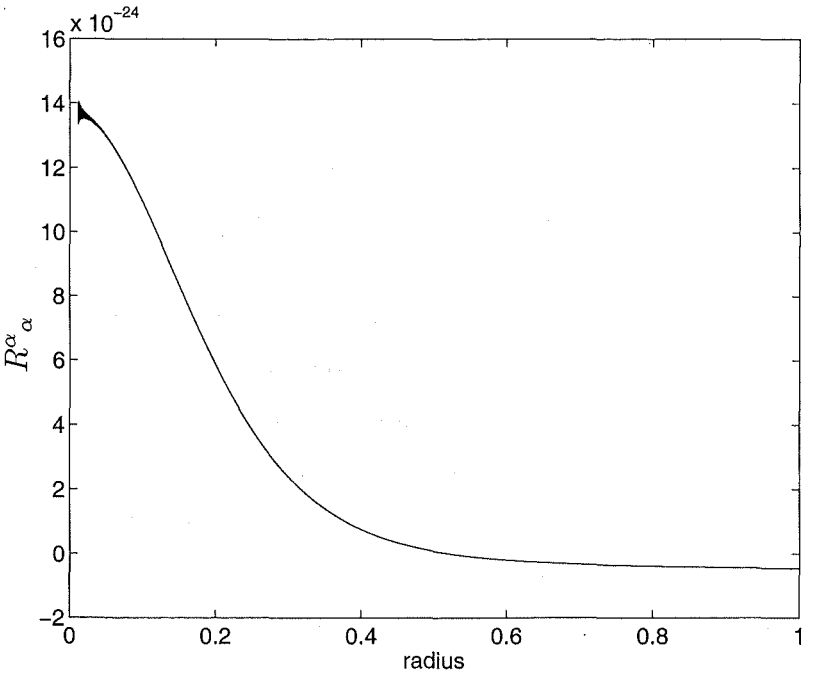

Figure 6.21: scalar curvature, polytrope $\alpha \sim 10^{22}$

transformed away perform well. Therefore, with solutions of the system with $\bar{a}$ transformed to one, we should obtain some limiting behaviour information that can help discriminate between the positive and negative α polytrope solutions.

6.2.2 Interior Solution in $\bar{b}$ and S

The radial field equation $W^{rr} = \frac{1}{4\alpha}T^{rr}$ and the S field equation of motion can be solved together to produce a reasonably simple pair of equations for the quantities $\bar{b}'''$ and S''. This allows the construction of a Runge-Kutta system for the interior problem, with the metric coefficient $\bar{a}$ conformally transformed away. This system is performing the initial procedures as mentioned in the literature, but not assuming that compatible transformations exist to reduce both the S and $\bar{a}$ fields to constants simultaneously. Such a system requires a close match between the interior section's value for the metric coefficient $\bar{b}(R)$ to that produced exterior, with no contributions from the other metric coefficient.

An engine was written to integrate this system of equations. This was not quite a cut down version of the three-variable system as the equations for the highest derivatives were different, given that the differential equations did not have to be solved for $\bar{a}$ derivatives in this case. The engine turned out to be quite robust and not as sensitive to the fine adjustment of parameters as the

three-variable engines tended to be, especially with respect to the limb values of the physical parameters pressure and density.

For this system, certain important parameters were identified, in this case the ratios pressure/density and alpha/pressure. The limb value of $\bar{b}(R)$ is determined almost completely, for a fixed pressure/density ratio, by the alpha/pressure ratio. Changing α or p, so long as their ratio is maintained (and ρ scaled appropriately) makes no change in the value of $\bar{b}(R)$ over a wide range of values of p and ρ. This, and the small variation of the values of $S'(R)$ with these parameters, indicate that the metric coefficient is driven mainly by the source term in pressure and that the structure of the scalar field has very little influence in the value of $\bar{b}(r)$. This is what we hoped to find, and matches well with the behaviour expected from the form of the equations. Conversely, the pressure and density both contribute strongly to the scalar field, and the metric coefficient can have significant effects on the final value $S'(R)$ takes.

More than one set of parameter values that match $\bar{b}(R)$ and $S'(R)$ can be found. However, two particular areas of the parameter space were identified — either the limb value of the metric coefficient gradient is of similar order to the exterior solution, or the scalar curvature can be forced to conserve sign. A solution where both of these properties held was not found. Given that the metric coefficient $\bar{b}$ cannot appeal to it's partner $\bar{a}$ to match the boundary condition in this particular choice of metric, the solution with good slope behaviour is favoured. The change of sign in the scalar curvature is not necessarily an obstacle as the scalar field is not constant in the region where $R^{\alpha}{}_{\alpha}$ crosses zero, as discussed above. The parameters for the preferred solution were given by:

α	3.47×10^{15}
ρ_0	$9.5 \times 10^{-23}\mathrm{m}^{-4}$
p_0	$3.43 \times 10^{-23}\mathrm{m}^{-4}$.

For this model, the pressure and density are modelled by a polytrope of order 3. This is currently taken to be the polytrope that best represents the bulk of the solar body, in terms of mass. It was found that the differences between polytropes of order 3 and 3/2 (the two most useful to consider) were small, with the features of the solutions coming out much the same for both and only a little tuning of parameters required to get from a viable solution of one order to a solution viable for the other order. This would indicate that it is the central value of pressure and density that have the greatest influence on the structure of the solutions.

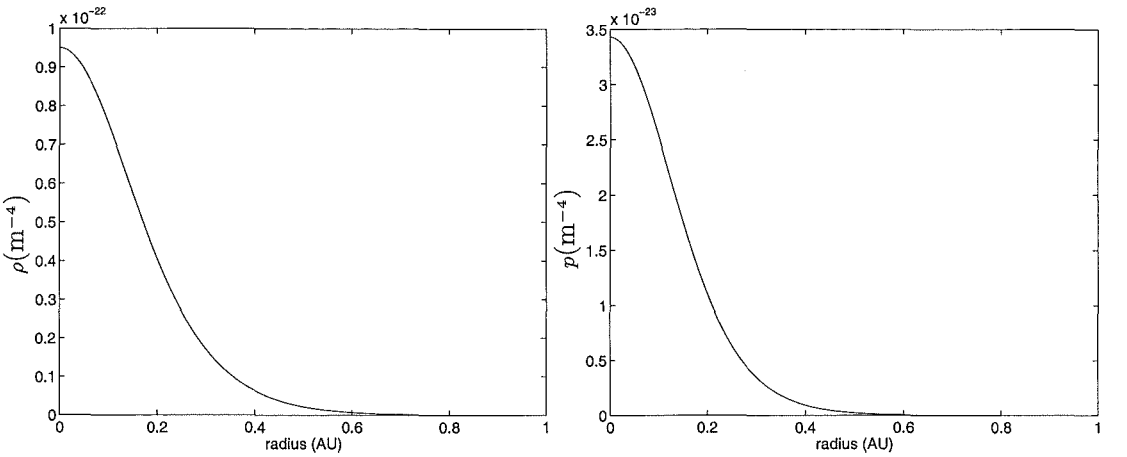

Figure 6.22: physical parameters - Lane-Emden polytrope order 3

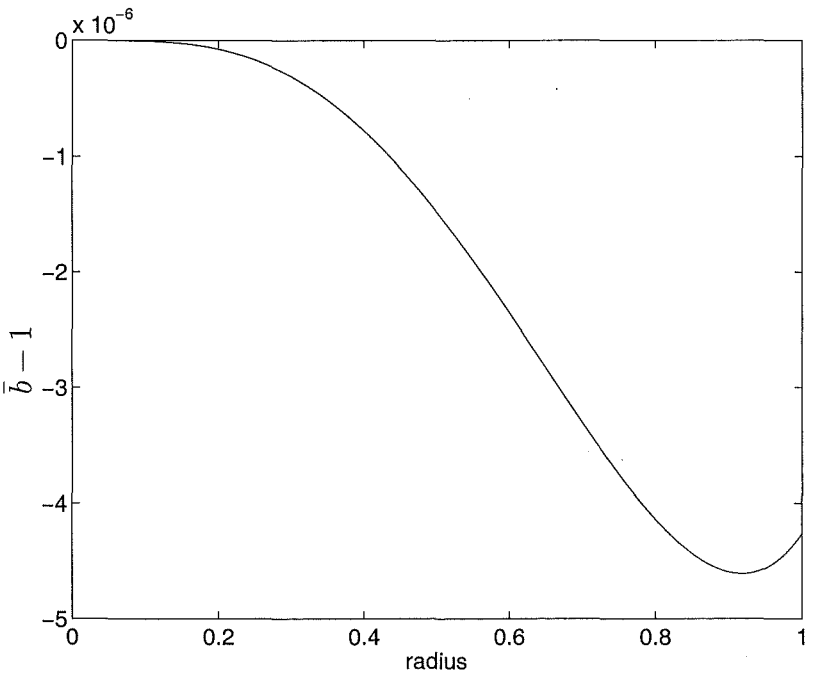

Figure 6.23: metric coefficient $\bar{b}$, $\alpha \sim 10^{15}$

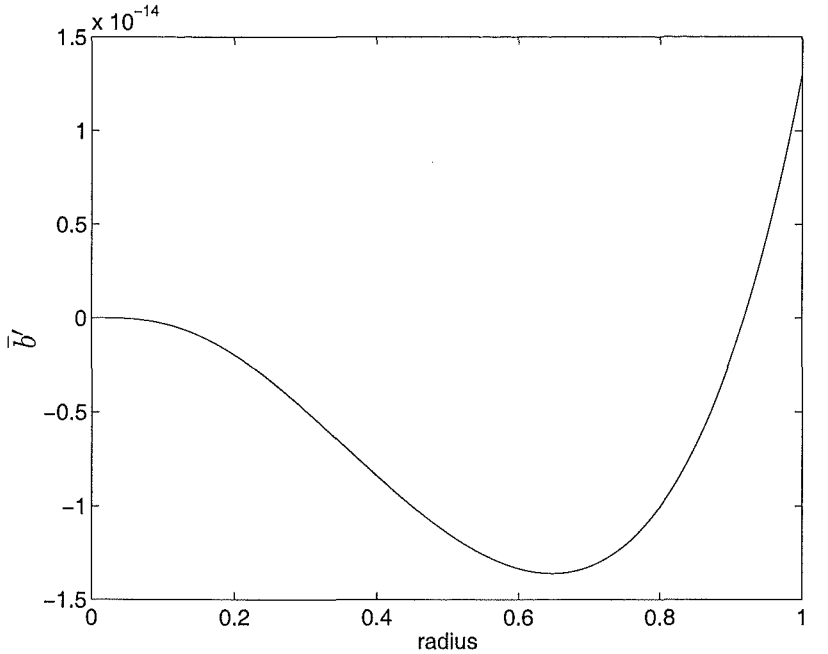

Figure 6.24: metric coefficient gradient $\bar{b}'$, $\alpha \sim 10^{15}$

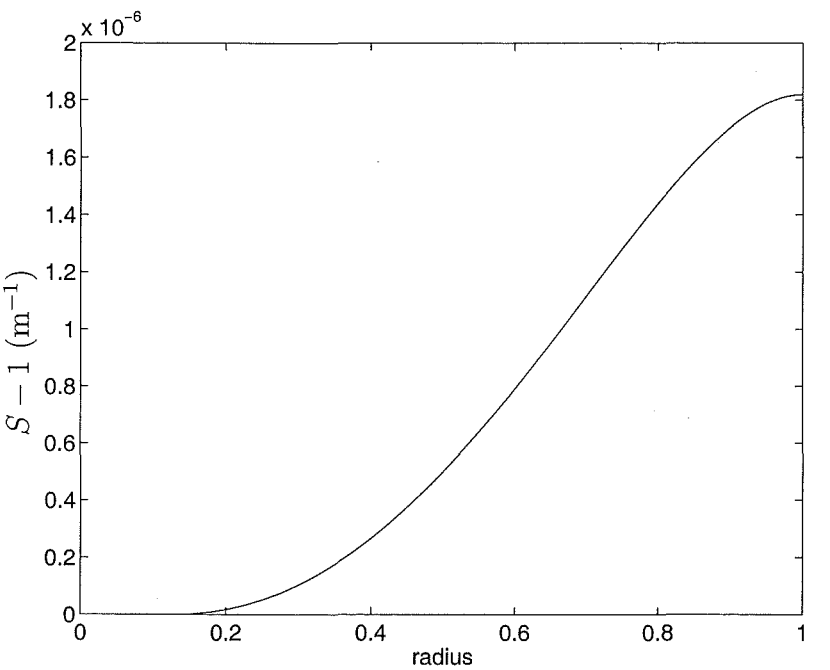

Figure 6.25: scalar field S, $\alpha \sim 10^{15}$

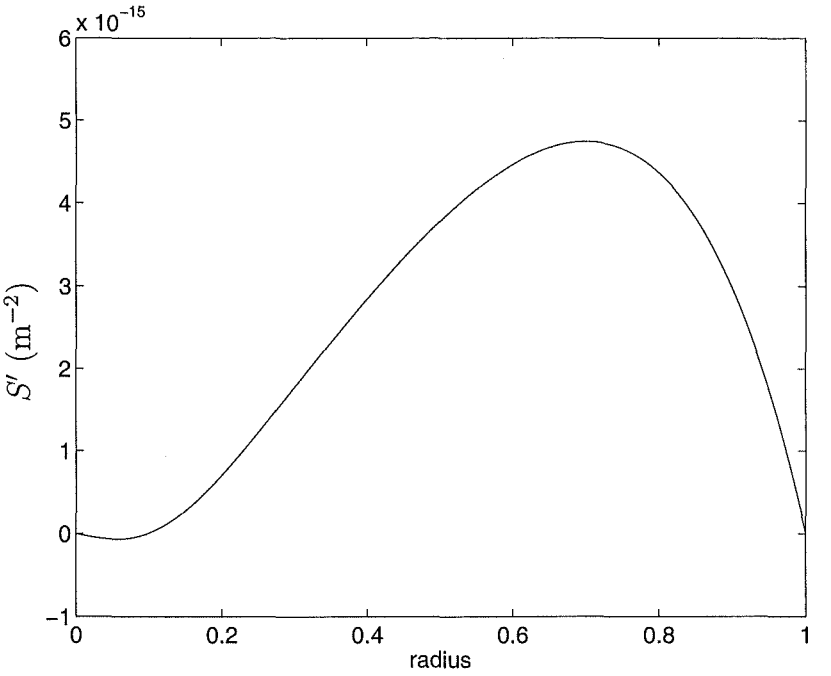

Figure 6.26: scalar field gradient, $\alpha \sim 10^{15}$

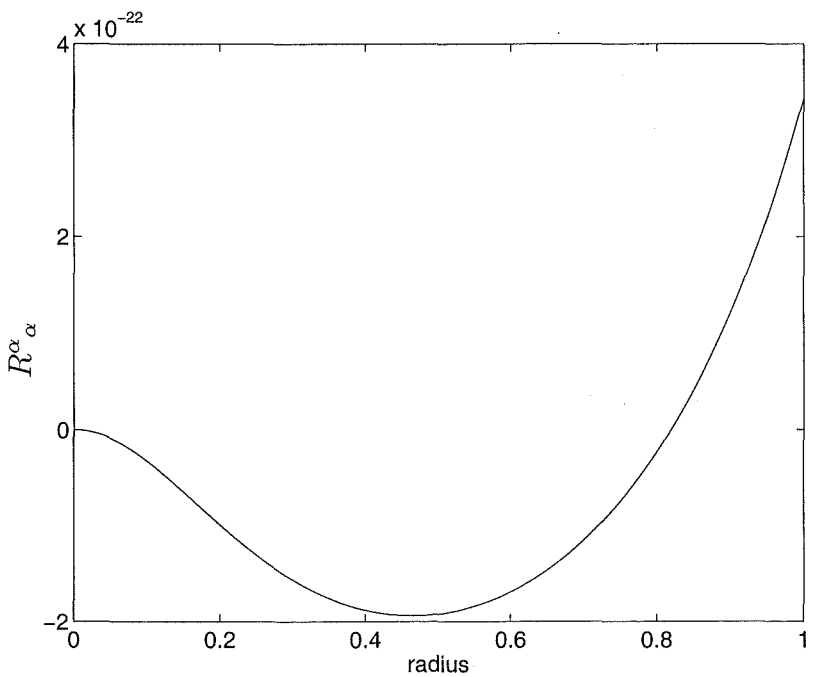

Figure 6.27: scalar curvature, $\alpha \sim 10^{15}$

The solution produced with these parameters agrees well with our viability criteria. The metric coefficient $\bar{b}$ has very satisfactory behaviour, in that it matches the boundary value by passing through a lower value and then rising again to the required value (figure 6.23). This gives a good matching of the derivatives of the metric coefficient (figure 6.24). The scalar field S is also very well behaved, rising gently across the interior domain and then levelling off as the boundary of the source is approached (figure 6.25), in good accordance with what we would expect from the exterior behaviour. The fields vary smoothly and without dramatic changes in magnitude, producing a quite intuitive and physically acceptable model.

The parameters for a representative of the other available type of solution, that where the scalar curvature is held to be of constant sign, are:

α	9.87×10^{17}
ρ_0	$7.0 \times 10^{-21}\mathrm{m}^{-4}$
p_0	$4.5945 \times 10^{-21}\mathrm{m}^{-4}$.

These produce a solution of the following form. The physical parameters follow exactly the same form but are of slightly different relative scaling.

This solution matches the boundary conditions that have been specified, but

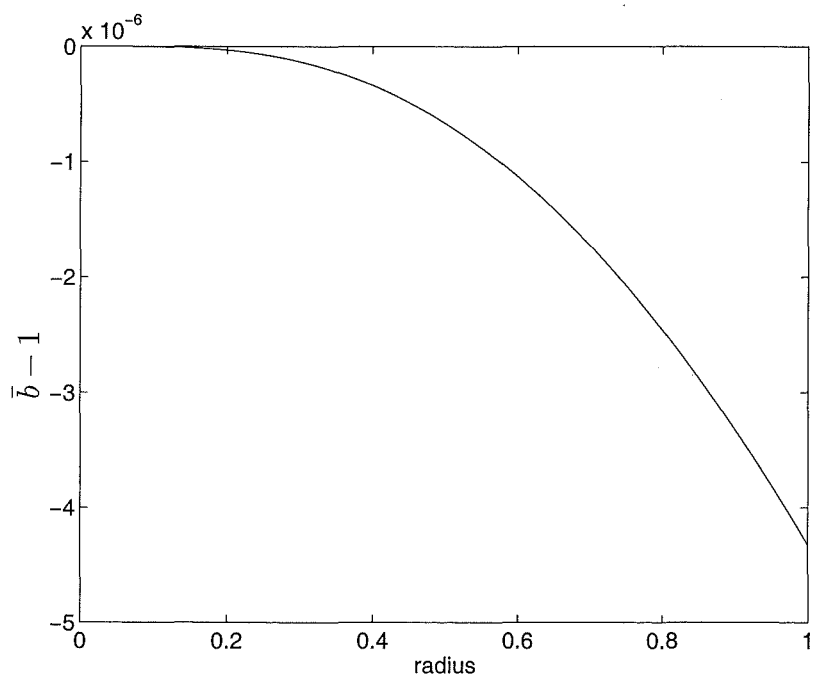

Figure 6.28: metric coefficient $\bar{b}$, $\alpha \sim 10^{17}$

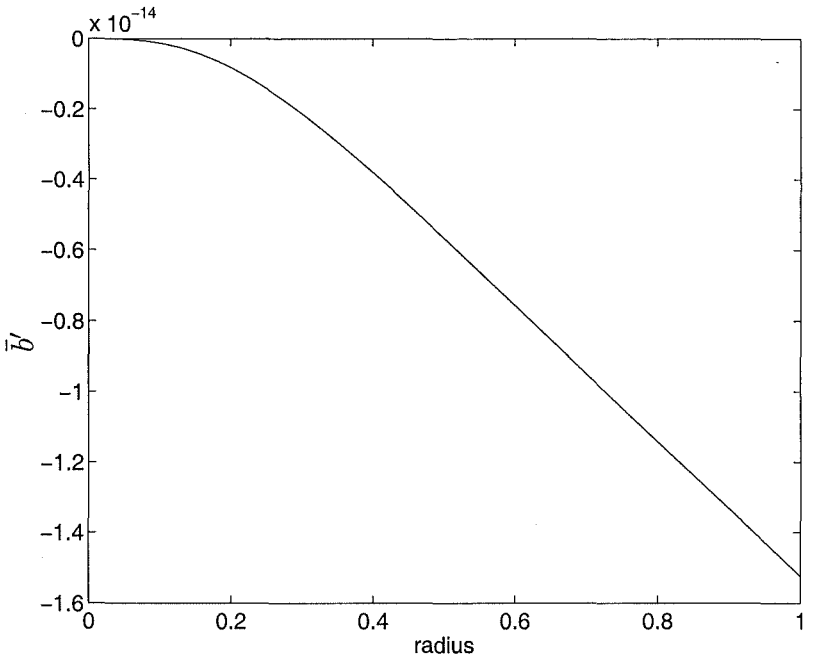

Figure 6.29: metric coefficient gradient $\bar{b}'$, $\alpha \sim 10^{17}$

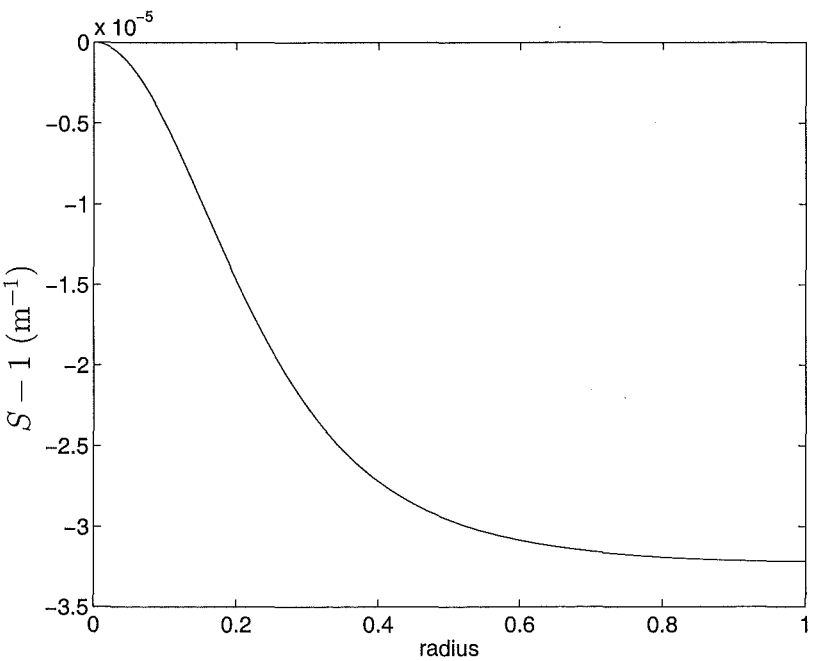

Figure 6.30: scalar field S, $\alpha \sim 10^{17}$

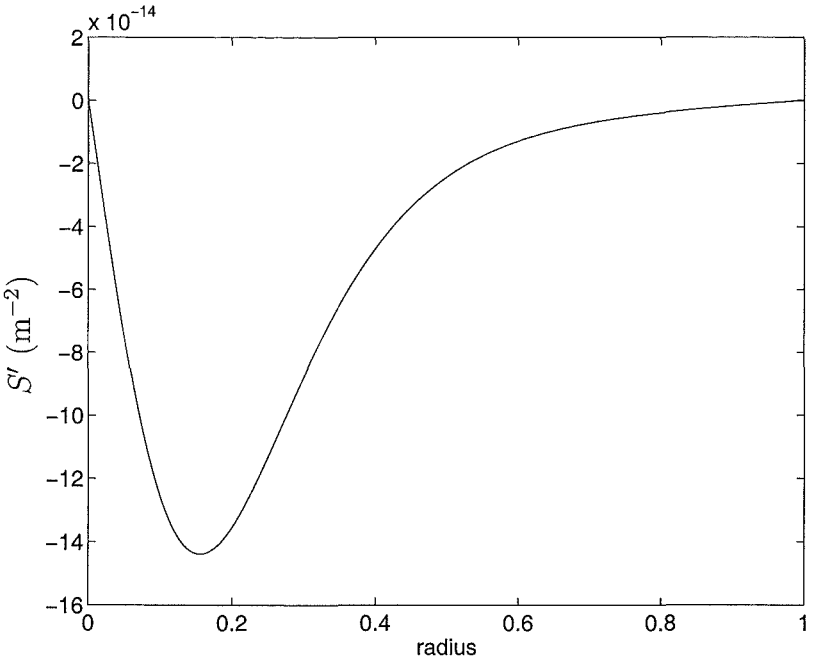

Figure 6.31: scalar field gradient, $\alpha \sim 10^{17}$

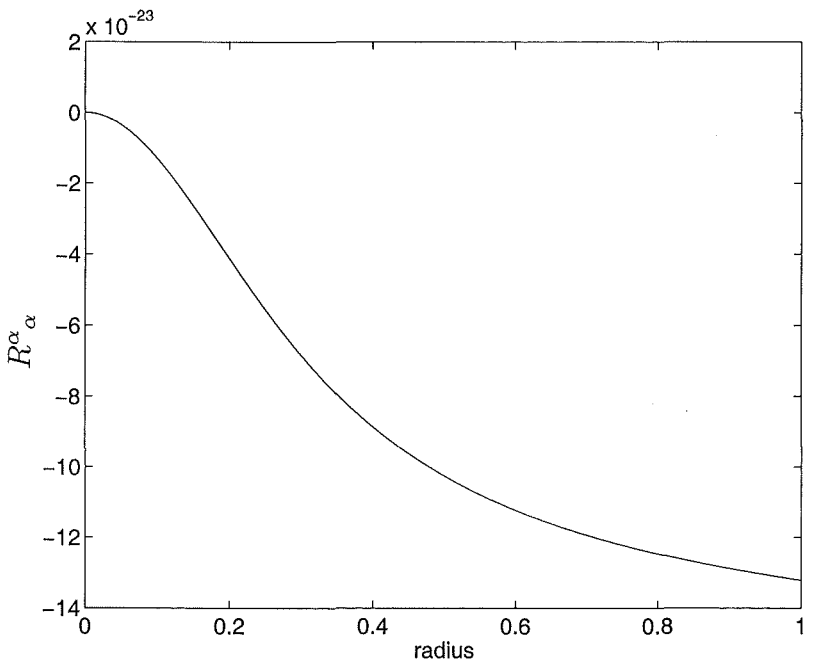

Figure 6.32: scalar curvature, $\alpha \sim 10^{17}$

its secondary features are not as satisfying as the previous model. The $\bar{b}$ field obtains the boundary value quite directly, but without the smooth change in slope that was observed above (figures 6.28, 6.29 c.f. figure 6.23). The boundary matching of the derivatives of the metric coefficient has been degraded by requiring the scalar curvature to preserve sign. The behaviour of the scalar field is also not as intuitive, the field varies smoothly but is decreasing across the interior region and only obtains a positive slope near the boundary of the source (figures 6.30, 6.31). The slope varies smoothly to give the required boundary value, but this profile for the scalar field is not as intuitive to match with the exterior behaviour where the field is increasing with radius in a region of weaker source. The scalar field gradient also varies across a larger range of magnitudes and more sharply than in the earlier model.

No solutions have been found that can match the boundary conditions with negative values of α. Negative α leads to an initially increasing $\bar{b}$ field, which is contradictory to physical expectation, and the field is subsequently driven negative by large density values, resulting in a negative $\bar{b}$ gradient throughout the rest of the domain. The solution does not produce a positive $\bar{b}$ gradient at the limb, and the strong density/pressure ratio required also means that the S gradient is much higher than the boundary conditions would allow. With this system, negative values of α are strongly disfavoured.

This feature can be used to determine which of the interior, three-variable solutions we should consider. Given that in the $\bar{a} = 1$ limit no viable negative α solutions were found, the positive $\alpha \sim 10^{22}$ solutions where $\bar{a} \neq 1$ are more favoured. As it turns out, this is the viable case in the exterior region as well. There is a large difference in the order of magnitude of α between the solutions with $\bar{a}$ and those without, but it should be remembered that the $\bar{a}$ derivatives play a very strong role in the source terms of the field equations, both in their own right and through the scalar curvature. The hydrostatic equilibrium equation (2.12) is a prime example showing the strength of the $\bar{a}$ derivative terms, where they come in to the same order as the terms on $\bar{b}$ and S. In the solutions that include $\bar{a}$, almost all of the metric structure appears in the $\bar{a}$ field.

The preferred solution of this system also has the desirable feature that an increase in pressure and density leads directly to a lower value of $\bar{b}(R)$, with stronger gradients for this field and the scalar field. (Increasing density alone can give a less strongly responding metric coefficient, but this would not be reasonable

as the solutions then have the opposite gradient in S at the limb, and would not be obeying the same hydrostatic equilibrium relations).

6.3 Consistent Interior/Exterior Solutions

The most promising internal solutions have produced an expected magnitude for the coupling constant α of order 10^{15}, and the expectation that α should be of positive sign. This value of α must be found to be compatible with exterior solutions as well as interior. In addition, the internal routines are compatible with the magnitude expected for λ required for the exterior solutions, that is around 10^{-45} or smaller. On theoretical grounds, λ is generally presumed to be positive for both the symmetry breaking and cosmological scale reasoning [40, 31]. As yet neither the interior nor exterior solution give much indication to confirm which sign λ should take — as the contribution from λ must be so small to avoid the production of anomalously large gradients, either sign would be acceptable to this test. Either sign is equally unacceptable for a larger magnitude of λ also, as each sign would cause unacceptably large gradients in a region where asymptotically decreasing gradients would be expected. Whether the solution blows up positively or negatively, its still not a reasonable solution!

The internal solutions that use this value of α match the boundary conditions for b and S very well. In addition, they match well to the expected Schwarzschild-like value of $b'(R)$. The solutions also have good responses to a range of values of pressure and density, in that increasing these parameters has the concomitant effect on the values of $b(R)$ and $b'(R)$ to maintain good agreement with the expected values close to those of the standard theory.

Exterior this value of α is acceptable as well. The near-limb Newton-Raphson test of the field equations in the presence of a scalar field performs well with α of order 10^{15}, producing the same kind of minor deviations from the initial solution as were found for the earlier compatibility studies (section 6.1). Solution for the metric coefficient $b(r)$ to large radius also performs well, producing a solution that is in good agreement with the standard treatment within the uncertainties of the method. A well set up Runge-Kutta method can take the metric field out to many AU with small uncertainties, and as the uncertainties are due to the numerical properties of the method, they become limited in magnitude. The solutions can be extended out to a radius of at least 40 AU with this limiting uncertainty, which agrees with the vacuum solution to at least one part in 10^5.

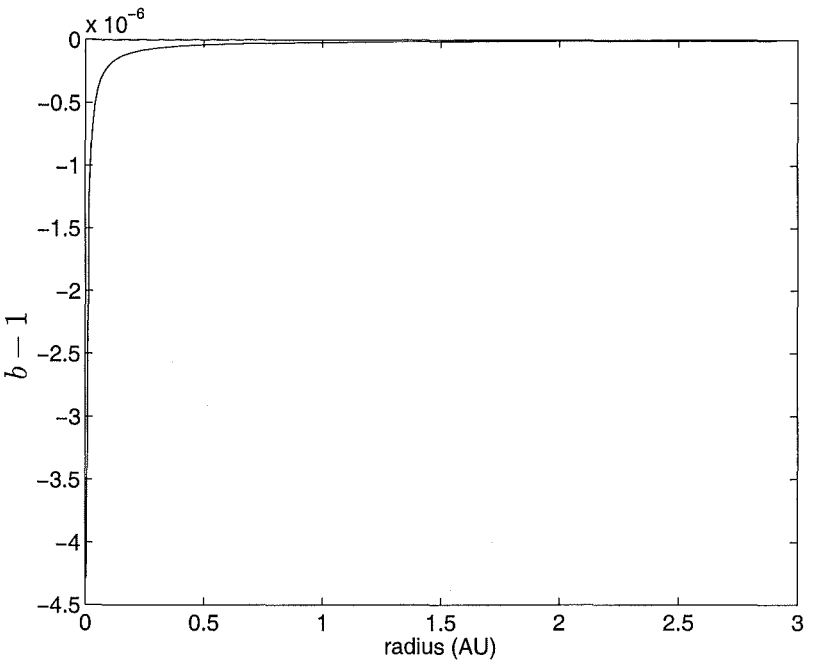

Figure 6.33: exterior b field, $\alpha \sim 10^{15}$, first 3 AU

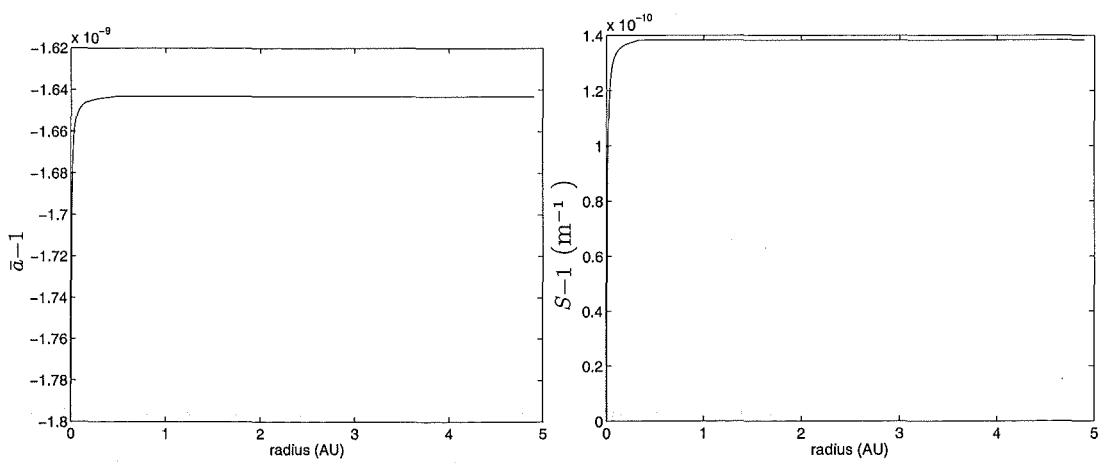

Figure 6.34: exterior $\bar{a}$ and S field Runge-Kutta

With a metric field b agreeing with Schwarzschild to good order, the field equation and equations of motion can be solved as before to find consistent S (and $\bar{a}$, depending on the model considered) fields. These methods are largely unchanged as the S field equation does not depend on α, and with a $b(r)$ agreeing with Schwarzschild (or the conformal vacuum solution (2.3)) to good order, then α cancels out of the field equation as well. The results produced for S are consistent with the original exterior results, whether performed individually or in conjunction with a solution for $\bar{a}(r)$ as well. The solutions generated for the field $\bar{a}(r)$ are close to being one everywhere and are of such a magnitude as to not significantly effect the value of $b(r)$. Note that the solutions with α of order 10^{15} are in the gauge where $\bar{a} = 1$ by transformation.

The matching of boundary conditions at the limb with α order 10^{15} is shown in the following figures (6.35, 6.36). The fields are continuous and the first derivatives match well, particularly the scalar field gradient. Discontinuities in the higher derivatives are expected as the model assumes a discontinuous drop to zero pressure and density at the limb, and the stepsize is large compared to the scale on which the pressure and density drop to zero. In addition, the S field equation is second order so there is no way in which the Runge-Kutta method would enforce continuity of the second derivative, as it is constructed at a point from the local values of only up to the first derivative in S.

Acceptable exterior solutions can also be produced with these methods for larger values of α, of order 10^{22}. Solutions with this value of α have better stability properties than the earlier α order 10^{15} routines for some of the Runge-Kutta methods, allowing good solutions in terms of b and S simultaneously. This order of magnitude for α is consistent with solutions for the interior region where both metric coefficients $\bar{a}$ and $\bar{b}$ are considered. The numerical engine is still susceptible to extrapolation errors but the magnitude of the mechanisms that appear to cause the uncertainty in one field to feed back into the errors in the other are damped down by the larger constant in the denominator of the source for the field equations, producing fields in reasonable agreement with the expected near-vacuum solutions. The agreement of the individual solutions for one field at a time is not as satisfactory as that found for $\alpha \sim 10^{15}$, and the magnitude of discrepancies can be larger (see discussion below). This is not unexpected considering the further complication of the system involving three variables instead of two, where the behaviour of the $\bar{a}$ field can be quite significant

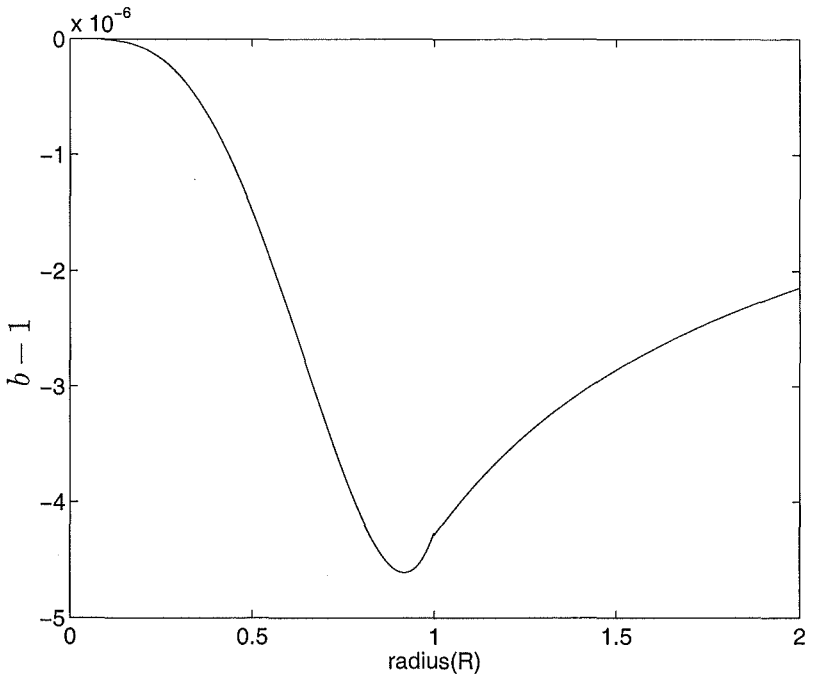

Figure 6.35: interior/exterior b field, $\alpha \sim 10^{15}$

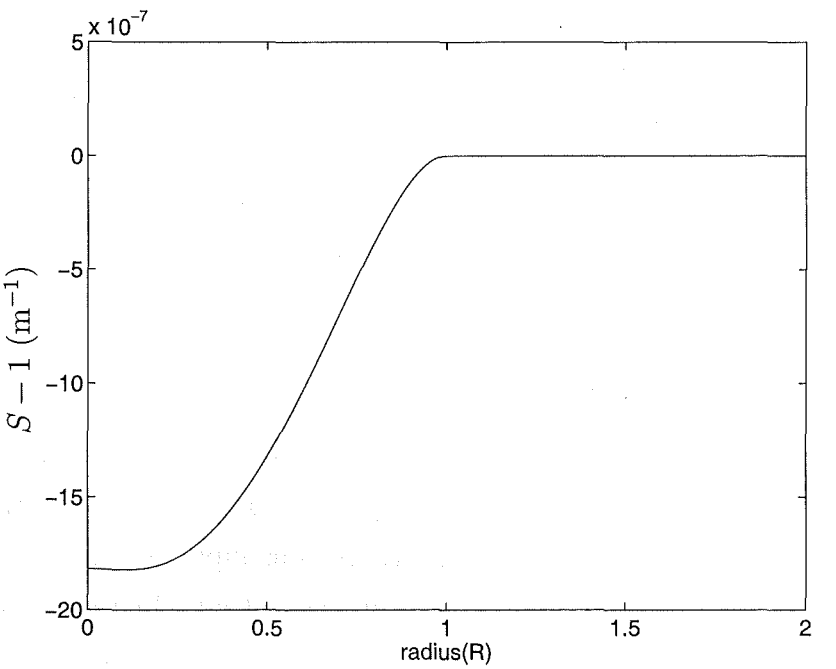

Figure 6.36: interior/exterior S field, $\alpha \sim 10^{15}$

near the limb, and when the equations are made more susceptible to error by containing higher orders in more variables. However, the simultaneous solution for b and S can be extended to a greater radius, about twenty to twenty-five solar radii.

The interior solutions that are consistent with α taking this value, which were the solutions including the three fields $\bar{a}(r), \bar{b}(r)$, and $S(r)$, can be found to match solar boundary requirements, though they are not quite as intuitively satisfactory as the later solutions where $\bar{a}$ has been conformally transformed to take the value one. In addition, their agreement with the boundary value of $b'(R)$ is not as good. The solutions have one further free parameter to be set, the initial value of $\bar{a}(r=0)$, which is currently determined by the success of the boundary value matching. When this matching is performed, the model responds well to changes in the massive properties of the source.

6.4 Discussion of the Methods

The results described above are the end product of a great many attempts at the problem, utilising different numerical techniques, forms of the metric, systems of equations, and sets of variables. These results are the set that best and most reliably describe the behaviour of the system. However, this is not to say that these results are without their own uncertainties or that better methods could not be found. Some suggestions for other techniques that could be used to improve these solutions will be made below.

In the matching process between the interior solutions and refined exterior solutions, further insight was made into the limitations and useful ranges of the various numerical methods employed. It is the most difficult aspect of the solution process that no single method has yet been produced that can successfully produce results across the entire domain in terms of all the required variables. The interior problem could be solved fully and for all the variables that were desired, with a good level of confidence, by use of Runge-Kutta methods. The results produced could be verified by using them as input to a Newton-Raphson system and retrieving good agreement from the output. In the exterior sector of the problem, however, it proved harder to find a single method that could produce acceptable and repeatable results across the whole domain. The successes of individual methods employed varied dependant on what variables were being solved for, and with what parameters. In addition, in the exterior domain the un-

derlying methods themselves became more obviously susceptible to certain kinds of error, particularly truncation or extrapolation errors that include components of spurious homogeneous solutions. While this limits the final accuracy obtainable using these methods, it is well to be aware of the limitations and to understand how they are changed with the different situations being investigated, and how that situation is being investigated.

In overview, it was generally found that the difficulties arose for the solution of the higher order field equations $W^{\mu\nu} = \frac{1}{4\alpha}T^{\mu\nu}$, especially when being solved simultaneously for more than one variable. Minor numerical errors, such as those introduced by roundoff, could easily shift the solutions between members of a family of near-homogenous solutions to the equations. Such errors are generally cumulative, especially for extrapolation methods. The solution of the second-order equation of motion in S proved much more robust, and could be extended across the entire solar system domain.

In the exterior region, the area in which it is most important to show that a compatible solution is possible for the metric and the scalar field is near the limb of the sun. This is the region where the source of the field equations, $T^{\mu\nu}$, is greatest, so this is where we can expect that the particular solutions of the differential equations will be strongest - that is, that the particular solution of the differential equation will pin down the solution of the equations and decrease any ambiguity coming from homogeneous contributions. All the methods proved to be at their most reliable in this region.

The Newton-Raphson iterations behaved very well in the region out to around ten solar radii , and could be tested against the known vacuum $T^{\mu\nu} = 0$ solution for reliability, which proved to be very good. This method could not be extended much further, as at about one AU (approx. 200 solar radii) the Newton-Raphson method was showing sensitivity to the stepsize of the method as well as the actual input fields. This is because the source expression is in terms of gradients of the fields which are becoming very small, small enough that truncation error can introduce values that correspond to homogeneous solutions of comparable magnitude to the particular solution we are attempting to solve for, and the finite-difference constraints are not enough to constrain the field to a global solution with the same homogeneous coefficients at every point.

The Runge-Kutta methods for higher order equations tended to be extensible to a radius of order several R, with a strong dependance on the parameters

of the system. However, systems that solved for multiple fields simultaneously were sensitive to feedback of errors between the equations - a small error, due to truncation or any other source, in the robust S field equation could introduce large errors in the field equation being solved for b that was using S as it's source. This in turn puts a further slight perturbation on S, and the process continues.

Some of these sensitivities can be attributed to the difficulties in solving systems of differential equations with parts of the solutions varying on different length scales. In this case, the differing length scales are between the metric field b and the scalar field, which is varying many orders of magnitude more slowly over the domain of interest. Such sets of equations are known as *stiff* systems of equations and often require different methods of solution to the traditional Runge-Kutta or Burlisch-Stoer methods, or else a very large number of steps to be taken to ensure that the solutions are tracked properly. However, stepsize is limited by the issue of truncation error, making quite a circular problem! That difficulties could be arising from these causes seems probable given that if the fields were solved for in an independent, self-consistent fashion then the solutions could be extended to a much greater radius, of order up to twenty or twenty-five AU with a good degree of reliability.

The Newton-Raphson engines also respond differently when applied to stiff systems of equations. For these methods, what can occur is that a slowly changing variable will require a large stepsize to show up the gradients in that field, as the difference in the field's value between any two points is small. However, a stepsize large enough to provide a good representation of the gradients in one field may be rather too large for the gradients in another field that is varying more quickly, and the finite-difference expressions for the derivatives no longer track the field as well with large stepsizes. This can occur for simultaneous solutions of equations in b and S where the scalar field is varying slowly, requiring a large stepsize which in turn produces a coarse representation of the derivatives in the metric field.

These methods were also showing signs of stepsize-related effects in the solution, variations in the solutions that depended on how the system was being solved, not on what the system being solved was. Such effects are usually very noticeable, due to the obviously structured patterns they produce in the solution, irrespective of what effect they might have on the accuracy of the solution. A clear example of stepsize-related effects on a solution is described in appendix D.

A Burlisch-Stoer engine was also tried in this part of the domain. Theoret-

ically, the results of the Burlisch-Stoer should be more accurate and also more efficient to compute to that higher accuracy. However, it appears that different scales for the variation of the fields prevent a standard implementation of this method from being very effective. The results obtained appeared satisfactory for the metric coefficient b but could not be produced with a great degree of accuracy for S, and the behaviour of the S field did not well match expectation or the results of the other methods. The large stepsize scale that the successful extrapolation of the b field allowed introduced error into the extrapolation for S, eventually driving the slope of S negative in contradiction to the successful earlier results and to theoretical expectation. This would make the system of equations for b and S a stiff system as mentioned above, which requires a different approach to implement a successful Burlisch-Stoer extrapolation. Use of this method was not taken any further, although its solutions for b are quite accurate if the S field does not have to be considered.

The consensus of the exterior methods was that near the limb the solutions agreed very closely to the $T^{\mu\nu} = 0$ vacuum solution, and with scalar field solutions that were produced based upon this assumption. The local Newton-Raphson methods showed a high degree of compatibility for solutions of this kind. These results could be extended to further radius in terms of b and S by assuming that $\bar{a} = 1$, as can be enforced by transformation (or appears to hold to high accuracy even when not transformed away, in regions beyond a radius of one or two AU). These results were consistent with the assumption that $b(r)$ is close to that of a vacuum solution.

These types of assumptions allow the extrapolation of b by Runge-Kutta methods to a further distance that depends strongly upon the value of α, the magnitude of S and S', and the stepsize. Equivalently, if b were to be assumed to agree with the vacuum solution (2.3) to good order, and a Runge-Kutta was used to solve for $\bar{a}$ and S, then this method was found to produce good results out to a large radius (up to twenty-five AU or better). However, the asymptotic behaviour observed by solving for these variables simultaneously was often broken by one of the field gradients passing through zero rather than asymptotically approaching it, and the point where this occurred (and to which field) could be varied by changing the stepsize h. Therefore, these kinds of high order equations had strong limits as to how far they could be extended with these methods.

This means that the far-field behaviour is dependant more strongly upon as-

sumed behaviour of the metric fields that we might have liked. These assumptions are verified to a good accuracy in the regions where the numerical methods are reliable, and it is expected that the deviations of the solution from the vacuum $T^{\mu\nu} = 0$ solution should decrease with increasing radius as the exterior source is dependant upon the scalar curvature and the S field gradients, both of which are decreasing. As the source decreases, the solution will become more closely matched to the vacuum solution. Therefore, the criterion used to make the assumptions are becoming more valid as radius increases.

Chapter 7

Conclusion

The aim of this thesis has been to determine the potential viability of conformal gravity theory incorporating dynamically generated massive particles. Numerical solutions to the field equations of this theory have been produced, which are to be compared with criterion based upon the observational evidence of how gravitation occurs on solar system distance scales. To recap, these criteria were that the deviation of the metric fields from the GR values cannot exceed reasonable experimental bounds, that the gradient of the scalar field be small enough that anomalously large accelerations are not generated, and that the scalar field does not become zero.

A series of numerical solutions to the field equations of conformal gravity were produced for models of increasing physical relevance and similarity to the established and successful models of the standard theory. These models were produced for a variety of different basic properties, particularly the assumption of whether the conformal symmetry can be used to reduce the metric component $\bar{a}$ to the value one, and the property of the sign given to the conformal coupling constant α. The models were constrained by the matching of their boundary conditions at the limb of the sun, which is the point where the last observable interior properties are obtained, and the point where the exterior fields have their strongest effects on the field equations. The solutions of the equations with these different properties allowed the selection of the possible solutions that best described the physical situation, based on the criteria described above.

Two categories of solution were found to be relevant, based upon the property of conformal symmetry described above. Solutions of the conformal field equations can be found that match the criterion of both the case when conformal symmetry has been invoked to reduce the number of metric coefficients, and the case when this has not been assumed and the metric is in terms of the two parameters $\bar{a}$ and $\bar{b}$. In both cases, the coupling constant α has been found to

preferentially assume the positive sign. The character of the solutions in these two categories are quite distinct, and some discussion of the differences will be made below.

In the category of solutions where conformal symmetry is invoked to simplify the metric, the coupling constant α is found to have a value of order 10^{15}. With a reasonable physical model of the interior of a stellar source, the numerical solutions of the field equations produce a metric field that is very close to the Schwarzschild solution in the exterior and matches well across the source boundary conditions at the limb of the sun. A scalar field is generated that has appropriately small gradients and matches well to the external requirements. Analytically, it is also found that for any reasonable scalar field the successes of the standard tests of general relativity theory in predicting deflection of light near the sun and the perihelion shift of planetary orbits will not be manifestly effected.

The solutions in which both metric coefficients have been retained have a quite different structure, with significant contributions to the source terms of the field equations arising due to the metric coefficient $\bar{a}$. With an appropriately higher value of α, of order 10^{22}, solutions can be produced in this system that also match well with the boundary requirements for the metric field b and the scalar field S. The solution of these equations can be more robust for complicated systems in the exterior region, however the self-consistent solution for the metric fields to large radius is not as stable.

In either of these systems, the combination of the various numerical methods that can be applied working from the limb of the source outwards indicate that the scalar field is very near constant and with asymptotically decreasing slope. It is also apparent that the metric fields agree well with the vacuum ($T^{\mu\nu} = 0$) solution to within the accuracy of the methods, that is $a = 1/b$ (or equivalently, $\bar{a} = 1$) and $b = 1 - 3\beta\gamma - \frac{\beta(2-3\beta\gamma)}{r} + \gamma r$, for very small or zero γ on solar system scales. The metric and scalar fields are compatible with each other and with the standard tests of gravitational motion.

In all cases, strong limits can be made to the values of some of the defining parameters of the theory. The scalar field self-coupling constant λ can be limited by far-field integrations of the scalar field equations of motion to have a magnitude of order 10^{-42} or smaller within the solar system. Larger values are not permitted as they would lead to exponentially increasing values of the scalar field at some

large radius, which is not mathematically or physically reasonable.

The magnitude of the scalar field gradient is also strongly limited. Initial analytical approximations at the photosphere limit the value of $S'(R)$ to a magnitude of order 10^{-14}. This limit was made more stringent once the methods were developed for consistent, simultaneous numerical solutions of the field equations that could be extended to large radius. A scalar field with limb gradient $S'(R) = 1.0 \times 10^{-17}$ is compatible with a metric field b that agrees with Schwarzschild to order 10^{-14} at a radius of twenty AU. At this range the Schwarzschild metric field would be of order $1 - 1.0 \times 10^{-9}$, so the deviation from flat space $b = 1$ is within one part in 10^5. Larger values of $S'(R)$ produce metric fields that agree with Schwarzschild less well, roughly according to a relationship of each order higher in S' increases the difference between the output metric field and Schwarzschild by one order of magnitude. Large deviations from Schwarzschild would not be supported by the observed motions of the planets.

Overall, the best solution produced is the system with $\bar{a}$ set equal to one by conformal symmetry, and α of order 10^{15}. This system produces good interior results that match well with the limb boundary conditions. The exterior solution is extensible to reasonable radius in a self-consistent manner. The resulting metric field agrees closely with the Schwarzschild and homogeneous conformal exterior solutions, with a weak scalar field gradient. These results are compatible with the criterion established above. The far-field scalar field solution is best performed with the extrapolated near-Schwarzschild metric field, and then produces a scalar field that agrees closely with the restricted analytic predictions (3.11) at appropriately large radius. The effective gravitational acceleration produced by these fields is compatible with observation, within the uncertainties of planetary ranging. The results of this modelling indicate that it is possible to find solutions of the conformal gravity field equations that match well with the standard observational tests, making conformal gravity with dynamical mass generation a viable theory for local gravitational phenomena, and worthy of further investigation.

It is found that the scalar field gradient has a functional dependance upon radius that closely resembles that suggested by the restricted analytic solution (3.11), that is approximately $S' \propto \frac{1}{r^2}$. This form of radial dependance means that the scalar field will not induce spurious accelerations with dependencies that deviate from the standard results. However, this is far from the near-constant gradient that would be required to produce a weak, near-constant acceleration

on spacecraft such as Pioneer 10/11. With a $\frac{1}{r^2}$ gradient the acceleration would be expected to drop by a factor of 4 over the range 30-60 AU, rather than remain nearly constant.

The implication of these features is that a scalar field with this radial profile does not produce an additional, weak constant acceleration of these spacecraft as it stands. However, the acceleration required may not be exactly constant. The anomalous acceleration of the Pioneer 10 spacecraft is quoted to be $(8.09 \pm 0.20) \times 10^{-10}\text{ms}^{-2}$, with no magnitude variation within a sensitivity of $2 \times 10^{-10}\text{ms}^{-2}$ over the range 40-60 AU [6]. The Pioneer 11 acceleration is measured to be $(8.56 \pm 0.15) \times 10^{-10}\text{ms}^{-2}$ at a range up to 30 AU, and that of the Ulysses spacecraft to be $(12 \pm 3) \times 10^{-10}\text{ms}^{-2}$ at ranges between $1.3 - 5.4$ AU. It would appear that there is some variation of this anomalous acceleration with range, though with a very slow radial dependance.

The exterior vacuum $T^{\mu\nu} = 0$ solution of the conformal field equations (2.3) includes a linear term that would produce a constant acceleration, however in order to reproduce the Pioneer 10 effect the magnitude of the linear coefficient γ would be large enough that the linear perturbations would be unacceptable in the solar system. Despite this, a linear term of smaller magnitude could contribute to a more constant acceleration, as the behaviour of the scalar field solution in far field is such that the presence of a moderately weak linear term in the metric produces S gradients that are notably closer to constant, through the presence of a nonzero scalar curvature. This would also be generated by cosmological terms, if present, and for solutions in which $\bar{a} \neq 1$.

The effect of the conformal gravity metric, if different from that of standard general relativity, is therefore to induce very weak near-constant accelerations through both the metric and the effect of the metric on the scalar field. If the complete solution for metric and scalar field could be carried out to radii of 30-60 AU this could be better investigated. Currently the accuracy of the methods is unreliable at these distances, the extrapolation from closer radii would not favour strong linear components, or a value of $\bar{a}$ that is far from one at large radius. Weak linear components are possible, as γ terms of the order of magnitude proposed for galactic rotation curves are too small to have any significant effect on the solar system results produced.

7.1 Suggestions for Further Work

The area that requires the most improvement in terms of accuracy is the exterior solution at large radius. This is the region that requires the most assumptions for its solution and is also most susceptible to numerical difficulties. Some of the numerical difficulties could potentially be reduced by reformulation of the equations in a carefully chosen manner to avoid those situations where the numerical limits become an issue, such as the example of systems where the derivative terms of a field become so small compared to the value of the field that they cannot alter it due to machine limitations.

The exterior solution could also potentially be solved better by semi-implicit Burlisch-Stoer methods, which handle stiff systems better than the standard algorithms. The semi-implicit Runge-Kutta methods that were used exterior were found to be more efficient, though subject to essentially the same limitations as the standard methods. The potentially increased accuracy of the Burlisch-Stoer methods applied to this kind of method could improve these results, especially if the equations are reformulated to avoid discrepancies in the relative magnitude of terms as described above.

In the interior region, the Burlisch-Stoer methods might also be used to improve accuracy. Given that the interior methods used were relatively stable, this was not attempted, but this could improve the models and the improved efficiency would most likely allow more rapid testing of different models.

Another area that would be useful to investigate is the application of the conformal symmetry to remove the metric coefficient a. The differences between solutions produced in terms of two metric coefficients and those in only one are quite distinct, and this would be a useful area to investigate. If some kind of limiting process between the two cases can be produced, this should provide a lot of insight into the effects of conformal symmetry, and give better criterion for what kind of model is the best description of the physics.

7.2 Acknowledgments

I would like to thank my supervisor Dr. William Moreau for his guidance, patience and encouragement when the results looked unusual, throughout the development of this thesis.

Thanks also to Dr. Brian Lawrence and Dr. Mike Reid for conversations about implementation and possible limitations of the numerical methods.

Thanks to the University of Canterbury for the Doctoral Scholarship, and to the Department of Physics and Astronomy for teaching opportunities.

Finally, thanks to Kate for proof-reading and being supportive through the hardest part of the work.

Appendix A

Algorithms of Extrapolation Methods

A.1 Runge-Kutta Methods

The methods of Runge-Kutta extrapolation are well established and have been under development for many years. An excellent reference for useful Runge-Kutta methods of many orders is *Numerical Recipes* [38], which describes the development, implementation, strengths and weaknesses of these methods. A precis of the algorithm for a standard fourth-order Runge-Kutta, as often used in this project, is as follows.

The Runge-Kutta algorithm has its roots in Euler's method of extrapolation

$$y_{n+1} = y_n + hf(x_n, y_n)$$

which takes a solution from x_n to $x_{n+1} \equiv x + h$. This method is simple but not very accurate, it is only accurate to one power of h smaller than the added correction.

However, by taking multiple steps the error order can be improved. The first step in this process is to take a step of half the distance to the midpoint of the interval, and then another step of the same size to the final point. By performing this process it is possible to cancel out the $O(h^2)$ terms in the expressions for the final value, improving the accuracy to $O(h^3)$. By performing different step combinations that all lead to the same final point, many orders of error can be eliminated. The most common order expansion that is used is the fourth-order expansion:

$$\begin{aligned} k_1 &= hf(x_n, y_n) \\ k_2 &= hf\left(x_n + \frac{h}{2}, y_n + \frac{k_1}{2}\right) \\ k_3 &= hf\left(x_n + \frac{h}{2}, y_n + \frac{k_2}{2}\right) \end{aligned}$$

$$\begin{aligned} k_4 &= hf\left(x_n + h, y_n + k_3\right) \\ y_{n+1} &= y_n + \frac{k_1}{6} + \frac{k_2}{3} + \frac{k_3}{3} + \frac{k_4}{6} + O\left(h^5\right). \end{aligned}$$

This process improves the error order of the method at the expense of more evaluations of the derivative functions. A performance increase would only result if the stepsize can be extended to take advantage of the improved error properties. However, this is often the case — and for the work done here the performance considerations were not a serious limiting factor, smaller stepsizes could be used with higher order methods to improve the accuracy of the results.

Beyond the standard fourth-order Runge-Kutta method, adaptive stepsize methods are implemented by producing methods that can combine the different expansions as above to produce two methods of getting to the end point, that are of different error order — the standard methods produce a fourth-order and a fifth-order extrapolation simultaneously. The advantage of having two different extrapolations is that the difference between the two can be used as an error estimate for the process, which can then be used to scale the stepsize to return values of a given accuracy. This allows fine stepsizes to be used in the regions where the function is varying quickly, and extends the stepsize to rapidly cover areas where the function is easily extrapolated to good accuracy.

A.2 Burlisch-Stoer Methods

The Burlisch-Stoer method is a descendant of the Runge-Kutta method that extends the power of variable stepsize schemes. These methods aim to find the best possible value of the extrapolated point by performing a series of evaluations with sequentially smaller stepsizes. Given that accuracy should improve with this process, the results of this sequence of evaluations are then extrapolated as a function of the stepsize to give a value that the extrapolated point would have if the stepsize were reduced to zero. In that limit the stepwise integration process would be returning the actual value of the real function.

This process is valuable not only because of potential accuracy gains, but because this accurate extrapolation method is particularly amenable to performing large skips across smooth areas of a function. With the overall stepsize being adaptive, a Burlisch-Stoer method can reliably use large stepsizes in regions where the function is varying slowly, while still being able to reduce to small stepsizes in areas where the function is more complicated. The exact methods

for determination of stepsizes to use based on error estimates from the previous step are quite involved, again I would refer the reader to *Numerical Recipes* [38] for a detailed description.

Appendix B

Algorithms of Relaxation Methods

The relaxation method that was used in this project was a finite-difference Newton-Raphson iteration on a regular mesh. Descriptions of finite-difference methods are available in the literature, a useful reference was *Numerical Algorithms with C* [41], which describes in some detail different approaches and algorithms.

The essence of the finite-difference method is to replace the differential equations of the problem with difference equations, by making substitutions of the form

$$y'(x_i) \rightarrow \frac{(y(x_{i+1}) - y(x_{i-1}))}{(x_{i+1} - x_{i-1})}$$

for a grid of evenly spaced points x_i. If the spacing between points is denoted h, then this would be written as

$$y'(x_i) \rightarrow \frac{1}{2h}(y(x_i + h) - y(x_i - h)),$$

which demonstrates that in the limit $h \rightarrow 0$ that this expression becomes the actual derivative by definition.

The finite-difference expressions for the derivatives (to various order) can be simply derived by considering Taylor expansions of the function and it's derivatives at a point. Expressions can be derived from different order of Taylor expansion, whereupon they will involve information from differing numbers of points on the mesh adjacent to the point of interest. For example, the second order expression above involves only the points one mesh spacing to either side of the point of interest, for the first derivative. Fourth order Taylor expansions produce equations in terms of the points up to two mesh spacings away, sixth order Taylor expansions involve the points three mesh spacings away, etc. The number of data points required also increases with the order of the derivative that the finite-difference expression is for.

Finite-Difference Expressions (fourth order)

$$
\begin{aligned}
y' &= \frac{1}{12h}\left(y_{i-2} - 8y_{i-1} + 8y_{i+1} - y_{i+2}\right) \\
y'' &= \frac{1}{12h^2}\left(-y_{i-2} + 16y_{i-1} - 30y_i + 16y_{i+1} - y_{i+2}\right) \\
y''' &= \frac{1}{8h^3}\left(y_{i-3} - 8y_{i-2} + 13y_{i-1} - 13y_{i+1} + 8y_{i+2} - y_{i+3}\right) \\
y'''' &= \frac{1}{6h^4}\left(-y_{i-3} + 12y_{i-2} - 39y_{i-1} + 56y_i - 39y_{i+1} + 12y_{i+2} - y_{i+3}\right)
\end{aligned}
$$

Finite-Difference Expressions (sixth order)

$$
\begin{aligned}
y' &= \frac{1}{60h}\left(-y_{i-3} + 9y_{i-2} - 45y_{i-1} + 45y_{i+1} - 9y_{i+2} + y_{i+3}\right) \\
y'' &= \frac{1}{180h^2}\left(2y_{i-3} - 27y_{i-2} + 270y_{i-1} - 490y_i + 270y_{i+1} - 27y_{i+2} + 2y_{i+3}\right)
\end{aligned}
$$

This feature of the finite-difference expressions comes in very useful for the implementation of the method, as a Jacobian matrix of the dependencies of the equation at each point depends only upon the values of the function at a very limited number of neighbouring points. This leads to a band diagonal (or block-band diagonal) structure to the matrix, for which simple and efficient algorithms are available for inversion.

This is the critical part of the method. As described above, the process involves producing a Jacobian matrix for the system and solving the matrix equation

$$Jx = f$$

for x. The Jacobian matrix is produced from the derivative of the difference equation with respect to its dependant variables at a point, and the vector f contains the values of the difference equations at the mesh points. The equations are set up homogeneously, making f a vector of residuals that should be approaching zero with successive iterations. The vector x is a 'descent direction' for the vector containing the fields of interest, that should bring the fields to a configuration that better solves the difference equations. The strengths of this method are that the entire domain of the grid is solved for simultaneously, and that convergence is rapid once the fields are close to a solution of the difference equations. On the

other hand, if the field vector is *not* close to a solution, then the system may not converge, or may find a local minimum as opposed to a global solution. Having a reasonable estimate of what the solution should be is very useful for extracting the best results from this method.

Boundary conditions are a major consideration in the setting up of a Newton-Raphson system. The finite-difference derivative expressions typically involve points on either side of the point of interest, so at the boundaries information is required that is outside the domain of the grid - that is, we need some additional mesh points specified outside the grid. The values that these mesh points take must be specified from the boundary conditions, either by taking fixed values, or by providing some relation between the mesh points such as requiring the first derivative to vanish. Some such condition must be found to allow construction of the additional mesh points.

Note also that point or slope boundary conditions involve, generally, only enough information to specify one external mesh point. This means that the order of the finite-difference expansion must be carefully selected, such that the structure of the Jacobian matrix is consistently workable. By this we mean that the finite-difference equations at the boundaries provide enough information to maintain the band diagonal structure without introducing many zeros that make the matrix ill-conditioned. This kind of problem can be reduced by finding asymmetrical finite-difference expressions for the boundaries that involve less external mesh points.

Assymetric Finite-Difference Expressions (fourth order)

$$
\begin{aligned}
y_0''' &= \frac{1}{2h^3}\left(-3y_{-1} + 10y_0 - 12y_1 + 6y_2 - y_3\right) \\
y_n''' &= \frac{1}{2h^3}\left(y_{n-3} - 6y_{n-2} + 12y_{n-1} - 10y_n + 3y_{n+1}\right)
\end{aligned}
$$

Once this setting up of a viable Jacobian matrix for the finite-difference system is complete, the program to implement the method can be constructed. The methods used to solve the matrix equation are LU decompositions for (block) band diagonal matrices. Block structure will be introduced when more than one equation is being solved for multiple variables, which is often the case. Algorithms of such decompositions are readily available for any order of band-diagonal structure [41]. This produces the vector of field adjustments x. It is generally wise to allow for the possibility of the descent direction overshooting the solution, so

it is best to have some fraction parameter δ that determines how much of the descent vector is added to the field vector, i.e. for field vector a_n at iteration n, the new field vector is given by $a_{n+1} = a_n + \delta x$. The process is repeated until a maximum number of iterations is reached, a minimum size of residual is obtained, the system becomes unstable, or the user interrupts. Limits to the number of iterations other than an expected residual size are important as if local minima are reached, or the solution oscillates around some set of values without approaching it, then the initial solution or δ factor will need to be adjusted.

The success of the method can be quite dependant on the exact formulation of the system of difference equations. The properties of the different expansions available can have a bearing on how the method behaves — for example, the asymmetric forms of the expansions that can be used at the boundaries can prove to be less stable than the central-difference expansions used interior to the domain. This could lead to the method becoming unstable, with dubious values being introduced from one end until the solution 'peels away' from a region of stability. Equally, for some slope boundary conditions the situation can be reversed and information about the limiting value of the slope is only slowly propagated out through the domain a few mesh points at a time as each iteration incorporates more mesh points that have been involved with information that originated at the boundary condition. In this case, a requirement of the solution propagates into the domain and the difference equations have to conform to that information.

The mathematical formulation of the differential equations can also have a bearing on the successful operation of a Newton-Raphson system. If the equations are only weakly dependant on some of the variables, or if there is a cancellation that produces near-zero dependencies on the variables, the Jacobian matrix can become ill conditioned. In this case the system tends to show divergent behaviour — once one inappropriate value has appeared in the field vector, the matrix becomes more ill conditioned and the system is not viable. This can often be resolved by appropriate transformations to scaled or shifted variables, for example an equation in asymptotically vanishing quantities can sometimes be made workable if the equations are rewritten in terms of new variables scaling the old variables by the radius, i.e. an equation in $a(r)$ is rewritten in terms of $\bar{a}(r) = a(r) \times r$.

Appendix C

Numerical Engine Code

Below are given the core parts of the C++ programs that were written to numerically solve the various differential equations in this project. Some of the numerical routines are derived from *Numerical Recipes in C* [38], others were coded from scratch for a given algorithm. The graphics handling section makes use of the freely available library *Allegro* (see http://www.talula.demon.co.uk/allegro/). The code is not necessarily the best constructed or most elegant, however it is functional and allows the problems to be set up relatively easily. Very large systems, in terms of the number of nodes, can be handled. The running time of most sensible problems was a matter of seconds (on a P333, 64 Mb RAM), only when the number of nodes was cranked up to excessive values (25 million or so, for the Runge-Kutta methods) in multi-variable problems was the running time sufficiently long as to warrant leaving it to run while you go find a coffee.

The programs all make use of a few standard routines for handling data, files, and graphic output. These are in the source files utils.cpp, gfx.cpp, and diskvect.cpp. The Newton-Raphson programs tended to extend the utility routines with more functional handling of small vectors and matrices, which is incidentally written in more modern, object-oriented code showing the development of techniques as the project progressed.

The programs then often have an object for handling the particular method involved, say a fourth-order Runge-Kutta method. This is paired up with files containing the information about the problem to be solved, typically called 'function.h' and 'function.cpp'. The first contains definitions and the constants of the problem, the second some initialisation routines and the actual equations to be solved. These objects are all controlled from the main program ('main.cpp') which provides storage space, loads data, runs the actual engine, and displays (and saves) the results. Results can be saved as binary files or as text output, the binary files are particularly easy to read into third party packages such as

Matlab.

The common source code files will be reproduced here, along with examples of 'function' files and the 'main' programs.

utils.h - memory allocation and general functions

```
static double dsqrarg;
#define SQR(a) ((dsqrarg=(a)) == 0.0 ? 0.0 : dsqrarg*dsqrarg)
static double dcubearg;
#define CUBE(a) ((dcubearg=(a)) == 0.0 ? 0.0 : dcubearg*dcubearg*dcubearg)

template <class T> inline const T& min( const T& t1, const T& t2 ){
   return t1>t2 ? t2 : t1;
}
template <class T> inline const T& max( const T& t1, const T& t2 ){
   return t1>t2 ? t1 : t2;
}

void uerror(char error_text[]);
double *vector(long nl, long nh);
double **matrix(long nrl, long nrh, long ncl, long nch);
double ***d3tensor(long nrl, long nrh, long ncl, long nch, long ndl, long ndh);
void free_vector(double *v, long nl, long nh);
void free_matrix(double **m, long nrl, long nrh, long ncl, long nch);
void free_d3tensor(double ***t, long nrl, long nrh, long ncl, long nch,
                   long ndl, long ndh);
int *ivector(long nl, long nh);
void free_ivector(int *v, long nl, long nh);
double dabs(double arg);
double sign(double a, double b);
```

utils.cpp

```
#include <stdlib.h>
#include "allegro.h"
#define ENDOFFSET 1

double dabs(double arg) {
   if (arg<0.0) return (-arg);
   return(arg);
}

double sign(double a, double b) {
   if (b>=0.0) return dabs(a);
   return (-dabs(a) );
}

void uerror(char error_text[]) { // standard error handler
   textprintf(screen,font,0,0,63,"%s \n (click mouse)",error_text);
   do{
   }while(!(mouse_b&1));
   exit(1);
}

double *vector(long nl, long nh){
   // allocate a double vector with subscript range v[nl..nh]
   double *v;
   v=(double *)malloc((size_t) ((nh-nl+1+ENDOFFSET)*sizeof(double)));
   if (!v) uerror("allocation failure in vector()");
   return v-nl+ENDOFFSET;
}

double **matrix(long nrl, long nrh, long ncl, long nch) {
   // allocate a double matrix with subscript range m[nrl..nrh][ncl..nch]
   long i, nrow=nrh-nrl+1,ncol=nch-ncl+1;
   double **m;
   /* allocate pointers to rows */
   m=(double **) malloc((size_t)((nrow+ENDOFFSET)*sizeof(double*)));
   if (!m) uerror("allocation failure 1 in matrix()");
   m += ENDOFFSET;
   m -= nrl;
   /* allocate rows and set pointers to them */
   m[nrl]=(double *) malloc((size_t)((nrow*ncol+ENDOFFSET)*sizeof(double)));
   if (!m[nrl]) uerror("allocation failure 2 in matrix()");
   m[nrl] += ENDOFFSET;
   m[nrl] -= ncl;
   for(i=nrl+1;i<=nrh;i++) m[i]=m[i-1]+ncol;
      /* return pointer to array of pointers to rows */
      return m;
}

double ***d3tensor(long nrl, long nrh, long ncl, long nch,
                   long ndl, long ndh){
/* allocate a double 3tensor with range t[nrl..nrh][ncl..nch][ndl..ndh] */
   long i,j,nrow=nrh-nrl+1,ncol=nch-ncl+1,ndep=ndh-ndl+1;
   double ***t;

   /* allocate pointers to pointers to rows */
   t=(double ***) malloc((size_t)((nrow+ENDOFFSET)*sizeof(double**)));
   if (!t) uerror("allocation failure 1 in d3tensor()");
   t += ENDOFFSET;
   t -= nrl;
   /* allocate pointers to rows and set pointers to them */
```

```
   t[nrl]=(double **) malloc((size_t)((nrow*ncol+ENDOFFSET)
                                      *sizeof(double*)));
   if (!t[nrl]) uerror("allocation failure 2 in d3tensor()");
   t[nrl] += ENDOFFSET;
   t[nrl] -= ncl;
   /* allocate rows and set pointers to them */
   t[nrl][ncl]=(double *) malloc((size_t)((nrow*ncol*ndep+ENDOFFSET)
                                          *sizeof(double)));
   if (!t[nrl][ncl]) uerror("allocation failure 3 in d3tensor()");
   t[nrl][ncl] += ENDOFFSET;
   t[nrl][ncl] -= ndl;
   for(j=ncl+1;j<=nch;j++) t[nrl][j]=t[nrl][j-1]+ndep;
   for(i=nrl+1;i<=nrh;i++) {
      t[i]=t[i-1]+ncol;
      t[i][ncl]=t[i-1][ncl]+ncol*ndep;
      for(j=ncl+1;j<=nch;j++) t[i][j]=t[i][j-1]+ndep;
   }
   /* return pointer to array of pointers to rows */
   return t;
}

void free_vector(double *v, long nl, long nh) {
   // free a double vector allocated with dvector()
   free((char *) (v+nl-ENDOFFSET));
}

void free_matrix(double **m, long nrl, long nrh, long ncl, long nch) {
   // free a double matrix allocated by dmatrix()
   free((char *) (m[nrl]+ncl-ENDOFFSET));
   free((char *) (m+nrl-ENDOFFSET));
}

void free_d3tensor(double ***t, long nrl, long nrh, long ncl, long nch,
                   long ndl, long ndh){
   /* free a double 3tensor allocated by f3tensor() */
   free((char *) (t[nrl][ncl]+ndl-ENDOFFSET));
   free((char *) (t[nrl]+ncl-ENDOFFSET));
   free((char *) (t+nrl-ENDOFFSET));
}

int *ivector(long nl, long nh){
/* allocate an int vector with subscript range v[nl..nh] */
   int *v;
   v=(int *)malloc((size_t) ((nh-nl+1+ENDOFFSET)*sizeof(int)));
   if (!v) uerror("allocation failure in ivector()");
   return v-nl+ENDOFFSET;
}

void free_ivector(int *v, long nl, long nh){
/* free an int vector allocated with ivector() */
   free((char *) (v+nl-ENDOFFSET));
}
```

gfx.h - screen setup and plotting routines

```
#define col_yellow  129
#define col_white   130
#define col_blue    131
#define col_cyan    132
#define dot_mode  0
#define line_mode 4
#define scale_largest 0
#define scale_range   1
#define draw_zero     2
#define draw_one      4
#define disable       128
#define d_width       1024
#define d_height      768

struct message{
   int   type;
   int   x;
   int   y;
   int   b;
   void  *box;
};

class display{
   void  setup();
   int   state;
public:
   int   d_w;
   int   d_h;
   int   nbox;
   display();
   display(int dw, int dh);
   ~display();
   message update();
   void    interact();
   void    *find_box();
   void    *boxes[10];
};

class context{
   int     bx,by;
   int     width,height;
   int     flags;
   int     clearcol;
   int     init_node;
   int     final_node;
   int     min_node;
   int     max_node;
   int     last_init_node;
   int     last_final_node;
   int     last_col;
   double  *last_vect;
   display *disp;
public:
   context(int bx, int by, int w, int h, int ccol, int flags,
           display *dispscr);
   context(float bx, float by, float w, float h, int ccol, int flags,
           display *dispscr);
   ~context();
   void  plot(double *ystore, int n,  int col, int mode);
   void  plot(double *ystore, int n,  int col, int mode, char *text);
```

```
    void  plot(double *yvect, int n, int col, char *text);
    void  plot(double *xvect, double *yvect, int n, int col, char *text);
    void  plot2(double *xvect, double *yvect, int n, int col);
    void  plot_mult(double *xvect, double **yvect, int n, int nv,
                    int col[],char *text);
    void  plot_range(int node1, int node2);
    void  reset_coords(int x, int y, int w, int h);
    void  clear();
    void  setflags(int newflags);
    int   inbox(int x, int y);
    void  setnode(int x, int node);
    void  replot();
    int   state;
};
```

gfx.cpp

```
#include "stdio.h"
#include "allegro.h"
#include "gfx.h"
#include "utils.h"
#include "assert.h"

void display::setup() {
   int   i;
   RGB   col;
   clear(screen);
   col.r=63; col.g=63; col.b=0; set_color(129,&col);
   col.r=63; col.g=63; col.b=63; set_color(130,&col);
   col.r=0; col.g=0; col.b=63; set_color(131,&col);
   col.r=0; col.g=63; col.b=63; set_color(132,&col);
   nbox=0;
   state=0;
   for (i=0;i<10;i++) {
      boxes[i]=NULL;
   }
   show_mouse(screen);
};

display::display() {
   allegro_init();
   install_keyboard();
   install_timer();
   install_mouse();
   set_gfx_mode(GFX_AUTODETECT,d_width,d_height,0,0); /* set grafix mode */
   d_w=d_width; d_h=d_height;
   setup();
};

display::display(int dw, int dh) {
   allegro_init();
   install_keyboard();
   install_timer();
   install_mouse();
   set_gfx_mode(GFX_AUTODETECT,dw,dh,0,0); /* set grafix mode */
   d_w=dw; d_h=dh;
   setup();
}

display::~display() {
   set_gfx_mode(GFX_TEXT,640,480,0,0); /* set grafix mode */
};

void *display::find_box() {
   int i;
   if (nbox>0) {
      for (i=0;i<nbox;i++) {
         if ( ( ((context *)boxes[i])->inbox(mouse_x,mouse_y)>0) )
             return (boxes[i]);
      }
   }
   return(NULL);
};

message display::update() {
   message msg;
   msg.type=0;
```

```
   msg.box=NULL;
   if ((mouse_b&1)>0) {
      do {
      }while((mouse_b&1)>0) ;
      msg.box=find_box();
      if (msg.box!=NULL) {
         msg.type=1;
         msg.x=mouse_x;
         msg.y=mouse_y;
      }
   }
   if ((mouse_b&2)>0) {
      do {
      }while((mouse_b&1)>0) ;
      msg.box=find_box();
      if (msg.box!=NULL) {
         msg.type=2;
         msg.x=mouse_x;
         msg.y=mouse_y;
      }
   }
   return(msg);
};

void display::interact() {
   message msg;
   context *ctx;

   show_mouse(screen);
   do{
      msg=update();
      if (msg.type==1) { //clicked on context
         ctx=(context *)msg.box;
         if (ctx->state==1) { //2nd click
            ctx->setnode(msg.x,2);
            ctx->state=0;
            ctx->clear();
            show_mouse(NULL);
            ctx->replot();
            show_mouse(screen);
         }
         else {
            ctx->state=1;
            ctx->setnode(msg.x,1);
         }
      }
      if (msg.type==2) { //r-clicked on context
         ctx=(context *)msg.box;
         if (ctx->state>0) {
            ctx->state=0;
         }
      }
   }while(!keypressed());
   clear_keybuf();
   show_mouse(NULL);
};

context::context(int x, int y, int w, int h, int ccol, int iflags,
                 display *dispscr){
   bx=x;
   by=y;
```

```
   width=w;
   height=h;
   clearcol=ccol;
   flags=iflags;
   rectfill(screen,bx,by,bx+w,by+h,ccol);
   init_node=1;
   final_node=2;
   min_node=1;
   max_node=2;
   state=0;
   last_vect=NULL;
   dispscr->boxes[dispscr->nbox]=(void *)this;
   dispscr->nbox++;
   disp=dispscr;
};

context::context(float x, float y, float w, float h, int ccol, int iflags,
                 display *dispscr){
   bx=dispscr->d_w*x;
   by=dispscr->d_h*y;
   width=dispscr->d_w*w;
   height=dispscr->d_h*h;
   clearcol=ccol;
   flags=iflags;
   rectfill(screen,bx,by,bx+w,by+h,ccol);
   init_node=1;
   final_node=2;
   min_node=1;
   max_node=2;
   state=0;
   last_vect=NULL;
   dispscr->boxes[dispscr->nbox]=(void *)this;
   dispscr->nbox++;
   disp=dispscr;
};

int context::inbox(int x, int y) {
   if ( (x>bx) & (x<(bx+width)) & (y>by) & (y<(by+height)) & (flags<disable) )
         return(1);
   return(0);
};

void context::plot_range(int node1, int node2){
   init_node=node1;
   final_node=node2;
};

void context::reset_coords(int x, int y, int w, int h) {
   bx=x; by=y; width=w; height=h;
};

void context::setnode(int x, int node) {
   float pixsep;
   int   w;
   pixsep=((float)(last_final_node-last_init_node)/(float)(width-20));
   if (node==1) {
      if (x>bx+10) { //in range
         init_node=last_init_node+(int)(pixsep*(x-bx-10.0));
      }
      else {
         init_node=1;
```

```
      }
   }
   else {
      if (x>bx+10) { //in range
         w=last_init_node+(int)(pixsep*(x-bx-10.0));
         if (w<init_node) {
            w=max_node;
            init_node=1;
         }
         final_node=w;
         if (final_node>max_node) final_node=max_node;
      }
      else { //reset
         state=0;
         init_node=last_init_node;
         final_node=last_final_node;
      }
   }
};

void context::replot() {
   plot(last_vect,0,last_col,dot_mode);
};

void context::plot(double *yvect, int n, int col, int mode, char *text){
   plot(yvect, n, col, mode);
   textprintf(screen,font,bx,by,col_white,text);
}

void context::plot(double *xvect, double *yvect, int n, int col, char *text){
   plot2(xvect, yvect, n, col);
   textprintf(screen,font,bx,by,col_white,text);
}

void context::plot(double *yvect, int n, int col, char *text){
   plot(yvect, n, col, dot_mode);
   textprintf(screen,font,bx,by,col_white,text);
}

void context::plot(double *yvect, int n, int col, int mode){
   int    i,j;
   double fmax=-1.0e-40;
   double fmin=0.0;
   double range;
   char   buffer[120];
   double xspace,xc;
   int    pixsep;
   double yscale=(height-20);
   double midy=by+0.5*height;
   int    node1;
   int    node2;
   int    refheight;
   assert(yvect!=NULL);

   if (n==0) {
      node2=final_node;
      node1=init_node;
   }
   else {
      node2=n;
      final_node=n;
```

```
   node1=1;
}
xspace=((double)(width-20)/(node2-node1));
pixsep=(int)((node2-node1)/(width-20));
rect(screen,bx+10,by+10,bx+width-10,by+height-10,20);
for (i=node1; i<=node2; i++) {
   if (yvect[i]>fmax) fmax=yvect[i];
}
if ((flags&scale_range)>0) { //range scale, min-max
   fmin=fmax;
   for (i=node1; i<node2; i++) {
      if (yvect[i]<fmin) fmin=yvect[i];
   }
   sprintf(buffer,"range: %e - %e   nodes: %d - %d",fmin,fmax,
                  init_node,final_node);
   textout(screen,font,buffer,bx,by+height-10,col_white);
   range=fmax-fmin;
   if ((flags&draw_zero)>0) {
      refheight=by+height-10-(int)((-fmin)/range*yscale);
      if ( (refheight<(by+height-9)) & (refheight>(by+9)) ) {
         hline(screen,bx+10,refheight,bx+width-10,col_blue);
         textout(screen,font,"0.0",0,refheight-4,col_white);
      }
   }
   if ((flags&draw_one)>0) {
      refheight=by+height-10-(int)((1.0-fmin)/range*yscale);
      if ( (refheight<(by+height-9)) & (refheight>(by+9)) ) {
         hline(screen,bx+10,refheight,bx+width-10,col_blue);
         textout(screen,font,"1.0",0,refheight-4,col_white);
      }
   }

   switch(mode) {
   case dot_mode:
      if (xspace<1.0) {
         j=node1;
         for (i=bx+10;i<bx+width-10;i++) {
            putpixel(screen,i,by+height-10-((yvect[j]-fmin)/range*yscale),col);
            j+=pixsep;
            if (j>node2) j=node2;
         }
      }
      else {
         xc=bx+10.0;
         for (i=node1; i<node2; i++) {
            putpixel(screen,xc,by+height-10-((yvect[i]-fmin)/range*yscale),col);
            xc+=xspace;
         }
      }
      break;
   case line_mode:
      for (i=node1; i<node2-1; i++) {
         line(screen,bx+10+i*xspace,by+height-10-((yvect[i]-fmin)/range*yscale),
              bx+10+i*xspace+xspace,
              by+height-10-((yvect[i+1]-fmin)/range*yscale),col);
      }
      break;
   }
}
else {//normal scale, 0-max
   sprintf(buffer,"scale: %e  nodes: %d - %d ",fmax, init_node, final_node);
```

```
      textout(screen,font,buffer,bx,by+height-10,col_white);
      hline(screen,bx,midy,bx+width,40);
      yscale*=0.5;
      switch(mode) {
      case dot_mode:
         if (xspace<1.0) {
            j=node1;
            for (i=bx+10;i<bx+width-10;i++) {
               putpixel(screen,i,midy-(yvect[j]/fmax*yscale),col);
               j+=pixsep;
            }
         }
         else {
            xc=bx+10.0;
            for (i=node1; i<node2; i++) {
               putpixel(screen,xc,midy-(yvect[i]/fmax*yscale),col);
               xc+=xspace;
            }
         }
         break;
      case line_mode:
         for (i=node1; i<node2-1; i++) {
            line(screen,bx+10+i*xspace,midy-(yvect[i]/fmax*yscale),
                 bx+10+i*xspace+xspace,midy-(yvect[i+1]/fmax*yscale),col);
         }
         break;
      }
   }
   if (last_vect==NULL) {
      min_node=1;
      max_node=node2;
   }
   last_vect=yvect;
   last_init_node=node1;
   last_final_node=node2;
   last_col=col;
};

void context::plot2(double *xvect, double *yvect, int n, int col){
   int    i,j;
   double fmax=0.0;
   double fmin=0.0;
   double deltar,pixsep;
   double range;
   char   buffer[120];
   double xspace,rc;
   double yscale=(height-20)/2;
   double midy=by+height/2;
   int    node1;
   int    node2;

   if (n==0) {
      node2=final_node;
      node1=init_node;
   }
   else {
      node2=n;
      final_node=n;
      node1=1;
   }
   deltar=xvect[node2]-xvect[node1];
```

```
   xspace=(deltar/(double)(node2-node1));
   pixsep=(double)(width-20)/deltar;
   hline(screen,bx,midy,bx+width,40);
   for (i=node1; i<=node2; i++) {
      if (yvect[i]>fmax) fmax=yvect[i];
   }
   if ((flags&scale_range)>0) { //range scale, min-max
      fmin=fmax;
      for (i=node1; i<node2; i++) {
         if (yvect[i]<fmin) fmin=yvect[i];
      }
      sprintf(buffer,"range: %e - %e   nodes: %d - %d",fmin,fmax,
                     init_node,final_node);
      textout(screen,font,buffer,bx,by+height-10,col_white);
      range=fmax-fmin;
      rc=0.0;
      for (j=node1; j<=node2; j++) {
         if (xvect[j]>(rc+xspace) ) { //next pixel at least
            putpixel(screen,bx+10+(xvect[j]-xvect[node1])*pixsep,
                     midy-((yvect[j]-fmin)/range*yscale),col);
            rc=xvect[j];
         }
      }
      if ((flags&draw_zero)>0) {
         line(screen,bx+10,midy-((-fmin)/range*yscale),
              bx+width-10,midy-((-fmin)/range*yscale),col_blue);
      }
   }
   else {//normal scale, 0-max
      sprintf(buffer,"scale: %e  nodes: %d - %d ",fmax, init_node, final_node);
      textout(screen,font,buffer,bx,by+height-10,col_white);
      rc=0.0;
      for (j=node1; j<=node2; j++) {
         if (xvect[j]>(rc+xspace) ) { //next pixel at least
            putpixel(screen,bx+10+(xvect[j]-xvect[node1])*pixsep,
                     midy-(yvect[j]/fmax*yscale),col);
            rc=xvect[j];
         }
      }
   }
   if (last_vect==NULL) {
      min_node=1;
      max_node=node2;
   }
   last_vect=yvect;
   last_init_node=node1;
   last_final_node=node2;
   last_col=col;
};

void context::plot_mult(double *xvect, double **yvect, int n, int nv, int col[],
                        char *text){
   int    i,j;
   double fmax=0.0;
   double fmin=0.0;
   double deltar,pixsep;
   double range;
   char   buffer[120];
   double xspace,rc;
   double yscale=(height-20)/2;
   double midy=by+height/2;
```

```
int    node1;
int    node2;

if (n==0) {
   node2=final_node;
   node1=init_node;
}
else {
   node2=n;
   final_node=n;
   node1=1;
}
deltar=xvect[node2]-xvect[node1];
xspace=(deltar/(double)(node2-node1));
pixsep=(double)(width-20)/deltar;
hline(screen,bx,midy,bx+width,40);
for (i=node1; i<=node2; i++) {
   if (yvect[0][i]>fmax) fmax=yvect[0][i];
}
if ((flags&scale_range)>0) { //range scale, min-max
   fmin=fmax;
   for (i=node1; i<node2; i++) {
      if (yvect[0][i]<fmin) fmin=yvect[0][i];
   }
   sprintf(buffer,"range: %e - %e   nodes: %d - %d",fmin,fmax,
          init_node,final_node);
   textout(screen,font,buffer,bx,by+height-10,col_white);
   range=fmax-fmin;
   rc=0.0;
   for (j=node1; j<=node2; j++) {
      if (xvect[j]>(rc+xspace) ) { //next pixel at least
         for (i=0; i<nv; i++) {
            putpixel(screen,bx+10+(xvect[j]-xvect[node1])*pixsep,
                     midy-((yvect[i][j]-fmin)/range*yscale),col[i]);
         }
         rc=xvect[j];
      }
   }
   if ((flags&draw_zero)>0) {
      line(screen,bx+10,midy-((-fmin)/range*yscale),bx+width-10,
           midy-((-fmin)/range*yscale),col_blue);
   }
}
else { //normal scale, 0-max
   sprintf(buffer,"scale: %e  nodes: %d - %d ",fmax, init_node, final_node);
   textout(screen,font,buffer,bx,by+height-10,col_white);
   rc=0.0;
   for (j=node1; j<=node2; j++) {
      if (xvect[j]>(rc+xspace) ) { //next pixel at least
         putpixel(screen,bx+10+(xvect[j]-xvect[node1])*pixsep,
                  midy-(yvect[i][j]/fmax*yscale),col[i]);
         rc=xvect[j];
      }
   }
}
if (last_vect==NULL) {
   min_node=1;
   max_node=node2;
}
last_vect=yvect[0];
last_init_node=node1;
```

```
   last_final_node=node2;
   last_col=col[0];
};

void context::clear() {
   rectfill(screen,bx,by,bx+width,by+height,clearcol);
};

void context::setflags(int newflags) {
   flags=newflags;
};

context::~context() {
   int i;
   int flag=0;

   for (i=0;i<disp->nbox;i++) {
      if (flag==0) {
         if (disp->boxes[i]=(void *)this) {
            flag=1;
         }
      }
      else {
         disp->boxes[i-1]=disp->boxes[i];
      }
   }
   disp->nbox--;
};
```

diskvect.h - standardised file routines for vector data

```
void create_diskvect(char*fname, int n, double value);
int  read_diskvect(char *fname, double *vect);
void write_diskvect(char*fname, int n, double *vect);
void write_diskvect_text(char*fname, int n, double *vect);
```

diskvect.cpp

```
#include "stdlib.h"
#include "stdio.h"
#include "diskvect.h"
#include "allegro.h"
#include "assert.h"

static FILE *f;

void create_diskvect(char*fname, int n, double value) {
   int i;
   f=fopen(fname,"wb");
   fwrite(&n,sizeof(int),1,f);
   for (i=0;i<n;i++) fwrite(&value,sizeof(double),1,f);
   fclose(f);
};

int read_diskvect(char *fname, double *vect) {
   int i,n;
   double w;
   f=NULL; //insurance!
   f=fopen(fname,"rb");
   if (f==NULL) {
      textprintf(screen,font,0,0,63,"Error reading: %s",fname);
      rest(2000);
      return(0);
   }
   fread(&n,sizeof(int),1,f);
   for (i=1;i<=n;i++) {
      fread(&w,sizeof(double),1,f);
      vect[i]=w;
   }
   fclose(f);
   return(n);
};

void write_diskvect(char*fname, int n, double *vect) {
   int i;
   double w;
   assert(vect!=NULL);
   f=fopen(fname,"wb");
   fwrite(&n,sizeof(int),1,f);
   for (i=1;i<=n;i++) {
      w=vect[i];
      fwrite(&w,sizeof(double),1,f);
   }
   fclose(f);
};

void write_diskvect_text(char*fname, int n, double *vect) {
   int i;
   double w;
   assert(vect!=NULL);
   f=fopen(fname,"wb");
   for (i=1;i<=n;i++) {
      w=vect[i];
      fprintf(f,"%e \n",w);
   }
   fclose(f);
};
```

rkengine.h - fourth-order Runge-Kutta implementation

```
void derivs(double x, double *y, double *dydx);
void rk4(double *y, double *dydx, int n, double x, double h, double *yout);
void rkdriver(double *vstart, int nvar, double x1, double x2, int nstep);
```

rkengine.cpp

```
#include "..\utils.h"
#include "stdio.h"
extern double **ystore, *xstore;

void derivs(double x, double *y, double *dydx);

void rk4(double *y, double *dydx, int n, double x, double h, double *yout){
   int i;
   double xh,hh,h6,*dym,*dyt,*yt;

   dym=vector(1,n);
   dyt=vector(1,n);
   yt=vector(1,n);
   hh=h*0.5;
   h6=h/6.0;
   xh=x+hh;
   for (i=1;i<=n;i++) yt[i]=y[i]+hh*dydx[i];
   derivs(xh,yt,dyt);
   for (i=1;i<=n;i++) yt[i]=y[i]+hh*dyt[i];
   derivs(xh,yt,dym);
   for (i=1;i<=n;i++) {
      yt[i]=y[i]+h*dym[i];
      dym[i] += dyt[i];
   }
   derivs(x+h,yt,dyt);
   for (i=1;i<=n;i++) yout[i]=y[i]+h6*(dydx[i]+dyt[i]+2.0*dym[i]);
   free_vector(yt,1,n);
   free_vector(dyt,1,n);
   free_vector(dym,1,n);
}

void rkdriver(double *vstart, int nvar, double x1, double x2, int nstep) {
   int i,k;
   double x,h;
   double *v,*vout,*dv;
   char buffer[40];

   v=vector(1,nvar);
   vout=vector(1,nvar);
   dv=vector(1,nvar);

   for (i=1;i<=nvar;i++) {
      v[i]=vstart[i];
      ystore[i][1]=v[i];
   }
   xstore[1]=x1;
   x=x1;
   h=(x2-x1)/nstep;
   for (k=1;k<nstep;k++) {
      derivs(x,v,dv);
      rk4(v,dv,nvar,x,h,vout);
      if ((double)(x+h) == x) uerror("Step size too small in driver");
      x += h;
      xstore[k+1]=x;
      for (i=1;i<=nvar;i++) {
         v[i]=vout[i];
         ystore[i][k+1]=v[i];
      }
   }
   free_vector(dv,1,nvar);
```

```
    free_vector(vout,1,nvar);
    free_vector(v,1,nvar);
}
```

function.h - an example showing solution of the exterior scalar field equation of motion

```
#define PI      3.141592
#define mass    1.5e3
#define gamma   1.0e-35
#define lambda  2.0e-45
#define kappa   0.0e-40

void derivs(double x, double *y, double *dydx);
void init(double *values);
void init_bfield(double *rfield,double *store,int n);
```

function.cpp

```
#include "..\utils.h"
#include "math.h"
#include "function.h"

void derivs(double x, double *y, double *dydx) {
   // provide dydx (x,y)
   double b=1-3*mass*gamma-mass/x*(2-3*mass*gamma)+gamma*x+kappa*x*x;

   dydx[1]=y[2];
   dydx[2]=-y[2]*(2/x + (((x*x-3*mass*mass)*gamma-2*kappa*x*x*x+2*mass)
          /((x*x*x-3*mass*x*x+3*mass*mass*x)*gamma-kappa*x*x*x*x+x*x-2*mass*x)))
          +y[1]/6*(6*gamma/x*(1-mass/x)-12*kappa)/b+4*lambda*y[1]*y[1]*y[1]/b;
};

void init(double *values){
   // inititalize values
   values[1]=1.0;
   values[2]=4.11e-18;
};

void init_bfield(double *rfield,double *store,int n) {
   //construct b field vector from b field expression and radius field vector
   int i;
   for (i=1;i<=n;i++) {
      store[i]=1-3*mass*gamma - mass*(2-3*mass*gamma)/rfield[i]
             + gamma*rfield[i] +kappa*rfield[i]*rfield[i];
   }
};
```

main.cpp - exterior S field Runge-Kutta example

```
#include <stdlib.h>
#include <math.h>
#include "allegro.h"
#include "..\utils.h"
#include "rkengine.h"
#include "function.h"
#include "..\gfx.h"
#include "stdio.h"
#include "..\diskvect.h"

int    n,n2;   //nodes
int    nvar;   //variables
double **ystore, *xstore;   //result storage
double xmin,xmax;
double *values;
double *bfield;
double h;

context *function;
context *deriv;

void main() {
   // s field eqn of motion rk, to give about S'/S=10^-26 at 30AU
   // use scaled field (S-bar)
   int   i;
   n=100001;
   nvar=2;
   xmin=1*7.0e8;
   xmax=40.0*200.0*7.0e8;   // in solar radii
   h=(xmax-xmin)/(n-1);

   xstore=vector(1,n);
   ystore=matrix(1,nvar,1,n);
   values=vector(1,nvar);
   bfield=vector(1,n);
   char buffer[50];

   display *dispscr;
   dispscr=new display(1280,1024);
   context function((float)0.0,0.025,1.0,0.47,0,scale_range,dispscr);
   context deriv((float)0.0,0.5,1.0,0.47,0,scale_range,dispscr);

   init(values);

   rkdriver(values,nvar,xmin,xmax,n);

   function.clear();
   deriv.clear();
   function.plot(ystore[1],n,col_white,"S field");
   deriv.plot(ystore[2],n,col_cyan,"S' field");
   dispscr->interact();

   //record results to disk
   //write_diskvect("sfield.vct",n,ystore[1]);
   //write_diskvect("r.vct",n,xstore);
   //write_diskvect("ds.vct",n,ystore[2]);
   //create_diskvect("afield.vct",n,1.0);
   //init_bfield(xstore,bfield,n);
   //write_diskvect("bfield.vct",n,bfield);
```

```
    free_vector(xstore,1,n);
    free_matrix(ystore,1,nvar,1,n);
    free_vector(values,1,nvar);
    free_vector(bfield,1,n);
}

END_OF_MAIN();
```

mat2.h - further matrix routines for Newton-Raphson solutions

```
class vec2 {
public:
   vec2();
   vec2(double a, double b);
   ~vec2();
   double a,b;
   inline vec2 operator-(const vec2& v) const{ return vec2(a-v.a, b-v.b);}
   inline vec2 operator*(const double fl) const{ return vec2(a*fl, b*fl);}
};

class vec3 {
public:
   vec3();
   vec3(double a, double b, double c);
   ~vec3();
   double a,b,c;
   inline vec3 operator-(const vec3& v) const{ return vec3(a-v.a, b-v.b, c-v.c);}
   inline vec3 operator*(const double fl) const{ return vec3(a*fl, b*fl, c*fl);}
};

class mat2 {
public:
   mat2();
   mat2(double a, double b, double c, double d);
   ~mat2();
   double a,b,c,d;
   mat2 inverse();
   inline mat2 operator+(const mat2& m) const{
                              return mat2(a+m.a, b+m.b, c+m.c, d+m.d);}
   inline mat2 operator-(const mat2& m) const{
                              return mat2(a-m.a, b-m.b, c-m.c, d-m.d);}
   inline mat2 operator*(const mat2& m) const{
          return mat2(a*m.a+b*m.c, a*m.b+b*m.d, c*m.a+d*m.c, c*m.b+d*m.d);}
   inline vec2 operator*(const vec2& v) const{
                              return vec2(a*v.a+b*v.b, c*v.a+d*v.b);}
};

class mat3 {
public:
   mat3();
   mat3(double e0, double e1, double e2, double e3, double e4, double e5,
        double e6, double e7, double e8);
   ~mat3();
   double e11,e12,e13,e21,e22,e23,e31,e32,e33;
   mat3   inverse();
   inline mat3 operator+(const mat3& m) const{ return mat3(e11+m.e11,
       e12+m.e12, e13+m.e13, e21+m.e21, e22+m.e22,
       e23+m.e23, e31+m.e31, e32+m.e32, e33+m.e33);}
   inline mat3 operator-(const mat3& m) const{ return mat3(e11-m.e11,
       e12-m.e12, e13-m.e13, e21-m.e21, e22-m.e22,
       e23-m.e23, e21-m.e31, e32-m.e32, e33-m.e33);}
   inline mat3 operator*(const mat3& m) const{ return
       mat3(e11*m.e11+e12*m.e21+e13*m.e31, e11*m.e12+e12*m.e22+e13*m.e32,
            e11*m.e13+e12*m.e23+e13*m.e33, e21*m.e11+e22*m.e21+e23*m.e31,
            e21*m.e12+e22*m.e22+e23*m.e32, e21*m.e13+e22*m.e23+e23*m.e33,
            e31*m.e11+e32*m.e21+e33*m.e31, e31*m.e12+e32*m.e22+e33*m.e32,
            e31*m.e13+e32*m.e23+e33*m.e33);}
   inline vec3 operator*(const vec3& v) const{ return
       vec3(e11*v.a+e12*v.b+e13*v.c, e21*v.a+e22*v.b+e23*v.c,
            e31*v.a+e32*v.b+e33*v.c);}
```

```
};
```

mat2.cpp

```
#include <stdlib.h>
#include <stdio.h>
#include <math.h>
#include <conio.h>
#include "..\utils.h"
#include "mat2.h"

mat2::mat2() {
   a=0.0;
   b=0.0;
   c=0.0;
   d=0.0;
};

mat2::~mat2() {
};

mat2::mat2(double ia, double ib, double ic, double id) {
   a=ia;
   b=ib;
   c=ic;
   d=id;
};

mat2 mat2::inverse() {
   double det=1/(a*b-c*d);
   return (mat2(det*d,-det*b,-det*c,det*a));
};

vec2::vec2() {
   a=0.0; b=0.0;
};

vec2::vec2(double ia, double ib) {
   a=ia; b=ib;
};

vec2::~vec2(){
};

mat3::mat3() {
   e11=0.0;e12=0.0;e13=0.0;
   e21=0.0;e22=0.0;e23=0.0;
   e31=0.0;e32=0.0;e33=0.0;
};

mat3::~mat3() {
};

mat3::mat3(double e0, double e1, double e2, double e3, double e4, double e5,
           double e6, double e7, double e8) {
   e11=e0;e12=e1;e13=e2;
   e21=e3;e22=e4;e23=e5;
   e31=e6;e32=e7;e33=e8;
};

mat3 mat3::inverse() {
   double det=1/((e11*e22-e12*e21)*e33+(e13*e21-e11-e23)*e32
                 +(e12*e23-e13*e22)*e31);
   return (mat3(
```

```
      det*(e22*e33-e23*e32), det*(e13*e32-e12*e33), det*(e12*e23-e13*e22),
      det*(e23*e31-e21*e33), det*(e11*e33-e13*e31), det*(e13*e21-e11*e23),
      det*(e21*e32-e22*e31), det*(e12*e31-e11*e32), det*(e11*e22-e12*e21)));
};

vec3::vec3() {
   a=0.0;b=0.0;c=0.0;
};

vec3::vec3(double ia, double ib, double ic) {
   a=ia;b=ib;c=ic;
};

vec3::~vec3(){
};
```

main.cpp - Newton-Raphson example in exterior $\bar{a}$ and S fields

```
#include <stdlib.h>
#include <stdio.h>
#include <math.h>
#include <conio.h>
#include "..\diskvect.h"
#include "allegro.h"
#include "..\gfx.h"
#include "..\utils.h"
#include "mat2.h"

#define afield 1
#define sfield 2
#define aresidual 3
#define sresidual 4
const int IT_count=275;

typedef unsigned char byte;
typedef unsigned int  word;

int    n,i;
double lambda;
double ln,l0;
double h,h2,h3,h4;
double alpha,beta,gamma,kappa;
double aippp,aipp,aip,ai,aim,aimm,aimmm;
double anppp,anpp,anp,a1m,a1mm,a1mmm;
double sippp,sipp,sip,si,sim,simm,simmm;
double snppp,snpp,snp,s1m,s1mm,s1mmm;
double rippp,ripp,rip,ri,rim,rimm,rimmm;
double rnppp,rnpp,rnp,r1m,r1mm,r1mmm;
double si2,si3,ai2,ai3,r,r2,bi,bi2,dbi,ddbi,dddbi,dbi2;
double si4,r3,r4;
double sip2,sim2,s1m2,snp2,ai4,ai5,aip2,aim2;

void   iterate();
void   invert();
void   getvar(int i);
double bval(double r);
double dbval(double r);
double ddbval(double r);
double dddbval(double r);
double calcf();
void   calcj();
void   equate(vec2 *v2, vec2 *v1);

byte var;
int  t;
char tempc[20];
double *avect, *svect, *rvect;
double *readvect;
void   scale_diskvect(char *fname, double *vect);
void   extract_vector(char idx);
mat2   *d,*e,*f,*al,*ga;
vec2   *b,*c,*x,*solnx,*solnx2;

void main() {
//nr for a,s with b assumed exsol
//general routine for inversion block-3diagonal,
//given appropriate classes for block matrices and vectors
```

```
byte    flag;
display *dispscr;
dispscr=new display(1280,1024);
context output((float)0.0,0.025,1.0,0.475,0,scale_range,dispscr);
context residual((float)0.0,0.5,1.0,0.475,0,scale_range,dispscr);
FILE    *fp;

n=251; l0=7.0e8; ln=10*200.0*7.0e8;

alpha=6.0e21; beta=1.5e3; gamma=1.0e-28; kappa=0.0e-50; lambda=1.0e-35;

rvect=vector(1,n);
svect=vector(1,n);
avect=vector(1,n);
scale_diskvect("svect.vct",svect);
scale_diskvect("avect.vct",avect);
d=new mat2[n];
e=new mat2[n];
f=new mat2[n];
al=new mat2[n];
ga=new mat2[n];
b=new vec2[n];
c=new vec2[n];
x=new vec2[n];
solnx=new vec2[n];
solnx2=new vec2[n];

h=(ln-l0)/(n);
h2=h*h;
h3=h2*h;
h4=h3*h;
flag=0;

//boundary conditions
double r;
s1m=1.0;
snp=svect[n]+1.0e-26*h;
snp2=snp*snp; s1m2=s1m*s1m;
a1m=1.0-1.782e-9;
anp=avect[n];

for (i=1;i<=n;i++) {
   rvect[i]=l0+i*h;
   solnx[i-1].a=avect[i];
   solnx[i-1].b=svect[i];
}


write_diskvect_text("rvect.txt",n,rvect);
equate(solnx2,solnx);

//starting solution
extract_vector(sfield);
extract_vector(afield);
output.plot(avect, n, col_yellow, "start a");
residual.plot(svect,n,col_yellow,"S field");
textprintf(screen,font,0,0,col_white,"h: %f",h);
dispscr->interact();

for (t=0; t<IT_count; t++) {
   iterate();
```

```
      textprintf(screen,font,180,0,62,"ITERATED ");
      output.clear();
      residual.clear();
      extract_vector(sresidual);
      residual.plot(svect, n, 75, "s residual");
      extract_vector(sfield);
      output.plot(svect, n, col_white, "s field");
      textprintf(screen,font,180,0,62,"PLOTTED  ");
   }

   output.clear();
   residual.clear();
   extract_vector(sresidual);
   residual.plot(svect, n, 75, "s residual");
   extract_vector(sfield);
   output.plot(svect, n, col_white, "S field");
   dispscr->interact();

   output.clear();
   residual.clear();
   extract_vector(aresidual);
   residual.plot(avect, n, 75, "a residual");
   extract_vector(afield);
   output.plot(avect, n, col_white, "a field");
   dispscr->interact();

   free_vector(rvect,1,n);
   free_vector(svect,1,n);
   free_vector(avect,1,n);
}
END_OF_MAIN();

void equate(vec2 *v2, vec2 *v1) {
   word limit=n;
   word i;
   for (i=0;i<limit;i++) {
      v2[i]=v1[i];
   }
};

void getvar(int i) {
   ai=solnx[i].a;
   si=solnx[i].b;
   ri=rvect[i+1];
   if (i==0) {
      sim=s1m;
      aim=a1m;
   }
   else {
      aim=solnx[i-1].a;
      sim=solnx[i-1].b;
   }

   if (i==(n-1)) {
      anp=ai; //fixme, zero slope bc
      sip=snp;
      aip=anp;
   }
   else {
      aip=solnx[i+1].a;
      sip=solnx[i+1].b;
```

```
   }

   bi=bval(ri);
   dbi=dbval(ri);
   ddbi=ddbval(ri);
   dddbi=dddbval(ri);
   si2=si*si;
   si3=si2*si;
   ai2=ai*ai;
   ai3=ai2*ai;
   bi2=bi*bi;
   r=ri;
   r2=ri*ri;
   si4=si3*si;
   r3=r2*ri;
   r4=r3*ri;
   sim2=sim*sim;
   sip2=sip*sip;
   aip2=aip*aip;
   aim2=aim*aim;
   ai4=ai2*ai2;
   ai5=ai3*ai2;
}

double calcf() {
   int i;

   //debugging log
   //FILE *fp=fopen("res.txt","wb");

   for (i=0; i<n; i++) {
      getvar(i);
      b[i].a= - ((ai2 * si4 * lambda)/bi) + ((sip2)/(8 * h2))
 - ((sim * sip)/(4 * h2)) - ((dbi * si * sip)/(12 * ai2 * h * r))
 - ((aip * bi * si * sip)/(12 * ai3 * h2 * r)) + ((aim * bi * si * sip)
/(12 * ai3 * h2 * r)) - ((aip * dbi * si * sip)/(24 * ai3 * h2))
 + ((aim * dbi * si * sip)/(24 * ai3 * h2)) + ((si * sip)/(3 * h2))
 - ((aip2 * bi * si * sip)/(24 * ai4 * h3)) + ((aim * aip * bi * si * sip)
/(12 * ai4 * h3)) - ((aim2 * bi * si * sip)/(24 * ai4 * h3))
+ ((sim2)/(8 * h2)) + ((dbi * si * sim)/(12 * ai2 * h * r))
+ ((aip * bi * si * sim)/(12 * ai3 * h2 * r)) - ((aim * bi * si * sim)
/(12 * ai3 * h2 * r)) + ((aip * dbi * si * sim)/(24 * ai3 * h2))
 - ((aim * dbi * si * sim)/(24 * ai3 * h2)) + ((si * sim)/(3 * h2))
 + ((aip2 * bi * si * sim)/(24 * ai4 * h3)) - ((aim * aip * bi * si * sim)
/(12 * ai4 * h3)) + ((aim2 * bi * si * sim)/(24 * ai4 * h3))
 + ((aip * si2)/(3 * ai * h * r)) - ((aim * si2)/(3 * ai * h * r))
 + ((dbi * si2)/(6 * bi * r)) - ((si2)/(6 * bi * r2)) + ((si2)/(6 * r2))
 + ((aip * dbi * si2)/(12 * ai * bi * h)) - ((aim * dbi * si2)/(12 * ai * bi * h))
 + ((aip2 * si2)/(8 * ai2 * h2)) - ((aim * aip * si2)/(4 * ai2 * h2))
 + ((aim2 * si2)/(8 * ai2 * h2)) - ((2 * si2)/(3 * h2));

      b[i].b= - 4 * si3 * lambda + ((bi * sip)/(ai2 * h * r))
 + ((dbi * sip)/(2 * ai2 * h)) + ((aip * bi * sip)/(2 * ai3 * h2))
 - ((aim * bi * sip)/(2 * ai3 * h2)) + ((bi * sip)/(ai2 * h2))
 - ((bi * sim)/(ai2 * h * r)) - ((dbi * sim)/(2 * ai2 * h))
 - ((aip * bi * sim)/(2 * ai3 * h2)) + ((aim * bi * sim)/(2 * ai3 * h2))
 + ((bi * sim)/(ai2 * h2)) + ((aip * bi * si)/(ai3 * h * r))
 - ((aim * bi * si)/(ai3 * h * r)) + ((2 * dbi * si)/(3 * ai2 * r))
 + ((bi * si)/(3 * ai2 * r2)) - (si/(3 * ai2 * r2)) + ((aip * dbi * si)
/(2 * ai3 * h)) - ((aim * dbi * si)/(2 * ai3 * h)) + ((aip * bi * si)
/(ai3 * h2)) + ((aim * bi * si)/(ai3 * h2)) - ((4 * bi * si)/(ai2 * h2))
```

```
 + ((ddbi * si)/(6 * ai2));

      //fprintf(fp,"res: %e %e , bi: %e, ai: %e, si: %e, ri: %e\n",
                b[i].a,b[i].b,bi,ai,si,ri);
   }

   //fclose(fp);
   return(0.0);
}

void calcj() {
   int i;

   //debugging log
   //FILE *fp=fopen("jac.txt","wb");
   //calc jmat

   for (i=0; i<n; i++) {
      getvar(i);

      //deqns/dvars(i)
      d[i].a= - ((2 * ai * si4 * lambda)/bi) + ((dbi * si * sip)
/(6 * ai3 * h * r)) + ((aip * bi * si * sip)/(4 * ai4 * h2 * r))
 - ((aim * bi * si * sip)/(4 * ai4 * h2 * r)) + ((aip * dbi * si * sip)
/(8 * ai4 * h2)) - ((aim * dbi * si * sip)/(8 * ai4 * h2))
 + ((aip2 * bi * si * sip)/(6 * ai5 * h3)) - ((aim * aip * bi * si * sip)
/(3 * ai5 * h3)) + ((aim2 * bi * si * sip)/(6 * ai5 * h3))
 - ((dbi * si * sim)/(6 * ai3 * h * r)) - ((aip * bi * si * sim)
/(4 * ai4 * h2 * r)) + ((aim * bi * si * sim)/(4 * ai4 * h2 * r))
 - ((aip * dbi * si * sim)/(8 * ai4 * h2)) + ((aim * dbi * si * sim)
/(8 * ai4 * h2)) - ((aip2 * bi * si * sim)/(6 * ai5 * h3))
 + ((aim * aip * bi * si * sim)/(3 * ai5 * h3)) - ((aim2 * bi * si * sim)
/(6 * ai5 * h3)) - ((aip * si2)/(3 * ai2 * h * r)) + ((aim * si2)
/(3 * ai2 * h * r)) - ((aip * dbi * si2)/(12 * ai2 * bi * h))
 + ((aim * dbi * si2)/(12 * ai2 * bi * h)) - ((aip2 * si2)/(4 * ai3 * h2))
 + ((aim * aip * si2)/(2 * ai3 * h2)) - ((aim2 * si2)/(4 * ai3 * h2));

      d[i].b= - ((4 * ai2 * si3 * lambda)/bi) - ((dbi * sip)/(12 * ai2 * h * r))
 - ((aip * bi * sip)/(12 * ai3 * h2 * r)) + ((aim * bi * sip)
/(12 * ai3 * h2 * r)) - ((aip * dbi * sip)/(24 * ai3 * h2))
 + ((aim * dbi * sip)/(24 * ai3 * h2)) + (sip/(3 * h2))
 - ((aip2 * bi * sip)/(24 * ai4 * h3)) + ((aim * aip * bi * sip)
/(12 * ai4 * h3)) - ((aim2 * bi * sip)/(24 * ai4 * h3))
 + ((dbi * sim)/(12 * ai2 * h * r)) + ((aip * bi * sim)/(12 * ai3 * h2 * r))
 - ((aim * bi * sim)/(12 * ai3 * h2 * r)) + ((aip * dbi * sim)/(24 * ai3 * h2))
 - ((aim * dbi * sim)/(24 * ai3 * h2)) + (sim/(3 * h2)) + ((aip2 * bi * sim)
/(24 * ai4 * h3)) - ((aim * aip * bi * sim)/(12 * ai4 * h3))
 + ((aim2 * bi * sim)/(24 * ai4 * h3)) + ((2 * aip * si)/(3 * ai * h * r))
 - ((2 * aim * si)/(3 * ai * h * r)) + ((dbi * si)/(3 * bi * r))
 - (si/(3 * bi * r2)) + (si/(3 * r2)) + ((aip * dbi * si)/(6 * ai * bi * h))
 - ((aim * dbi * si)/(6 * ai * bi * h)) + ((aip2 * si)/(4 * ai2 * h2))
 - ((aim * aip * si)/(2 * ai2 * h2)) + ((aim2 * si)/(4 * ai2 * h2))
 - ((4 * si)/(3 * h2));

      d[i].c= - ((2 * bi * sip)/(ai3 * h * r)) - ((dbi * sip)/(ai3 * h))
 - ((3 * aip * bi * sip)/(2 * ai4 * h2)) + ((3 * aim * bi * sip)/(2 * ai4 * h2))
 - ((2 * bi * sip)/(ai3 * h2)) + ((2 * bi * sim)/(ai3 * h * r)) + ((dbi * sim)
/(ai3 * h)) + ((3 * aip * bi * sim)/(2 * ai4 * h2)) - ((3 * aim * bi * sim)
/(2 * ai4 * h2)) - ((2 * bi * sim)/(ai3 * h2)) - ((3 * aip * bi * si)
/(ai4 * h * r)) + ((3 * aim * bi * si)/(ai4 * h * r)) - ((4 * dbi * si)
/(3 * ai3 * r)) - ((2 * bi * si)/(3 * ai3 * r2)) + ((2 * si)/(3 * ai3 * r2))
```

```
 - ((3 * aip * dbi * si)/(2 * ai4 * h)) + ((3 * aim * dbi * si)/(2 * ai4 * h))
 - ((3 * aip * bi * si)/(ai4 * h2)) - ((3 * aim * bi * si)/(ai4 * h2))
 + ((8 * bi * si)/(ai3 * h2)) - ((ddbi * si)/(3 * ai3));

      d[i].d= - 12 * si2 * lambda + ((aip * bi)/(ai3 * h * r))
 - ((aim * bi)/(ai3 * h * r)) + ((2 * dbi)/(3 * ai2 * r)) + (bi/(3 * ai2 * r2))
 - (1/(3 * ai2 * r2)) + ((aip * dbi)/(2 * ai3 * h)) - ((aim * dbi)/(2 * ai3 * h))
 + ((aip * bi)/(ai3 * h2)) + ((aim * bi)/(ai3 * h2)) - ((4 * bi)/(ai2 * h2))
 + (ddbi/(6 * ai2));

      //deqns/dvars(i-1)
      if (i>0) {
         e[i].a=((bi * si * sip)/(12 * ai3 * h2 * r)) + ((dbi * si * sip)
/(24 * ai3 * h2)) + ((aip * bi * si * sip)/(12 * ai4 * h3))
 - ((aim * bi * si * sip)/(12 * ai4 * h3)) - ((bi * si * sim)/(12 * ai3 * h2 * r))
 - ((dbi * si * sim)/(24 * ai3 * h2)) - ((aip * bi * si * sim)/(12 * ai4 * h3))
 + ((aim * bi * si * sim)/(12 * ai4 * h3)) - ((si2)/(3 * ai * h * r))
 - ((dbi * si2)/(12 * ai * bi * h)) - ((aip * si2)/(4 * ai2 * h2))
 + ((aim * si2)/(4 * ai2 * h2));

         e[i].b= - (sip/(4 * h2)) + (sim/(4 * h2)) + ((dbi * si)
/(12 * ai2 * h * r)) + ((aip * bi * si)/(12 * ai3 * h2 * r))
 - ((aim * bi * si)/(12 * ai3 * h2 * r)) + ((aip * dbi * si)/(24 * ai3 * h2))
 - ((aim * dbi * si)/(24 * ai3 * h2)) + (si/(3 * h2)) + ((aip2 * bi * si)
/(24 * ai4 * h3)) - ((aim * aip * bi * si)/(12 * ai4 * h3))
 + ((aim2 * bi * si)/(24 * ai4 * h3));

         e[i].c= - ((bi * sip)/(2 * ai3 * h2)) + ((bi * sim)/(2 * ai3 * h2))
 - ((bi * si)/(ai3 * h * r)) - ((dbi * si)/(2 * ai3 * h)) + ((bi * si)/(ai3 * h2));

         e[i].d= - (bi/(ai2 * h * r)) - (dbi/(2 * ai2 * h)) - ((aip * bi)
/(2 * ai3 * h2)) + ((aim * bi)/(2 * ai3 * h2)) + (bi/(ai2 * h2));
      }
      else {
         e[i].a=0.0;
         e[i].b=0.0;
         e[i].c=0.0;
         e[i].d=0.0;
      }

      //deqns/dvars(i+1)
      f[i].a= - ((bi * si * sip)/(12 * ai3 * h2 * r)) - ((dbi * si * sip)
/(24 * ai3 * h2)) - ((aip * bi * si * sip)/(12 * ai4 * h3))
 + ((aim * bi * si * sip)/(12 * ai4 * h3)) + ((bi * si * sim)/(12 * ai3 * h2 * r))
 + ((dbi * si * sim)/(24 * ai3 * h2)) + ((aip * bi * si * sim)/(12 * ai4 * h3))
 - ((aim * bi * si * sim)/(12 * ai4 * h3)) + ((si2)/(3 * ai * h * r))
 + ((dbi * si2)/(12 * ai * bi * h)) + ((aip * si2)/(4 * ai2 * h2))
 - ((aim * si2)/(4 * ai2 * h2));

      f[i].b=(sip/(4 * h2)) - (sim/(4 * h2)) - ((dbi * si)/(12 * ai2 * h * r))
 - ((aip * bi * si)/(12 * ai3 * h2 * r)) + ((aim * bi * si)/(12 * ai3 * h2 * r))
 - ((aip * dbi * si)/(24 * ai3 * h2)) + ((aim * dbi * si)/(24 * ai3 * h2))
 + (si/(3 * h2)) - ((aip2 * bi * si)/(24 * ai4 * h3)) + ((aim * aip * bi * si)
/(12 * ai4 * h3)) - ((aim2 * bi * si)/(24 * ai4 * h3));

      f[i].c=((bi * sip)/(2 * ai3 * h2)) - ((bi * sim)/(2 * ai3 * h2))
 + ((bi * si)/(ai3 * h * r)) + ((dbi * si)/(2 * ai3 * h)) + ((bi * si)/(ai3 * h2));

      f[i].d=(bi/(ai2 * h * r)) + (dbi/(2 * ai2 * h)) + ((aip * bi)/(2 * ai3 * h2))
 - ((aim * bi)/(2 * ai3 * h2)) + (bi/(ai2 * h2));
```

```
      //fprintf(fp,"e: %e %e %e %e  d: %e %e %e %e\n",
      //e[i].a,e[i].b,e[i].c,e[i].d,d[i].a,d[i].b,d[i].c,d[i].d);
   }
   //fclose(fp);
}

void iterate() {
   int i;

   double oldf,frac;

   textprintf(screen,font,180,0,62,"ENTERED  ");
   oldf=calcf();
   textprintf(screen,font,180,0,62,"CALCED F ");
   calcj();
   textprintf(screen,font,180,0,62,"CALCED J ");

   // calc inverse j
   invert();
   textprintf(screen,font,180,0,62,"INVERTED ");

   frac=1.0;
   equate(solnx2,solnx);

   //calc x vector (new iteration)
   for (i=0; i<n; i++) {
      solnx[i]=solnx[i]-(x[i]*frac);
   }
   equate(solnx2,solnx);
}

void invert() {
   int j;

   al[0]=d[0];
   ga[0]=f[0]*al[0].inverse();

   for (j=1;j<(n-1);j++) {
      al[j]=d[j]-e[j]*ga[j-1];
      ga[j]=f[j]*al[j-1].inverse();
   };

   al[n-1]=d[n-1]-e[n-1]*ga[n-2];
   c[0]=d[0].inverse()*b[0];
   for (j=1;j<n;j++) {
      c[j]=al[j].inverse()*(b[j]-e[j]*c[j-1]);
   };

   x[n-1]=c[n-1];
   for (j=n-2; j>=0; j--) {
      x[j]=c[j]-ga[j]*x[j+1];
   };

}

void scale_diskvect(char *fname, double *vect) {
   int i,j,skip,nr;
   double w;
   FILE *f;

   f=NULL; f=fopen(fname,"rb");
```

```
   if (f==NULL) {
      textprintf(screen,font,0,0,63,"Error reading: %s",fname);
      rest(2000);
   }

   fread(&nr,sizeof(int),1,f);
   readvect=vector(1,nr);
   for (i=1;i<=nr;i++) {
      fread(&w,sizeof(double),1,f);
      readvect[i]=w;
   }
   fclose(f);

   //subsample
   skip=(nr-1)/(n-1);
   j=1;
   vect[1]=readvect[1];
   for(i=2;i<=n;i++) {
      j+=skip;
      vect[i]=readvect[j];
   }
   free_vector(readvect,1,nr);
};

double bval(double r) {
   return(1-beta/r-3*beta*gamma+gamma*r+kappa*r*r);
};

double dbval(double r) {
   return(beta/(r*r)+gamma+2*kappa*r);
};

double ddbval(double r) {
   return(-2*beta/(r*r*r)+2*kappa);
};

double dddbval(double r) {
   return(6*beta/(r*r*r*r));
};

void extract_vector(char idx) {
   int i;

   for (i=0;i<n;i++) {
      switch (idx) {
      case afield:
         avect[i+1]=solnx[i].a;
         break;
      case sfield:
         svect[i+1]=solnx[i].b;
         break;
      case aresidual:
         avect[i+1]=b[i].a;
         break;
      case sresidual:
         svect[i+1]=b[i].a;
         break;
      };
   };
}
```

Appendix D

Effects of Numerical Limitations on Solutions

The most illustrative example of the methodical uncertainties is the near-limb solution for b. When performed by Runge-Kutta methods, the region of confidence of the results was effected by the value of α, and showed features due to both the analytical and the numerical properties of the system.

For the exterior system with α of order 10^{15}, the uncertainties are of a small magnitude, and have the useful feature of being essentially evenly distributed around the standard solution (figures D.1, D.2). The deviations from the standard Schwarzschild solution with this value of α do not have appreciable bias either positively or negatively, and in fact possess a regular structure which is most obviously connected to the method's parameter h, the step size (or equivalently to n, the number of intervals). By extending the domain of the integration, it is found that this structure continues out to very large radius and the perturbations from Schwarzschild become oscillatory and of a fixed amplitude. The magnitude and onset of the oscillations is controlled by α, smaller values of α result in the oscillations not becoming apparent until further out in radius, and the oscillations grow more slowly to their maximum amplitude. With larger values, such as the 10^{22} value that makes simultaneous solution for b and S more stable, the oscillations set in earlier and have larger magnitude and longer period (fig. D.3). By examining the behaviour of the higher derivatives of b, it is found that they vanish quite quickly with increasing radius, and that this is accelerated by higher values of α. Once they are small enough compared to the machine accuracy ϵ_m, the structure of the differential equations resembles that of a sinusoidal function i.e. something like $b''' + b' = 0$. At this point the numerical accuracy is no longer sufficient to solve the actual differential equation we started with.

The stepsize dependant structure to the deviation from Schwarzschild is due

to the fixed spacing of the evaluation of the function. With different stepsizes, the function is sampled at differing intervals and produces quite different seeming patterns. The sinusoidal features can be observed by increasing the number of points (reducing h) or by integrating with a larger value of α. In effect, the exact structure observed for low values of α is an aliasing effect on a sinusoidal variation, i.e. sampling a sinusoid at different rates and producing differently structured results (figures D.1, D.2). The scatter of the points is found is to increase to a fixed maximum scale around the vacuum solution, where the numerical method is tracking the oscillations of the far-field solution with high accuracy.

The stepsize dependant variation can also generate error in the method in its own right, in the form of truncation errors in regions where the fields' difference between any pair of mesh points is becoming small compared to the machine accuracy ϵ_m. This kind of effect can be quite apparent from plots of the function and its derivative, where the derivative can vary smoothly yet the function shows an abrupt change in slope. This occurs when individual Runge-Kutta steps cannot change the value of the field due to the change in the field being less than ϵ_m, resulting in the field remaining constant until the gradient increases above this threshold. This effect can sometimes be alleviated by reformulating the equations in terms of (say) $(b-1)$ rather than b, in which case the Runge-Kutta step produces an increment which is no longer order ϵ_m less than the previous value of the field, so that it may be effectively added.

Due to effects of this kind, the size of the domain over which the integration can be satisfactorily performed is quite sensitive to the value of α, larger values damping down the contribution of the $\bar{a}$ and S fields to the source of the field equations and extending the region of stability. With α of order 10^{15}, the Runge-Kutta solutions for b and S simultaneously could not be extended satisfactorily beyond a few solar radii, but for larger values of the coupling constant α the fields can be produced for a reasonable range — up to several AU. Beyond this stability region the fields need to be solved for on an individual, self-consistent basis.

The results of the fourth-order Runge-Kutta used to perform these integrations were confirmed by use of third party routine as a check. In this case, Matlab routines were used to solve the same system. This also provided an opportunity to use a stiff system solving routine, which produced very similar results to the routine written in-house. The Matlab routines provided essentially

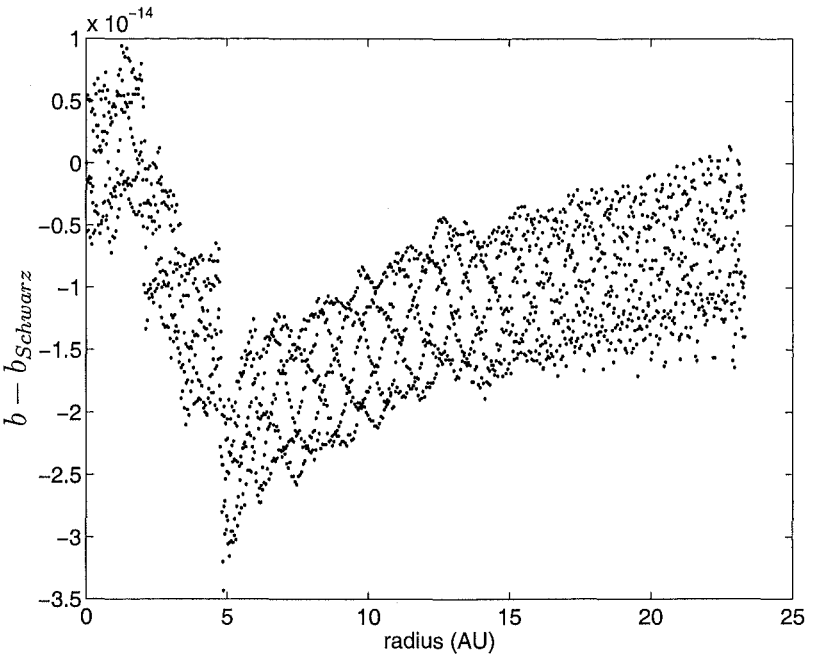

Figure D.1: b difference from Schwarzschild - $n = 500,000$, $\alpha \sim 10^{15}$

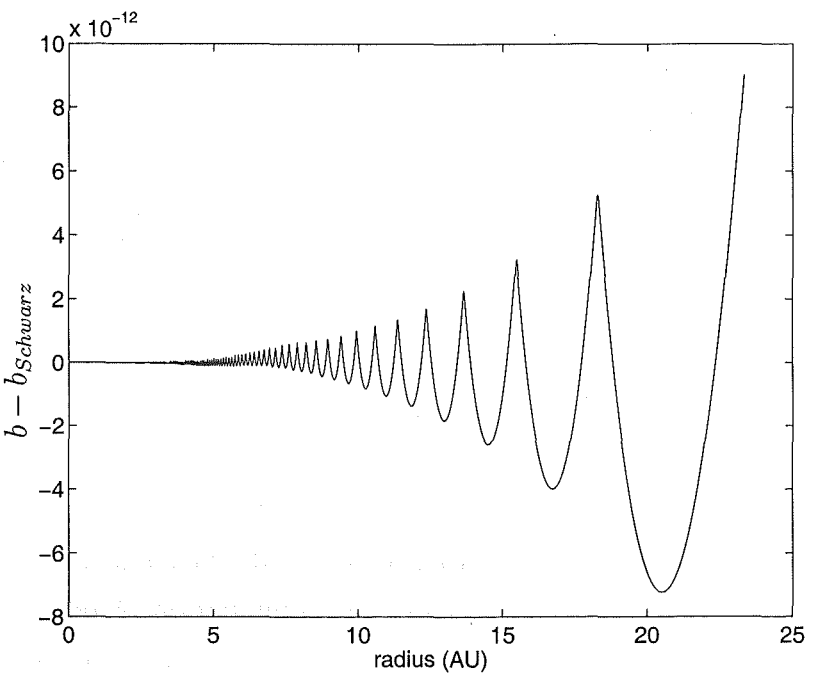

Figure D.2: b difference from Schwarzschild - $n = 5,000,000$, $\alpha \sim 10^{15}$

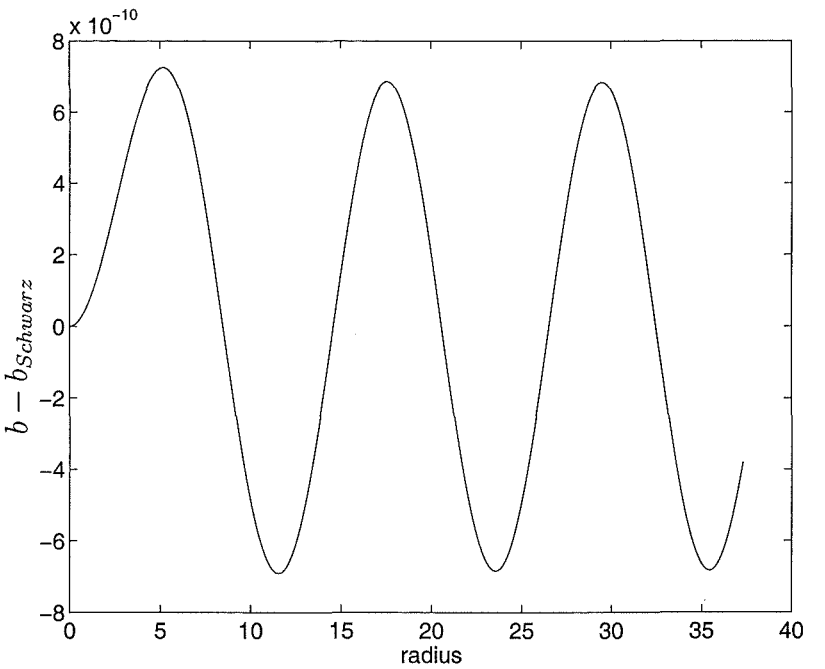

Figure D.3: b difference from Schwarzschild, $\alpha \sim 10^{22}$

identical results to what had been produced previously, though not to as fine a tolerance. This gives extra confidence in our results. The effect of changing α was also confirmed, low-α integrations could not be carried out to the same distances as higher α systems. The $\alpha \sim 10^{22}$ two-variable system had the same limits as before, around twenty to twenty-five solar radii. In addition, due to Matlab having more provisions built in to handle near-singular values, and by using variable stepsizes to step around them, the nature of the region where the low-α routines break down can be investigated further. Beyond any feedback effects as described above, it also seems that some of the difficulties are being introduced by an unfortunate combination of terms in the formulation that can become near-singular at some point. This would be suggested by a spike or gaussian-like feature appearing in the S derivative for low α, beyond the region where the results seem acceptable. This kind of effect has been observed before in single-variable systems, and can often be removed by changing the formulation of the system of equations. In this case, the combination of terms responsible has not yet been singled out. Such a feature does not occur for larger values of α, and does not effect the success of solving for each field individually with the values of α that were investigated.

Appendix E

Field Equation Derivation

The usual method for deriving the metric form of the Weyl field equations is by taking a variational approach. Given an action $I = \int d^4x\,(-g)^{\frac{1}{2}}\,L$ for Lagrangian density L, the elements of the tensor $W^{\mu\nu}$ can be found according to

$$\begin{aligned} g^{\frac{1}{2}}W^{rr} &= \frac{\delta I}{\delta g_{rr}} \\ &= \frac{\partial}{\partial a}\left(g^{\frac{1}{2}}L\right) - \frac{\partial}{\partial r}\left(g^{\frac{1}{2}}\frac{\partial L}{\partial a'}\right) + \frac{\partial^2}{\partial r^2}\left(g^{\frac{1}{2}}\frac{\partial L}{\partial a''}\right) \end{aligned}$$

where the second equality has assumed a standard line element of the form

$$ds^2 = -b\,(r)\,dt^2 + a\,(r)\,dr^2 + c\,(r)\,d\theta^2 + d\,(r,\theta)\,d\phi^2.$$

This is a simple procedure involving only ordinary differentiation for this line element, and can be easily carried out by many symbolic manipulation software packages or by hand. When more complicated line elements are used, say the manifestly conformal,spherically symmetric line element

$$ds^2 = \bar{a}^2\,(r)\left(-b\,(r)\,dt^2 + \frac{dr^2}{b\,(r)} + r^2\left(d\theta^2 + \sin^2\theta d\phi^2\right)\right)$$

the differentiation process becomes more involved and is sometimes beyond the standard abilities of the symbolic packages. For this particular example, the equations can be derived in the conformal $\bar{a} = 1$ gauge and then transformed to an arbitrary $\bar{a}$ gauge, but it would be good to have a more general method in only for confirmation of these derivations.

The alternative method to produce the field tensors $W^{\mu\nu}$ in terms of the metric is by working directly in terms of the metric and curvature tensors that make up $W^{\mu\nu}$. The expansion of the field tensor was found above to give

$$\begin{aligned} W_{\mu\nu} &= \frac{g_{\mu\nu}}{3}\left(R^{\alpha}{}_{\alpha}\right)^{;\beta}{}_{;\beta} + R_{\mu\nu}{}^{;\beta}{}_{;\beta} - R_{\mu}{}^{\beta}{}_{;\nu;\beta} - R_{\nu}{}^{\beta}{}_{;\mu;\beta} - 2R_{\mu}{}^{\beta}R_{\nu\beta} + \frac{g_{\mu\nu}}{2}R_{\alpha\beta}R^{\alpha\beta} \\ &\quad + \frac{2}{3}\left(R^{\alpha}{}_{\alpha}\right)_{;\mu;\nu} + \frac{2}{3}R^{\alpha}{}_{\alpha}R_{\mu\nu} - \frac{g_{\mu\nu}}{6}\left(R^{\alpha}{}_{\alpha}\right)^2, \end{aligned}$$

a rather complicated expression in multiple covariant derivatives. Expansion of these double covariant derivatives will produce a vast number of terms in summations on dummy indices. Fortunately, for the cases considered in this work, a few important simplifications reduce the number of terms to something manageable for symbolic packages to work out.

The simplifications used all come back to the static, spherically symmetric system that has been chosen to be investigated. Because of these symmetries, any ordinary derivative terms will only contribute when in terms of the radial variable. This allows the simplification on many terms. Even more useful is the result that the metric and Ricci tensors are diagonal. This property allows the reduction of many pairs of dummy indices to fixed values.

The general procedure used was as follows:

- covariant derivatives are expanded (following Weinberg [24], outer derivatives first), with additional dummy indices, which may be repeated in different terms if only present for the summation,
- cancel/add terms of the same form in the free indices (generally μ, ν),
- set ordinary derivatives to be derivatives with respect to r, with indices so changed set equal to r everywhere within a term,
- appeal to the diagonality of $g_{\mu\nu}$, etc. to equate disparate indices in these diagonal quantities,
- sum on the free indices, by hand or (preferably!) with a symbolic package.

The process can also appeal to raising or lowering indices in the double covariant derivative terms with factor of the metric tensor, to put these terms into the familiar form. The Christoffel symbols are also limited by the diagonal structure of the metric tensor to only be nonzero for certain combinations of indices.

With these methods in hand, it is possible to produce a symbolic script that will produce the field tensor elements in terms of an arbitrary metric. An example of this is the following expression to produce the field tensor element W_{rr} with the symbolic package Macsyma. First, the results of the expansion of the field tensor terms are shown, followed by the eventual Macsyma script. The result of running this script agree exactly with those produced by the variational method in the standard metric, and the equivalent expression in the conformal line element.

The various tensor elements in the scripting are labeled according to the following table.

rauad	$R^{\alpha}{}_{\alpha}$
ug[μ, ν]	$g^{\mu\nu}$
lg[μ, ν]	$g_{\mu\nu}$
mcs[α, β, λ]	$\Gamma^{\lambda}{}_{\alpha\beta}$
rll[μ, ν]	$R_{\mu\nu}$

$$\begin{aligned} R^{\alpha}{}_{\alpha}{}^{;\beta}{}_{;\beta} &\rightarrow g^{\gamma\beta}\left(\frac{\partial}{\partial x^{\beta}}\left(R^{\alpha}{}_{\alpha;\gamma}\right)+\Gamma^{\alpha}{}_{\lambda\beta}R^{\lambda}{}_{\alpha;\gamma}-\Gamma^{\rho}{}_{\alpha\beta}R^{\alpha}{}_{\rho;\gamma}-\Gamma^{\sigma}{}_{\gamma\beta}R^{\alpha}{}_{\alpha;\sigma}\right) \\ &\rightarrow \ldots \\ &\rightarrow g^{rr}R^{\alpha}{}_{\alpha,rr}-g^{\beta\beta}\Gamma^{r}{}_{\beta\beta}R^{\alpha}{}_{\alpha,r} \end{aligned}$$

$$\begin{aligned} R^{\alpha}{}_{\alpha;r;r} &\rightarrow \frac{\partial}{\partial x^{r}}\left(R^{\alpha}{}_{\alpha;r}\right)+\Gamma^{\alpha}{}_{\lambda r}R^{\lambda}{}_{\alpha;r}-\Gamma^{\rho}{}_{\alpha r}R^{\alpha}{}_{\rho;r}-\Gamma^{\sigma}{}_{rr}R^{\alpha}{}_{\alpha;\sigma} \\ &\rightarrow \ldots \\ &\rightarrow R^{\alpha}{}_{\alpha,rr}-\Gamma^{r}{}_{rr}R^{\alpha}{}_{\alpha,r} \end{aligned}$$

$$\begin{aligned} R_{rr}{}^{;\beta}{}_{;\beta} &\rightarrow g^{\gamma\beta}\left(\frac{\partial}{\partial x^{\beta}}\left(R_{rr;\gamma}\right)-\Gamma^{\lambda}{}_{r\beta}R_{\lambda r;\gamma}-\Gamma^{\rho}{}_{r\beta}R_{r\rho;\gamma}-\Gamma^{\sigma}{}_{\gamma\beta}R_{rr;\sigma}\right) \\ &\rightarrow \ldots \\ &\rightarrow g^{rr}R_{rr,rr}-2g^{rr}\Gamma^{r}{}_{rr,r}R_{rr}-4g^{rr}\Gamma^{r}{}_{rr}R_{rr,r}-g^{\beta\beta}\Gamma^{r}{}_{\beta\beta}R_{rr,r} \\ &\quad +2g^{\beta\beta}\Gamma^{\lambda}{}_{r\beta}\Gamma^{r}{}_{\lambda\beta}R_{rr}+2g^{\beta\beta}\left(\Gamma^{\lambda}{}_{r\beta}\right)^{2}R_{\lambda\lambda}+2g^{\beta\beta}\Gamma^{\sigma}{}_{\beta\beta}\Gamma^{r}{}_{r\sigma}R_{rr} \end{aligned}$$

$$\begin{aligned} R_{r}{}^{\beta}{}_{;r;\beta} &\rightarrow g^{\gamma\beta}\left(\frac{\partial}{\partial x^{\beta}}\left(R_{r\gamma;r}\right)-\Gamma^{\lambda}{}_{r\beta}R_{\lambda\gamma;r}-\Gamma^{\rho}{}_{\gamma\beta}R_{r\rho;r}-\Gamma^{\sigma}{}_{r\beta}R_{r\gamma;\sigma}\right) \\ &\rightarrow \ldots \\ &\rightarrow g^{rr}R_{rr,rr}-2g^{rr}\Gamma^{r}{}_{rr,r}R_{rr}-3g^{rr}\Gamma^{r}{}_{rr}R_{rr,r}-g^{\beta\beta}\Gamma^{\beta}{}_{r\beta}R_{\beta\beta,r} \\ &\quad -g^{\beta\beta}\Gamma^{r}{}_{\beta\beta}R_{rr,r}+2g^{\beta\beta}\Gamma^{\lambda}{}_{r\beta}\Gamma^{\beta}{}_{\lambda r}R_{\beta\beta}+g^{\beta\beta}\Gamma^{\lambda}{}_{\beta\beta}\Gamma^{\lambda}{}_{rr}R_{\lambda\lambda} \\ &\quad +g^{\beta\beta}\Gamma^{\rho}{}_{\beta\beta}\Gamma^{r}{}_{\rho r}R_{rr}+g^{\beta\beta}\Gamma^{\sigma}{}_{r\beta}\Gamma^{r}{}_{\rho\sigma}R_{rr} \end{aligned}$$

```
t1: expand(-1/6*lg[2,2] * (ug[2,2]*diff(rauad,r,2)
- sum(ug[beta,beta] * mcs[beta,beta,2] * diff(rauad,r),beta,1,4)))
t2: ug[2,2]*diff(rll[2,2],r,2) - 2*ug[2,2] * diff(mcs[2,2,2],r) * rll[2,2]
 - 4*ug[2,2] * mcs[2,2,2] * diff(rll[2,2],r) - sum(ug[beta,beta] * mcs[beta,beta,2]
 * diff(rll[2,2],r),beta,1,4) + 2 * sum(sum(ug[beta,beta] * mcs[2,beta,lam]
 * mcs[lam,beta,2] * rll[2,2],lam,1,4),beta,1,4)
 + 2*sum(sum(ug[beta,beta] * mcs[2,beta,lam]^2 * rll[lam,lam],lam,1,4),beta,1,4)
 + 2*sum(sum(ug[beta,beta] * mcs[beta,beta,sigma]
 * mcs[2,sigma,2] * rll[2,2],sigma,1,4),beta,1,4)$
t3: -2*( ug[2,2]*diff(rll[2,2],r,2) - 2*ug[2,2] * diff(mcs[2,2,2],r) * rll[2,2]
 - 3*ug[2,2] * mcs[2,2,2] * diff(rll[2,2],r)
 - sum(ug[beta,beta] * mcs[2,beta,beta] * diff(rll[beta,beta],r),beta,1,4)
 - sum(ug[beta,beta] * mcs[beta,beta,2] * diff(rll[2,2],r),beta,1,4)
 + 2*sum(sum(ug[beta,beta] * mcs[2,beta,lam]
* mcs[lam,2,beta] * rll[beta,beta],beta,1,4),lam,1,4)
 + sum(sum(sum( ug[beta,beta] * mcs[2,beta,lam]
 * mcs[beta,2,sigma] * rll[lam,sigma] ,sigma,1,4),lam,1,4),beta,1,4)
 + sum(sum(ug[beta,beta] * mcs[beta,beta,lam]
 * mcs[2,2,lam] * rll[lam,lam],lam,1,4),beta,1,4)
 + sum(sum(ug[beta,beta] * mcs[beta,beta,rho]
 * mcs[rho,2,2] * rll[2,2],rho,1,4),beta,1,4)
 +sum(sum(ug[beta,beta] * mcs[2,beta,sigma]
 * mcs[beta,sigma,2] * rll[2,2],sigma,1,4),beta,1,4) )$
t4: 2/3*(diff(rauad,r,2)-mcs[2,2,2]*diff(rauad,r))$
ts: expand(-2*rll[2,2]*rlu[2,2] + 1/2*lg[2,2]*sum(rll[beta,beta] * ruu[beta,beta],beta,1,4)
 + 2/3*rauad * rll[2,2] -1/6*lg[2,2] * rauad^2)
wrr: expand(t1+t2+t3+t4+ts)
```

Appendix F

Scalar Field Conservation Identity

It is stated in [19] that the following identity holds:

$$S^{\mu}\left(S^{\alpha}{}_{;\alpha}+\frac{SR^{\alpha}{}_{\alpha}}{6}-4\lambda S^{3}\right)=\begin{pmatrix}\frac{2S^{\mu}S^{\nu}}{3}-\frac{g^{\mu\nu}S^{\alpha}S_{\alpha}}{6}-\frac{SS^{\mu;\nu}}{3}+\frac{g^{\mu\nu}SS^{\alpha}{}_{;\alpha}}{3}\\ -\frac{S^{2}}{6}\left(R^{\mu\nu}-\frac{g^{\mu\nu}}{2}R^{\alpha}{}_{\alpha}\right)-g^{\mu\nu}\lambda S^{4}\end{pmatrix}_{;\nu}.$$

As this is not necessarily obvious, a derivation for the systems that are considered in this thesis is presented here.

Consider the individual terms of the derivative expression.

$$\begin{aligned}
\left(\frac{2S^{\mu}S^{\nu}}{3}\right)_{;\nu} &= \frac{2}{3}S^{\mu}{}_{;\nu}S^{\nu}+\frac{2}{3}S^{\mu}S^{\nu}{}_{;\nu} && \text{(F.1)}\\
\left(-\frac{g^{\mu\nu}S^{\alpha}S_{\alpha}}{6}\right)_{;\nu} &= \left(-\frac{1}{6}\right)\left(g^{\mu\nu}S^{\alpha}{}_{;\nu}S_{\alpha}+g^{\mu\nu}S^{\alpha}S_{\alpha;\nu}\right)\\
&= \left(-\frac{1}{6}\right)\left(g^{\mu\nu}S_{\alpha}S^{\alpha}{}_{;\nu}+g^{\mu\nu}S^{\alpha}\left(g_{\alpha\beta}S^{\beta}\right)_{;\nu}\right)\\
&= \left(-\frac{1}{6}\right)\left(g^{\mu\nu}S_{\alpha}S^{\alpha}{}_{;\nu}+g^{\mu\nu}S_{\beta}S^{\beta}{}_{;\nu}\right)\\
&= \left(-\frac{1}{3}\right)g^{\mu\nu}S_{\alpha}S^{\alpha}{}_{;\nu} && \text{(F.2)}\\
\left(-\frac{SS^{\mu;\nu}}{3}\right)_{;\nu} &= \left(-\frac{1}{3}\right)\left(S_{\nu}S^{\mu;\nu}+SS^{\mu;\nu}{}_{;\nu}\right)\\
&= \left(-\frac{1}{3}\right)\left(S^{\nu}S^{\mu}{}_{;\nu}+SS^{\mu;\nu}{}_{;\nu}\right) && \text{(F.3)}\\
\left(\frac{g^{\mu\nu}SS^{\alpha}{}_{;\alpha}}{3}\right)_{;\nu} &= \left(\frac{1}{3}\right)\left(g^{\mu\nu}S_{\nu}S^{\alpha}{}_{;\alpha}+g^{\mu\nu}SS^{\alpha}{}_{;\alpha;\nu}\right)\\
&= \left(\frac{1}{3}\right)\left(S^{\mu}S^{\alpha}{}_{;\alpha}+g^{\mu\nu}SS^{\alpha}{}_{;\alpha;\nu}\right) && \text{(F.4)}\\
\left(-\frac{S^{2}}{6}\left(R^{\mu\nu}-\frac{g^{\mu\nu}}{2}R^{\alpha}{}_{\alpha}\right)\right)_{;\nu} &= -\frac{1}{3}SS_{\nu}\left(R^{\mu\nu}-\frac{g^{\mu\nu}}{2}R^{\alpha}{}_{\alpha}\right)-\frac{S^{2}}{6}\left(R^{\mu\nu}-\frac{g^{\mu\nu}}{2}R^{\alpha}{}_{\alpha}\right)_{;\nu}\\
&= -\frac{1}{3}SS_{\nu}R^{\mu\nu}+\frac{1}{6}SS^{\mu}R^{\alpha}{}_{\alpha} && \text{(F.5)}\\
\left(-g^{\mu\nu}\lambda S^{4}\right)_{;\nu} &= -4g^{\mu\nu}\lambda S^{3}S_{\nu}
\end{aligned}$$

$$= -4\lambda S^3 S^\mu \tag{F.6}$$

In these steps, indices have been raised and lowered using the metric tensor and in the fifth term expression, the covariant conservation of the Einstein tensor has been used.

Summing up these terms, we obtain

$$\begin{aligned}
&\frac{1}{3}S^\mu{}_{;\nu}S^\nu + \frac{2}{3}S^\mu S^\nu{}_{;\nu} - \frac{1}{3}g^{\mu\nu}S_\alpha S^\alpha{}_{;\nu} - \frac{1}{3}SS^{\mu;\nu}{}_{;\nu} + \frac{1}{3}\left(S^\mu S^\alpha{}_{;\alpha} + g^{\mu\nu}SS^\alpha{}_{;\alpha;\nu}\right) \\
&-\frac{1}{3}SS_\nu R^{\mu\nu} + \frac{1}{6}SS^\mu R^\alpha{}_\alpha - 4\lambda S^3 S^\mu \\
= \; & S^\mu\left(S^\alpha{}_{;\alpha} + \frac{SR^\alpha{}_\alpha}{6} - 4\lambda S^3\right)
\end{aligned}$$

which results in the condition that

$$\frac{1}{3}S^\mu{}_{;\nu}S^\nu + \frac{2}{3}S^\mu S^\nu{}_{;\nu} - \frac{1}{3}g^{\mu\nu}S_\alpha S^\alpha{}_{;\nu} - \frac{2}{3}S^\mu S^\alpha{}_{;\alpha} + \frac{1}{3}g^{\mu\nu}SS^\alpha{}_{;\alpha;\nu} - \frac{1}{3}SS^{\mu;\nu}{}_{;\nu} - \frac{1}{3}SS_\nu R^{\mu\nu} = 0.$$

Consider first the terms in covariant divergence:

$$\begin{aligned}
& \frac{1}{3}S^\nu S^\mu{}_{;\nu} - \frac{1}{3}g^{\mu\nu}S_\alpha S^\alpha{}_{;\nu} + \frac{2}{3}S^\mu S^\nu{}_{;\nu} - \frac{2}{3}S^\mu S^\alpha{}_{;\alpha} \\
\Rightarrow \; & \frac{1}{3}g^{\mu\nu}\left(S_\mu S^\mu{}_{;\nu} - S_\alpha S^\alpha{}_{;\nu}\right) + \frac{2}{3}S^\mu\left(S^\nu{}_{;\nu} - S^\alpha{}_{;\alpha}\right) \\
\Rightarrow \; & \frac{1}{3}g^{\mu\nu}\left(g_{\mu\nu}S^\nu S^\mu{}_{;\nu} - g_{\alpha\nu}S^\nu S^\alpha{}_{;\nu}\right) + \frac{2}{3}S^\mu\left(S^\nu{}_{;\nu} - S^\alpha{}_{;\alpha}\right) \\
\Rightarrow \; & \frac{1}{3}g^{\mu\nu}\left(S^\nu S_{\nu;\nu} - S^\nu S_{\nu;\nu}\right) + \frac{2}{3}S^\mu\left(S^\nu{}_{;\nu} - S^\alpha{}_{;\alpha}\right) \\
\Rightarrow \; & 0
\end{aligned}$$

as both α and ν are indices to be summed over, the covariant divergence terms cancel.

Now, note that in the specific cases we are studying we have a system which is static and spherically symmetric. This has the consequences that both the metric and Ricci tensors are diagonal, and that the Christoffel symbols $\Gamma^\lambda_{\mu\nu}$ are symmetric under interchange of the indices μ, ν. The remaining terms become

$$\frac{1}{3}g^{\mu\nu}SS^\alpha{}_{;\alpha;\nu} - \frac{1}{3}SS^{\mu;\nu}{}_{;\nu} - \frac{1}{3}SS_\nu R^{\mu\nu} = 0.$$

The Ricci tensor term can be expanded, using relations about commutation of covariant derivatives [24] as

$$S_\nu R^{\mu\nu} = S_{;\nu}{}^{;\mu;\nu} - S_{;\nu}{}^{;\nu;\mu}.$$

However, if the Ricci tensor $R^{\mu\nu}$ is diagonal, when $\mu \neq \nu$ the tensor element is zero. Thus this expansion has the same property, leading to:

$$\begin{aligned} S_\nu R^{\mu\nu} &= S_{;\nu}{}^{;\mu;\nu} - S_{;\nu}{}^{;\nu;\mu} = 0 \text{ if } \mu \neq \nu \\ &= S_{;\nu}{}^{;\nu;\nu} - S_{;\nu}{}^{;\nu;\nu} = 0 \text{ if } \mu = \nu. \end{aligned}$$

The remaining terms are

$$\frac{1}{3} g^{\mu\nu} S S^{\alpha}{}_{;\alpha;\nu} - \frac{1}{3} S S^{\mu;\nu}{}_{;\nu} = 0.$$

A little rearrangement gives

$$\begin{aligned} & \frac{1}{3} g^{\mu\nu} S \left(S^{\alpha}{}_{;\alpha;\nu} - S^{\mu}{}_{;\mu;\nu} \right) \\ = \; & \frac{1}{3} g^{\mu\nu} S \left(S^{\alpha}{}_{;\alpha} - S^{\mu}{}_{;\mu} \right)_{;\nu} \\ = \; & 0 \end{aligned}$$

as in the covariant divergence the indices α and μ are both summed over the range 0..3. Thus the identity holds in this case of diagonal Ricci tensor, which arises from the symmetries of the situation being considered.

Bibliography

[1] Einstein A. Die grundlage der allgemeinen Relativitätstheorie. *Ann. Phys.*, 49:769, 1916.

[2] Weinberg S. *Dreams of a Final Theory.* Hutchinson Radius, London, 1993.

[3] Schmidt B. P., Suntzeff N. B., and Phillips M. M., *et. al.* The high-Z supernova search: Measuring cosmic deceleration and global curvature of the universe using type 1a supernovae. *Ap. J*, 507:46–63, 1998.

[4] Riess A. G., Filippenko A. V., and Challis P., *et. al.* Observational evidence from supernovae for an accelerating universe and a cosmological constant. *Astron. J.*, 116:1009–1038, 1998.

[5] Perlmutter S., Turner M. S., and White M. Constraining dark energy with type 1a supernovae and large-scale structure. *Phys. Rev. Lett*, 83(4):670–673, 1999.

[6] Anderson J. D., Laing P. A., Lau E. L., Liu A. S., Nieto M. M., and Turyshev S. G. Indication, from Pioneer 10/11, Galileo, and Ulysses data, of an apparent anomalous, weak, long-range acceleration. *Phys. Rev. Lett.*, 81:2858–2861, 1998.

[7] Guruprasad V. The correct analysis and explanation of the Pioneer-Galileo anomalies. Preprint astro-ph 9907363, September 1999.

[8] Mbelek J. P. and Lachiéze-Rey M. Long-range acceleration induced by a scalar field external to gravity and the indication from Pioneer 10/11, Galileo and Ulysses data. Preprint gr-qc 9910105, October 1999.

[9] Weyl H. *Math. Zeit.*, 2:384, 1918.

[10] Ohanian H. C. and Ruffini R. *Gravitation and Spacetime.* W. W. Norton and Co., second edition, 1994.

[11] Fiedler B. and Schimming R. Exact solutions of the Bach field equations of general relativity. *Rept. Math. Phys.*, 17:15, 1980.

[12] Reigert R. J. *Classical and Quantum Conformal Gravity.* PhD thesis, University of California, San Diego, 1986.

[13] Mannheim P. D. and Kazanas D. Exact vacuum solution to conformal Weyl gravity and galactic rotation curves. *Ap. J.*, 342:635–638, 1989.

[14] Mannheim P. D. and Kazanas D. Newtonian limit of conformal gravity and the lack of necessity of the second order Poisson equation. *Gen. Rel. Gravit.*, 26(4):337–361, 1994.

[15] Mannheim P. D. Conformal cosmology with no cosmological constant. *Gen. Rel. Gravit.*, 22(3):289–298, 1990.

[16] Mannheim P. D. Linear potentials and galactic rotation curves. *Ap. J.*, 419:150–154, 1993.

[17] Mannheim P. D. Are galactic rotation curves really flat? *Ap. J.*, 479:659–664, 1997.

[18] Perlick V. and Chongming X. Matching exterior to interior solutions in weyl gravity:comment on "Exact vacuum solution to conformal Weyl gravity and galactic rotation curves". *Ap. J*, 449:47–51, 1995.

[19] Mannheim P. D. Dynamical mass and geodesic motion. *Gen. Rel. Gravit.*, 25(7):697–715, 1993.

[20] de Bernardis P., et. al. A flat universe from high-resolution maps of the cosmic microwave background radiation. *Nature*, 404:955, 2000.

[21] McGaugh S. Distinguishing between cold dark matter and modified Newtonian dynamics: Predictions for the microwave background. *Ap. J.*, 523:L99, 1999.

[22] McGaugh S. Boomerang data suggest a purely baryonic universe. *Ap. J.*, 541:L33, 2000.

[23] Sellwood J. A. and Kosowsky A. Does dark matter exist? In Hibbard J E Rupen M P and van Gorkom J H, editors, *Gas and Galaxy Evolution, ASP Conference Series*, pages 24–89. 2000. Preprint astro-ph/0009074.

[24] Weinberg S. *Gravitation and Cosmology.* Wiley, New York, 1972.

[25] Bach R. *Math. Zeit.*, 9:110, 1921.

[26] DeWitt B. S. Dynamical theory of groups and fields. In C. DeWitt and B. S. DeWitt, editors, *Relativity, Groups and Topology*, page 719. Gordon and Breach, 1964.

[27] Edery A. and Paranjape M. B. Classical tests for Weyl gravity: Deflection of light and time delay. *Phys. Rev. D*, 58:024011, 1998.

[28] Edery A. and Paranjape M. B. Causal structure of vacuum solutions to conformal (Weyl) gravity. *Gen. Rel. Gravit.*, 31(7):1031 – 1047, 1999.

[29] Walker M. A. Lensing in alternative gravity. *Ap. J*, 430:463, 1994.

[30] Mannheim P. D. and Kazanas D. Energy-momentum tensor of fields in the standard cosmology. *Gen. Rel. Gravit.*, 20(3):201–220, 1988.

[31] Mannheim P. D. Implications of cosmic repulsion for gravitational theory. *Phys. Rev. D*, 58:103511, 1998.

[32] Jones B. F. Gravitational deflection of light: solar eclipse of 30 June 1973 II. Plate reductions. *Astron. J*, 81:455, 1976.

[33] Robertson D. S, Carter W. E., and Dillinger W. H. New measurement of solar gravitational deflection of radio signals using VLBI. *Nature*, 349:768, 1991.

[34] Reasenberg R. D., Shapiro I. I., MacNeil P. E., Goldstein R. B., Breidenthal J. C., Brenkle J. P., Cain D. L., Kaufman T. M., Komarek T. A., and Zygielbaum A. I. Viking relativity experiment: Verification of signal retardation by solar gravity. *Ap. J*, 234:L219, 1979.

[35] Barabash O. V. and Shtanov Y. V. Newtonian limit of conformal gravity. *Phys. Rev. D*, 60:064008, 1999.

[36] Wood K. S. and Nemiroff R. J. Constraints on Weyl gravity on subgalactic distance scales. *Ap. J*, 369:54–56, 1991.

[37] Mannhiem P. D. Fourth order theories without ghosts. Preprint hep-th 0001115, January 2000.

[38] Press W.H., Teukolsky S.A., Flannery W.T., and Vetterling W.T. *Numerical Recipes, The Art of Scientific Programming.* Cambridge University Press, second edition, 1992.

[39] Vernazza J. E., Avrett E. H., and Loeser R. Structure of the solar chromosphere. II. The underlying photosphere and temperature-minimum region. *Ap. J. Suppl*, 30:1–60, 1976.

[40] Mannheim P. D. Conformal gravity and the flatness problem. *Ap. J.*, 391:429–432, 1992.

[41] Engeln-Müllges G. and Uhlig F. *Numerical Algorithms with C.* Springer-Verlag, 1996.